

# Quantum Scalar Field Dynamics On A Maximally Sliced Two-sided AdS Black Hole Spacetime

Anurag Kaushal\*, Naveen S. Prabhakar† and Spenta R. Wadia‡

*International Centre for Theoretical Sciences*

*Tata Institute of Fundamental Research, Shivakote, Bengaluru 560089, India.*

We study the semi-classical dynamics of a scalar field in the background of a black hole in an asymptotically AdS (AAAdS) spacetime, in the framework of the Hamiltonian formulation of General Relativity. The small diffeomorphism (gauge) symmetries generated by the Hamiltonian and momentum constraints are completely fixed by the maximal slicing and spatial harmonic/Dirac gauge conditions after which the residual phase space degrees of freedom are gauge invariant. While many of our results are valid for AAAdS<sub>d+1</sub> spacetimes, we mainly discuss the  $d = 2$  case of the static BTZ solution. We present the explicit solution for the smooth maximal slicing of the fully extended BTZ solution where the spatial slices cut across the horizons, asymptote to the usual Schwarzschild slices, do not include the past and future singularities, and for which the lapse remains non-zero at the bifurcate point. We also derive unique large diffeomorphisms that asymptote to time translations on both boundaries in the maximal slicing gauge.

We present the solution of the scalar field wave equation in this gauge in terms of its boundary values which correspond to boundary CFT operators by the AdS/CFT dictionary. We explicitly construct the finite, time-dependent Hamiltonian in terms of a discrete set of mode functions of the scalar field that are smooth and differentiable across the horizons of the fully extended BTZ black hole. These modes mix the boundary operators from the two sides and are appropriate linear combinations of the Hartle-Hawking-Unruh modes. This Hamiltonian is an operator in the product of the two CFTs associated to the two boundaries and describes the time evolution of CFT operators. Our results are valid for evolution times smaller than the scrambling time during which the fully extended BTZ solution continues to be a valid saddle point of the quantum gravity path integral.

---

\*anuragkaushal314@gmail.com

†naveen.s.prabhakar@gmail.com

‡spenta.wadia@icts.res.in

# Contents

<b>1</b>	<b>Introduction</b>	<b>3</b>
<b>2</b>	<b>Gauge fixing in the Hamiltonian formulation</b>	<b>5</b>
2.1	The maximal slicing gauge	7
2.2	Gauge fixing the momentum constraints	10
2.3	The reduced phase space	12
2.4	Large diffeomorphisms and equations for the lapse and shift	12
2.5	Gauge fixing in perturbation theory	13
2.5.1	The perturbation expansion	14
2.5.2	Gauge fixing the linearized constraints	15
2.5.3	Diffeomorphism invariance of the scalar field	15
<b>3</b>	<b>Hamiltonian formulation in 2 + 1 dimensional AAdS spacetimes</b>	<b>15</b>
3.1	The maximal slicing gauge condition in $d = 2$	16
3.2	Spatial harmonic gauge for the momentum constraints	16
3.3	Solving the constraint equations	17
<b>4</b>	<b>The BTZ black hole in the maximal slicing gauge</b>	<b>19</b>
4.1	A review of the BTZ black hole solution	20
4.2	Solving Einstein's equations in the maximal slicing gauge using the areal radial coordinate	22
4.3	Wormhole coordinates	26
4.4	Symmetric maximal slices	27
4.5	A second family of maximal slices	29
4.6	Large diffeomorphisms	31
<b>5</b>	<b>A probe scalar field in the maximally sliced BTZ black hole</b>	<b>32</b>
5.1	The scalar field mode expansion	35
5.1.1	Mode expansion in Region I	35
5.1.2	Mode expansion in Region II	36
5.1.3	Mode expansions in Regions F and P	37
5.2	A smooth, global expression for the scalar field	38
5.2.1	The Hartle-Hawking modes	38
5.2.2	Divergences in the derivatives of the Hartle-Hawking modes	39
5.2.3	Smoothing the divergences at the horizons	39
5.2.4	The smeared modes	41
5.3	Hamiltonian for maximal slicing	42
<b>A</b>	<b>The Lichnerowicz equation</b>	<b>44</b>
<b>B</b>	<b>Details of the perturbation theory analysis</b>	<b>46</b>
<b>C</b>	<b>More details of the maximally sliced BTZ black hole solution</b>	<b>50</b>

C.1	Solving the constraint equations in maximal slicing gauge	51
C.2	Solving for the lapse and shift	51
C.3	Diffeomorphism to the BTZ black hole	53
C.4	The wormhole coordinate	56
C.5	ADM masses	57
C.6	Asymptotic falloff of the extrinsic curvature $K_{ij}$ and the boundary stress tensor	58
<b>D</b>	<b>Maximal slices in the BTZ black hole from a variational principle</b>	<b>60</b>
D.1	The variational principle	60
D.2	The spacetime metric in maximal slicing coordinates	63
<b>E</b>	<b>Solutions of the Klein-Gordon equation in the BTZ spacetime</b>	<b>64</b>
E.1	Separation of variables	64
E.2	Solution in Region I	65
E.3	Solution in region II	67
E.4	Solution in Region F	68
E.5	Solution in Region P	69
E.6	Analytic continuation to regions F and P	70
E.7	The Hartle-Hawking modes and Bogoliubov coefficients	74
E.8	Normalization of the Klein-Gordon mode functions	74

## 1 Introduction

In this paper we revisit and study the problem of quantum dynamics of matter fields in the background of a black hole in an asymptotically AdS (AAdS) spacetime. We study this problem in the framework of the Hamiltonian formulation of General Relativity in AAdS spacetimes. We pay special attention to the problem of gauge fixing corresponding to the Hamiltonian and momentum constraints using the constrained Hamiltonian formalism of Dirac [1, 2]. Correctly fixing gauge without residual small gauge transformations allows us to describe the physics in terms of quantities which are gauge invariant under small gauge transformations. The use of gauge invariant quantities in the gravity theory allows us to correctly interpret the results in the dual CFT via the AdS/CFT correspondence.

The Hamiltonian and momentum constraints of general relativity are first class constraints and generate gauge transformations, i.e., spacetime diffeomorphisms, on phase space via the Poisson bracket. We choose the maximal slicing condition  $g_{ij}\pi^{ij} = 0$  as the gauge condition corresponding to the Hamiltonian constraint and demonstrate that there are no residual small diffeomorphisms in this gauge using Dirac's method. We review results from mathematical relativity regarding the Lichnerowicz equation in AAdS spacetimes which isolates the independent degrees of freedom in phase space. We also discuss gauge fixing conditions for the momentum constraints which fix gauge completely.

Once the gauge corresponding to all constraints is correctly fixed without any residual small diffeomorphisms, the next step is to replace the Poisson bracket on phase space by the Dirac bracket. Recall that the Dirac bracket is well-defined only if there are no residual diffeomorphisms

in our gauge choice. As shown by Dirac, the Dirac bracket of any function on phase space with any of the constraints and gauge conditions is zero:

$$\{\mathcal{C}, f\}_D = 0, \quad (1.1)$$

where  $\{\cdot, \cdot\}_D$  is the Dirac bracket,  $\mathcal{C}$  stands for any of the constraints or the gauge conditions, and  $f$  is any function on phase space.<sup>1</sup> The key implication of this fact is that any function on phase space is now *gauge invariant under small gauge transformations*. The above results hold even in the presence of matter degrees of freedom, provided that in the scalar case, the potential energy of the scalar field satisfies  $V(\phi) \leq 0$  (the same condition is encountered for similar reasons in the analysis of the Lichnerowicz equation in the Einstein-scalar system [3–8]). This excludes the simple case of a free scalar field with a positive mass, but we remark that this case can be treated in perturbation theory about a pure gravity background.

We also discuss large diffeomorphisms in AAdS spacetimes. It has been shown in the Hamiltonian formalism by [9, 10] that the large diffeomorphisms that preserve AAdS boundary conditions all asymptote to the algebra of isometries  $\mathfrak{so}(d, 2)$  of  $\text{AdS}_{d+1}$  for  $d > 2$ , and the Virasoro algebra for  $d = 2$ . However, for a given element of the asymptotic symmetry algebra, there are an infinite number of large diffeomorphisms that asymptote to it, all differing by small diffeomorphisms. Since we have fixed small diffeomorphism redundancy completely in the maximal slicing gauge, one obtains a unique representative large diffeomorphism for any element of the asymptotic symmetry algebra. In  $2 + 1$  dimensions, we explicitly derive the unique large diffeomorphisms which are compatible with the maximal slicing and spatially harmonic gauge that corresponds to asymptotic time translations.

We specialize to  $2 + 1$  dimensional AAdS spacetimes and describe all the steps of Dirac’s method in explicit detail. In particular, we choose the maximal slicing gauge for the Hamiltonian constraint and the spatial harmonic gauge for the momentum constraints (a similar analysis was done in [11, 12] for the case of compact spatial slices, and the AAdS<sub>2+1</sub> constraint equations were considered in the recent paper [13]). Since we are interested in the maximally extended black hole solutions which have two AAdS boundaries, we focus on the case where the spatial manifold is a cylinder  $\mathbf{R} \times \mathbf{S}^1$ . This procedure automatically gives a maximally sliced foliation of the fully extended BTZ black hole [14, 15].

We then proceed to explicitly construct the maximally sliced foliation of the fully extended BTZ black hole by solving Einstein’s equations. Though we work with the BTZ black hole, similar calculations can be performed for AdS black holes in higher dimensions as well. We present the solution in the ‘wormhole coordinates’ which are globally valid. The main feature of the maximally sliced solution is that the spatial slices cut across the horizons and asymptote to the usual Schwarzschild slices at the two boundaries. Another important point is that the maximally sliced solution does not include the black hole and white hole singularities.

Next, we discuss the dynamics of a probe massive scalar field (as an example) in the maximally sliced black hole background. We do a careful semi-classical expansion in the coupling constant  $\kappa = \sqrt{16\pi G_N}$  up to quadratic order in the fluctuations of both the scalar and metric degrees of freedom, and note that the scalar field does not mix with the metric fluctuations in the

---

<sup>1</sup>In the quantum theory, it is the Dirac bracket that goes over to the commutator and not the Poisson bracket.

Hamiltonian at this order. For concreteness, we restrict the discussion to  $2 + 1$  dimensions, in which case there are no local degrees of freedom for the gravitational field.

Our main aim is to obtain a well-defined scalar field Hamiltonian which propagates the field modes in the time coordinate corresponding to the maximal slicing foliation of the BTZ black hole. Since the maximal slicing solution is time dependent, the Hamiltonian operator will be time dependent as well. The standard expansion of the scalar field in terms of the Hartle-Hawking modes is not well-suited for computing the Hamiltonian since their derivatives at the horizon are divergent. To cure this divergence, we introduce a discrete basis of modes which also annihilate the Hartle-Hawking state. Using these modes, we obtain a finite expression for the Hamiltonian operator. This gives a well-defined time evolution for the operator modes of the scalar field and we can study the time evolution of the entangled Hartle-Hawking state and its excitations along the maximal slicing. We would like to emphasize that, while we have stated the above results for a scalar field in a BTZ black hole, they are of a universal nature and the same conclusions would be valid for matter fields in higher dimensional AdS black holes.

Since the maximal slices cut across the black hole horizon, we can study infalling states in a completely well defined way. Since our entire treatment is in a correctly gauge fixed setup, we can interpret these results correctly in the dual product CFT on the two boundaries. The expression for the Hamiltonian in fact involves the modes of the boundary operators, since these are related to the bulk scalar field modes by the AdS/CFT dictionary [16–23]. The boundary operators enter in the Hartle-Hawking-Unruh combination of the two boundary CFTs; thus, the evolution of states using the maximal slicing Hamiltonian necessarily involves the entangled degrees of freedom of the two CFTs. In [24–26], a CFT operator which describes the time evolution of infalling observers in the black hole background was obtained using algebraic QFT methods. Related ideas and questions have been discussed in [27–31].

We would like to emphasize that this description of dynamics of the scalar field in the BTZ black hole background is valid for times  $\bar{t}$  much smaller than the scrambling time  $t_*$ . This is because, at times of order  $t_*$ , we expect that the given black hole background may not be the dominant saddle point due to backreaction effects becoming important [32]. We can also infer this from the observation that the dual CFT four-point OTOC ceases to factorize into the product of two two-point functions at times of order  $t_* \sim \frac{\beta}{2\pi} \log N$  [33]. This indicates that the large  $N$  saddle point analysis in the dual CFT is no longer valid at times of order  $t_*$ .

## 2 Gauge fixing in the Hamiltonian formulation

In this section we discuss the Hamiltonian formulation of General Relativity in asymptotically AdS (AAdS) spacetimes with two boundaries, with emphasis on gauge fixing corresponding to the first class Hamiltonian and momentum constraints.

The Hamiltonian formulation requires that spacetime be locally of the form  $\Sigma \times \mathbf{R}$  where  $\mathbf{R}$  corresponds to the Lorentzian time direction. The configuration space of general relativity is  $\text{Met}$ , the space of Riemannian metrics  $g_{ij}$  on the  $d$ -dimensional space  $\Sigma$ . The unconstrained phase space is the cotangent bundle  $T^*\text{Met}$  whose points are labelled by  $(g_{ij}, \pi^{ij})$  where  $\pi^{ij}$  is the canonically conjugate momentum to  $g_{ij}$ . When matter fields are present, we have to include them in the phase space as well. For illustration, we consider a scalar field  $\phi$  with conjugate

momentum  $\pi_\phi$ .

The Poisson brackets are given by

$$\{g_{ij}(x), \pi^{kl}(x')\} = \delta_{(i}^{(k} \delta_{j)}^{l)} \delta(x, x') , \quad \{\phi, \pi_\phi\} = \delta(x, x') . \quad (2.1)$$

The Hamiltonian of general relativity is

$$H = \int_{\Sigma} d^d x (N \mathcal{H}_{\perp} + N_i \mathcal{H}^i) + \oint_{\partial\Sigma} d^{d-1} \sigma \mathcal{B} , \quad (2.2)$$

where

1.  $N, N_i$  are the auxiliary lapse and shift fields, with the lapse  $N$  being constrained to be nowhere zero on  $\Sigma$  in the classical theory.
2.  $\mathcal{H}_{\perp}$  and  $\mathcal{H}^i$  are resp. the Hamiltonian and momentum constraints

$$\begin{aligned} \mathcal{H}_{\perp} &= \kappa^2 \frac{1}{\sqrt{g}} \left( \pi^{ij} \pi_{ij} - \frac{1}{d-1} \pi^2 \right) - \frac{1}{\kappa^2} \sqrt{g} (R - 2\Lambda) + \frac{\pi_\phi^2}{2\sqrt{g}} + \sqrt{g} \left( \frac{1}{2} g^{ij} \partial_i \phi \partial_j \phi + V(\phi) \right) , \\ \mathcal{H}^i &= -2D_j \pi^{ij} + g^{ij} \pi_\phi \partial_j \phi . \end{aligned} \quad (2.3)$$

$\Lambda$  is the cosmological constant, and in this paper we take  $\Lambda < 0$ . The AdS length  $\ell$  is defined as  $\Lambda = -1/\ell^2$ . The constant  $\kappa^2 = 16\pi G_N$  is the gravitational coupling which is set to 1 unless indicated otherwise.

3. The boundary term  $\mathcal{B}$  is present to make the functional partial derivatives of  $H$  with respect to  $g_{ij}$  and  $\pi^{ij}$  well-defined [9, 10, 34]. For the choice of Dirichlet boundary conditions on all the fields, with appropriate fall-off conditions as one approaches the asymptotic boundary, the boundary terms are

$$\mathcal{B} = -\frac{2}{\kappa^2} N \sqrt{\sigma} k + 2r_i N_j \pi^{ij} - \mathcal{B}_{\text{ct}} , \quad (2.4)$$

where  $\sigma$  is the determinant of the induced metric on  $\partial\Sigma$ ,  $k = g^{ij} D_i r_j$  is the trace of the extrinsic curvature of the boundary  $\partial\Sigma$  embedded in  $\Sigma$ , and  $r^i$  is its outward pointing unit normal vector (unit norm with respect to the spatial metric  $g_{ij}$ ). The subtraction  $\mathcal{B}_{\text{ct}}$  are holographic counterterms that are required to remove the divergence present in the first term [35–39]. For  $d = 2$ , the counterterm is simply  $\mathcal{B}_{\text{ct}} = \frac{2}{\kappa^2 \ell} N \sqrt{\sigma}$  which subtracts  $1/\ell$  from  $k$  above.

The equations of motion for the lapse and shift are  $\mathcal{H}_{\perp} \approx 0$  and  $\mathcal{H}^i \approx 0$  respectively, where the notation  $\approx$  indicates that they are imposed as weak constraints on phase space. The dynamics generated by the Hamiltonian (2.2) must respect these constraints. The Hamiltonian and momentum constraints are first class constraints and their algebra is

$$\begin{aligned} \{\mathcal{H}_{\perp}(x), \mathcal{H}_{\perp}(x')\} &= (g^{ij} \mathcal{H}_j(x) + g^{ij} \mathcal{H}_j(x')) \delta_{,i}(x, x') , \\ \{\mathcal{H}_i(x), \mathcal{H}_{\perp}(x')\} &= \mathcal{H}_{\perp}(x) \delta_{,i}(x, x') , \\ \{\mathcal{H}_i(x), \mathcal{H}_j(x')\} &= \mathcal{H}_i(x) \delta_{,j}(x, x') + \mathcal{H}_j(x) \delta_{,i}(x, x') , \end{aligned} \quad (2.5)$$

where the derivatives on the  $\delta$ -functions are all with respect to the first argument. The geometric interpretation of  $\mathcal{H}_\perp$  and  $\mathcal{H}_i$  is that they generate deformations of the surface  $\Sigma$  in the normal and tangential directions respectively with respect to a given coordinate embedding in spacetime [2, 40, 41]. In other words, they generate the action of ‘small local’ spacetime diffeomorphisms on the fields defined on the surface  $\Sigma$ .

Arbitrary diffeomorphisms of spacetime (including global transformations) are generated by a linear combination of these constraints including appropriate surface terms. The Hamiltonian (2.2) is precisely of this form, and it generates diffeomorphisms specified by the functions  $N$  and  $N^i$ .

There has been an extensive discussion in the literature on gauge fixing the diffeomorphism invariance; for instance, see [42] and the references therein for a detailed description. In this paper, we discuss one of the earliest and well-studied choices of gauge for the Hamiltonian constraint – the maximal slicing condition [43]<sup>2</sup>. We make use of mathematical relativity results on the maximal slicing gauge condition in AAdS spacetimes [6–8, 44–46].

## 2.1 The maximal slicing gauge

The maximal slicing gauge choice corresponds to setting the trace of the canonical momentum  $\pi = g_{ij}\pi^{ij}$  to zero on  $\Sigma$ :

$$\pi \approx 0 . \tag{2.6}$$

Note that this must be imposed a weak constraint on phase space, hence the  $\approx$ . One immediate consequence of this is that the Hamiltonian constraint has a positive definite kinetic term:

$$\mathcal{H}_\perp = \frac{1}{\sqrt{g}} \left( \pi^{ij}\pi_{ij} - \frac{1}{2} \underbrace{\pi^2}_0 \right) - \sqrt{g}(R - 2\Lambda) . \tag{2.7}$$

For a gauge choice to be correct, the orbits of the gauge group should intersect the gauge slice transversally, that is, gauge transformations must take any point on the gauge slice out of the slice. Infinitesimal gauge transformations are generated by Poisson bracket with the constraints. Hence, we must check that the Poisson bracket of the gauge condition with the constraints are not all zero. This is the next step in Dirac’s method. Note that  $\pi$  has a trivial Poisson bracket with the momentum constraints on the gauge slice:

$$\{\mathcal{H}_i(x), \pi(x')\} = D_i\delta(x, x')\pi(x') \approx 0 . \tag{2.8}$$

This means that the spatial diffeomorphisms generated by  $\mathcal{H}_i$  act tangentially on the gauge slice  $\pi \approx 0$  and preserve the gauge condition. Hence one has to separately impose  $d$  gauge fixing conditions for each of the  $d$  generators  $\mathcal{H}^i$ . We will discuss these gauge conditions later on.

---

<sup>2</sup>Also known as the zero mean curvature condition.

Next, we compute the Poisson bracket of  $\pi$  with  $\mathcal{H}_\perp$ :

$$\begin{aligned}
& \{\mathcal{H}_\perp(x), \pi(x')\} \\
&= \left( -\frac{d}{2} \mathcal{G}_{ijkl} \pi^{ij} \pi^{kl} - \frac{d}{2} \sqrt{g} (R - 2\Lambda) + \sqrt{g} (R + (d-1)D^2) \right. \\
&\quad \left. - \frac{d}{2} \frac{\pi_\phi^2}{2\sqrt{g}} + \frac{d}{2} \sqrt{g} \left( \frac{1}{2} g^{ij} \partial_i \phi \partial_j \phi + V(\phi) \right) - \frac{1}{2} \sqrt{g} g^{ij} \partial_i \phi \partial_j \phi \right) \delta(x, x'), \\
&\approx (d-1) \sqrt{g} \left( D^2 - \frac{\pi^{ij} \pi_{ij} - \frac{1}{d-1} \pi^2 + \frac{1}{2} \pi_\phi^2}{g} + \frac{2\Lambda + V(\phi)}{d-1} \right) \delta(x, x'), \\
&\approx (d-1) \sqrt{g} \left( D^2 - \frac{1}{g} (\pi^{ij} \pi_{ij} + \frac{1}{2} \pi_\phi^2) + \frac{2\Lambda + V(\phi)}{d-1} \right) \delta(x, x'). \tag{2.9}
\end{aligned}$$

where we have used the Hamiltonian constraint  $\mathcal{H}_\perp \approx 0$  in going to the second line, and  $\pi \approx 0$  in going to the last line. Thus, on the subspace simultaneously constrained by  $\mathcal{H}_\perp \approx 0$  and  $\pi \approx 0$ , the Poisson bracket is given by the above differential operator. If the operator has zero modes, then a small diffeomorphism corresponding to a zero mode preserves the gauge slice  $\pi \approx 0$  and hence the diffeomorphism orbit is not transversal.

We show that the operator in the last line of (2.9) has no zero modes corresponding to *small diffeomorphisms*, i.e., diffeomorphisms which fall-off fast enough to zero as one approaches the boundary. Suppose there is a diffeomorphism parameter  $(\xi_\perp, \xi^i)$  that is a zero mode. Then, we have

$$\left( D^2 - \frac{1}{g} (\pi^{ij} \pi_{ij} + \frac{1}{2} \pi_\phi^2) + \frac{2\Lambda + V(\phi)}{d-1} \right) \xi_\perp = 0. \tag{2.10}$$

Multiplying by  $\xi_\perp$  and integrating over  $\Sigma$ , we have

$$\int_\Sigma d^d x \sqrt{g} \xi_\perp D^2 \xi_\perp = \int_\Sigma d^d x \sqrt{g} \left( \frac{\pi^{ij} \pi_{ij} + \frac{1}{2} \pi_\phi^2}{g} - \frac{2\Lambda + V(\phi)}{d-1} \right) \xi_\perp^2. \tag{2.11}$$

Integrating by parts on the left hand side, we get

$$\int_{\partial\Sigma} d^{d-1} \sigma r^i \sqrt{\sigma} \xi_\perp \partial_i \xi_\perp = \int_\Sigma d^d x \sqrt{g} \left( g^{ij} D_i \xi_\perp D_j \xi_\perp + \frac{\pi^{ij} \pi_{ij} + \frac{1}{2} \pi_\phi^2}{g} \xi_\perp^2 - \frac{2\Lambda + V(\phi)}{d-1} \xi_\perp^2 \right). \tag{2.12}$$

The right hand side is positive definite if the potential  $V(\phi)$  satisfies

$$V(\phi) \leq 0. \tag{2.13}$$

Suppose this is so.<sup>3</sup> Also, suppose  $\xi_\perp$  is a small diffeomorphism for which the boundary contribution is zero.<sup>4</sup> Since the right hand side is non-negative, the only small diffeomorphism that satisfies the above equation is then  $\xi_\perp = 0$  identically everywhere. The absence of non-trivial zero modes implies that there is no non-trivial small diffeomorphism that preserves the  $\pi \approx 0$

<sup>3</sup>In case the potential does not satisfy  $V(\phi) \leq 0$ , the analysis as written cannot be carried through. However, in perturbation theory, the potential can be positive since it appears at subleading order in the coupling constant  $\kappa$ . This means that leading part of the differential operator to be inverted does not involve  $V(\phi)$ .

<sup>4</sup>For spatial metrics  $g_{ij}$  which approach the AdS<sub>d</sub> spatial metric  $\frac{dr^2}{r^2} + r^2 d\Omega_{d-1}^2$ , the fall-off condition on  $\xi_\perp$  that ensures that the boundary contribution is zero is  $\xi_\perp \sim r^{-(d-1+\epsilon)}$ .



gauge slice.

The above discussion does not rule out the existence of zero modes  $(\xi_\perp, \xi_i)$  for which the boundary contribution on the left-hand side of (2.12) is non-zero (and possibly infinite). These are the *large diffeomorphisms*, which we discuss in Section 2.4 below.

Now that we have shown that the Poisson bracket  $\{\mathcal{H}_\perp, \pi\}$  is invertible, one can form the Dirac bracket  $\{\cdot, \cdot\}_D$  by the standard procedure (see for instance [1, 47]). It is a standard fact that the Dirac bracket of  $\mathcal{H}_\perp$  and  $\pi$  with any observable  $f[g_{ij}, \pi^{ij}]$  is zero:

$$\{\mathcal{H}_\perp, f\}_D = 0, \quad \{\pi, f\}_D = 0. \quad (2.14)$$

This is the statement that, with respect to this Dirac bracket, any observable is *gauge invariant*; that is, invariant under small gauge transformations generated by  $\mathcal{H}_\perp$  and  $\pi$  via the Dirac bracket. Then,  $\mathcal{H}_\perp \approx 0$  and  $\pi \approx 0$  can now be elevated to strong conditions  $\mathcal{H}_\perp = 0$  and  $\pi = 0$  on phase space. Solving these strong constraints then leads to a description of the reduced phase space in terms of independent degrees of freedom as we discuss next.

### Independent degrees of freedom of the phase space on the maximal slice

We will now discuss the issue of the degrees of freedom of the phase space constrained by  $\pi = 0$  and  $\mathcal{H}_\perp = 0$  [6–8, 44, 45]. Consider a general point  $(g'_{ij}, \pi^{ij})$  in the  $\pi = 0$  slice. We consider  $g'_{ij}$  as a point on the orbit of the Weyl group, i.e.,  $g'_{ij} = \gamma^{4/(d-2)} g_{ij}^0$ , where  $\gamma^{4/(d-2)}$  denotes an element of the Weyl group and  $g_{ij}^0$  is an arbitrary reference metric that is our chosen representative of the Weyl orbit. We omit the  $\gamma$  dependence of  $g'_{ij}$  for notational convenience. The following discussion applies to all points in a given Weyl orbit.

The scalar field is Weyl invariant, and hence it is not important for the following discussion, except for the extra terms it contributes to the Lichnerowicz equation below.

To proceed further, we use the result that any metric  $g'_{ij}$  that satisfies  $R' = 2\Lambda$  asymptotically in  $\Sigma$  can be uniquely Weyl transformed to a metric  $\tilde{g}_{ij} = \chi^{4/(d-2)} g'_{ij}$  with  $\tilde{R} = 2\Lambda$  everywhere on  $\Sigma$  [44, 45].<sup>5</sup> The Weyl factor  $\chi$  has to approach 1 asymptotically since we are looking at AAdS spacetimes for which the curvature approaches  $2\Lambda$  asymptotically. The above Weyl factor arises as the unique solution of the Yamabe equation

$$D^2\chi - \frac{d-2}{4(d-1)}R'\chi + \frac{d-2}{2(d-1)}\Lambda\chi^{\frac{d+2}{d-2}} = 0.$$

Thus, for every metric  $g'_{ij}$  in the Weyl class of some reference metric  $g_{ij}^0$ , there exists a unique Weyl factor  $\chi$  which transforms it to a metric  $\tilde{g}_{ij}$  with constant curvature  $2\Lambda$ . This effectively removes the freedom to perform Weyl transformations on the metric, and reduces the configuration space of metrics  $\text{Met}$  to the space of Weyl orbits  $\text{Met}/\text{Weyl}$  where Weyl is the group of Weyl transformations. In particular, we might as well choose this constant curvature metric  $\tilde{g}_{ij}$  to be the representative of the Weyl class.

Now that we have eliminated the freedom to perform a Weyl transformation, we focus on the subspace in the  $\pi = 0$  slice of phase space where the metrics satisfy  $R = 2\Lambda$ . That is, the subspace consisting of configurations  $(\tilde{g}_{ij}, \tilde{\pi}^{ij})$  with  $\tilde{R} = 2\Lambda$  and  $\tilde{\pi} = 0$ . However, it is not yet

<sup>5</sup>We denote the scalar curvature of the metric  $g'_{ij}$  by  $R'$ , and that of  $\tilde{g}_{ij}$  by  $\tilde{R}$ .

guaranteed that every configuration in this subspace of phase space satisfies the Hamiltonian constraint  $\mathcal{H}_\perp = 0$ . To obtain such a subspace of  $\pi = 0$ , we start with a point  $(\tilde{g}_{ij}, \tilde{\pi}^{ij})$  in the  $\tilde{\pi} = 0, \tilde{R} = 2\Lambda$  subspace and Weyl transform the pair to  $g_{ij} = \psi^{4/(d-2)}\tilde{g}_{ij}, \pi^{ij} = \psi^{-4/(d-2)}\tilde{\pi}^{ij}$ . Recall that we need  $\psi \rightarrow 1$  asymptotically to preserve the condition  $R = 2\Lambda$ . Next, demanding that  $(g_{ij}, \pi^{ij})$  satisfy the Hamiltonian constraint  $\mathcal{H}_\perp \approx 0$  gives the Lichnerowicz equation for the Weyl factor  $\psi$ :

$$\begin{aligned} \tilde{D}^2\psi - \frac{d-2}{4(d-1)}(\tilde{R} - \frac{1}{2}\tilde{g}^{ij}\partial_i\phi\partial_j\phi)\psi + \frac{d-2}{4(d-1)}\frac{1}{\tilde{g}}(\tilde{\pi}^{ij}\tilde{\pi}^{kl}\tilde{g}_{ik}\tilde{g}_{jl} + \frac{1}{2}\pi_\phi^2)\psi^{\frac{2-3d}{d-2}} \\ + \frac{d-2}{4(d-1)}(2\Lambda + V(\phi))\psi^{\frac{d+2}{d-2}} = 0. \end{aligned} \quad (2.15)$$

where  $\tilde{R}$  has to be substituted by  $2\Lambda$  in the second term above. This equation can be shown to have a unique solution for  $\psi$  [6–8, 44, 45]. This implies that for every Weyl orbit in the  $\pi = 0$  subspace represented by  $(\tilde{g}_{ij}, \tilde{\pi}^{ij})$  with  $\tilde{R} = 2\Lambda, \tilde{\pi} = 0$ , there is a corresponding unique point in the  $\mathcal{H}_\perp = 0, \pi = 0$  subspace. Thus, solutions of the Hamiltonian constraint in the gauge  $\pi = 0$  are characterized by the independent degrees of freedom which are Weyl classes of metrics  $\text{Conf} = \text{Met}/\text{Weyl}$  and traceless momenta.

### The Lichnerowicz equation and its relation to the Poisson bracket $\{\mathcal{H}_\perp, \pi\}$

Suppose the starting point  $(\tilde{g}_{ij}, \tilde{\pi}^{ij}; \phi, \pi_\phi)$  with  $\tilde{R} = 2\Lambda$  also satisfies the Hamiltonian constraint. Then,  $\psi = 1$  satisfies the Lichnerowicz equation. Since the equation has a unique solution,  $\psi = 1$  is the only solution. Let us derive the linearized version of the above statement. Starting from the known solution  $\psi = 1$ , we ask if there are any nearby solutions to the Lichnerowicz equation. Writing the Weyl factor in (2.15) as  $\psi = 1 + u$  with  $u$  suitably small, and retaining only terms up to order  $u$ , we get

$$\tilde{D}^2u - \frac{1}{\tilde{g}}(\tilde{g}_{ik}\tilde{g}_{jl}\tilde{\pi}^{ij}\tilde{\pi}^{kl} + \frac{1}{2}\pi_\phi^2)u + \frac{2\Lambda + V(\phi)}{d-1}u = 0. \quad (2.16)$$

The uniqueness of the solution of the Lichnerowicz equation shows that the only solution of the above equation which goes to 0 at infinity is  $u = 0$ . This can also be seen by noting that the above differential operator is precisely the one appearing on the right hand side of the Poisson bracket  $\{\mathcal{H}_\perp, \pi\}$  (2.9), which indeed does not have zero modes that fall-off to zero at the boundary.

In the discussion after (2.9)  $u$  was interpreted as a parameter for an infinitesimal diffeomorphism rather than as a infinitesimal Weyl transformation. This shows the dual nature of the Poisson bracket  $\{\mathcal{H}_\perp, \pi\}$ : it can be either thought of as diffeomorphism of  $\pi$  or as a Weyl transformation of  $\mathcal{H}_\perp$ . The latter point of view leads to the linearized Lichnerowicz equation (2.16) with infinitesimal parameter  $u$ .

## 2.2 Gauge fixing the momentum constraints

As we saw earlier, the Poisson bracket of  $\pi$  with the momentum constraint  $\mathcal{H}_i$  is zero on the constrained subspace  $\pi \approx 0$ , and hence the spatial diffeomorphisms are not gauge fixed at all. We must choose additional gauge fixing conditions to fix these diffeomorphisms. One choice is to

pick coordinates on  $\Sigma$  which are harmonic with respect to the metric  $g_{ij}$ . That is,

$$D^2 x^i = 0, \quad i = 1, \dots, d. \quad (2.17)$$

Note that the index  $i$  is simply a label for the solutions of the Laplace equation and is not treated as a vector index. Then, the Laplacian is just the scalar Laplacian. Evaluating it in the coordinate system  $x^i$  itself, we get

$$\frac{1}{\sqrt{g}} \frac{\partial}{\partial x^j} \left( \sqrt{g} g^{jk} \frac{\partial x^i}{\partial x^k} \right) = 0 \quad \Rightarrow \quad \frac{\partial}{\partial x^j} (\sqrt{g} g^{ij}) = 0. \quad (2.18)$$

As discussed by Dirac [43], the above conditions do not have zero Poisson bracket with  $\pi$  for  $d > 2$ . Since it is desirable to have all the gauge conditions commute with each other, he proposed a slight variant of the above which indeed has zero Poisson bracket with  $\pi$ :

$$\mathcal{D}^i \equiv \frac{\partial}{\partial x^j} (g^{1/d} g^{ij}) = 0. \quad (2.19)$$

It is easy to see that this has zero Poisson bracket with  $\pi$  since  $g^{1/d} g^{ij}$  has zero Weyl weight. The condition (2.19), known in the literature as the *Dirac gauge*, applies to the constant curvature metric  $\tilde{g}_{ij}$  as well since (2.19) is conformally invariant. Note that the harmonic gauge is the same as the Dirac gauge in  $d = 2$ . Thus, choosing harmonic coordinates has all the virtues of the Dirac gauge in  $d = 2$ . This will be useful in our  $d = 2$  analysis in Section 3.

Let us check the correctness of the Dirac gauge for the momentum constraints. The Poisson bracket of  $\mathcal{H}_i$  with  $\mathcal{D}^j$  is

$$\begin{aligned} \{\mathcal{H}^i(x), \mathcal{D}^j(x')\} &= \{-2D_k \pi^{ik}, \partial_l (g^{1/d} g^{jl})\} \\ &= -2D_k \partial_l (g^{1/d} (\frac{1}{d} g^{ik} g^{jl} - \frac{1}{2} (g^{ji} g^{kl} + g^{jk} g^{il}))) \delta(x, x'). \end{aligned} \quad (2.20)$$

The Dirac gauge constraints have a non-trivial Poisson bracket with the Hamiltonian constraint as well:

$$\{\mathcal{H}_\perp(x), \mathcal{D}^j(x')\} = 2K_{ik} \partial_l (g^{1/d} (\frac{1}{d} g^{ik} g^{jl} - \frac{1}{2} (g^{ji} g^{kl} + g^{jk} g^{il}))) \delta(x, x'), \quad (2.21)$$

where  $K_{ik}$  is the extrinsic curvature that is related to the conjugate momentum as (with  $K = g^{ij} K_{ij}$ )

$$K_{ij} = \frac{1}{\sqrt{g}} (\pi_{ij} - \frac{1}{d-1} \pi), \quad \pi^{ij} = \sqrt{g} (K^{ij} - g^{ij} K). \quad (2.22)$$

For small spatial diffeomorphisms to be fixed completely, we need to show that the small diffeomorphisms generated by the Hamiltonian (2.2) do not preserve the gauge. Indeed, suppose there is a small diffeomorphism  $(\xi_\perp, \xi_i)$  that preserves the Dirac gauge. Then, it must satisfy the differential equation

$$\partial_l (g^{1/d} (2\xi_\perp K^{kl} - 2D^{(k} \xi^{l)} + \frac{2}{d} g^{kl} D_i \xi^i)) = 0, \quad (2.23)$$

Since we have previously shown that  $\xi_\perp = 0$  is the only small diffeomorphism that preserves the

$\pi = 0$  condition, we set it to zero in the above and get

$$\partial_l(g^{1/d}(-2D^{(k}\xi^l) + \frac{2}{d}g^{kl}D_i\xi^i)) = 0 . \quad (2.24)$$

If the differential operator above is invertible when acting on the space of  $\xi^i$  that fall-off fast enough to zero near the boundaries, then the only such solution would be  $\xi^i = 0$ . This would mean that the Dirac gauge would fix the small spatial diffeomorphisms completely as well. An attempt was made by Dirac [43] to invert this differential operator in a short distance expansion. However it is not clear if this method captures all the properties of the exact solution.<sup>6</sup> Next section onwards, our focus will be on  $d = 2$  in which case we can indeed show that the Dirac gauge fixes small spatial diffeomorphisms completely.

### 2.3 The reduced phase space

The gauge fixed phase space is thus obtained by solving the Hamiltonian and momentum constraints in conjunction with the maximal slicing gauge condition and  $d$  gauge conditions for the momentum constraints. This reduced phase space has the structure of a cotangent bundle  $T^*(\text{Conf}/\text{Diff})$  [7, 8, 11, 12, 48–50] where  $\text{Conf} = \text{Met}/\text{Weyl}$  is the space of conformal classes, i.e., Weyl orbits, of AAdS metrics on  $\Sigma$ , and  $\text{Diff}$  is the group of small diffeomorphisms on  $\Sigma$ . We realize the above fact explicitly in the case of  $d = 2$  in Section 3, with  $\Sigma$  being the cylinder  $\mathbf{S}^1 \times \mathbf{R}$ .

### 2.4 Large diffeomorphisms and equations for the lapse and shift

We have discussed the gauge-fixing of small diffeomorphism redundancies and shown that the maximal slicing gauge condition completely fixes the  $\xi_\perp$  component of a small diffeomorphism. We also expect small spatial diffeomorphisms to be completely gauge fixed in the Dirac gauge, and we indeed demonstrate this for  $d = 2$  in Section 3.

Recall that small diffeomorphisms fall-off fast enough to identity as one approaches the boundary. The diffeomorphisms that do not approach identity at the boundary are the *large diffeomorphisms*. In the context of AAdS $_{d+1}$  spacetimes, large diffeomorphisms are simply those which approach an element of the asymptotic AdS symmetry algebra  $\mathfrak{so}(d, 2)$  with a particular fall-off, for  $d > 2$ ; the asymptotic symmetry is enhanced to the Virasoro algebra in  $d = 2$  [9, 10]. Given a particular element of the asymptotic symmetry, there are an infinite number of diffeomorphisms which approach it at the boundary, all of them differing by small diffeomorphisms. Thus, to completely specify a large diffeomorphism, one needs give an element of the asymptotic symmetry algebra as well as a particular way of smoothly continuing the element into the interior of the spacetime.

In the Hamiltonian formulation, any spacetime diffeomorphism is implemented on  $g_{ij}$  and  $\pi^{ij}$

---

<sup>6</sup> Note that the differential operator is elliptic; it may be possible to use tools from elliptic operator theory to show that the differential operator is invertible on a suitable function space of  $\xi^i$  with appropriate fall-off conditions. The presence of asymptotic boundaries where the metric diverges presents additional complications since the elliptic operator degenerates at the boundaries. See [45] for a detailed exposition on such issues.

via Poisson bracket by the Hamiltonian (2.2):

$$H = \int_{\Sigma} d^d x (N\mathcal{H}_{\perp} + N_i\mathcal{H}^i) + \oint_{\partial\Sigma} d^{d-1}\sigma \mathcal{B} . \quad (2.25)$$

To get a unique large diffeomorphism described by  $N$  and  $N^i$  that asymptote a given element of the asymptotic symmetry algebra, we demand that  $H$  preserve the maximal slicing (2.6) and Dirac gauge conditions (2.19)

$$\{H, \pi(x)\} \approx (d-1)\sqrt{g} \left( D^2 - \frac{1}{g}(\pi^{ij}\pi_{ij} + \frac{1}{2}\pi_{\phi}^2) + \frac{2\Lambda + V(\phi)}{d-1} \right) N(x) = 0 , \quad (2.26)$$

$$\{H, \mathcal{D}^j(x)\} \approx \partial_l (g^{1/d}(2NK^{jl} - 2D^{(j}N^{l)} + \frac{2}{d}g^{jl}D_iN^i)) = 0 . \quad (2.27)$$

In this paper, we assume that there exists solutions of the above differential equations for any choice of boundary condition corresponding to any asymptotic symmetry, on physical grounds. Then, given a choice of non-trivial asymptotic boundary conditions, such a solution is unique if the above gauge conditions completely fix the small diffeomorphism redundancy. We have demonstrated this for (2.26) in Section 2.1. A similar analysis maybe possible for (2.27) as discussed in Footnote 6.

Time evolution is a large diffeomorphism corresponding to the boundary conditions  $N \sim r/\ell$  and  $N_i \sim 0$  as one approaches the boundary. We solve the above differential equations explicitly with this boundary condition for the case of 2 + 1 dimensional BTZ black hole and obtain a unique solution in Sections 4.2 - 4.4 below.

## 2.5 Gauge fixing in perturbation theory

In this subsection, we carefully consider the question of gauge fixing in perturbation theory about a pure gravity background, i.e., a classical solution in which the scalar field is zero. To have a consistent perturbation theory, one must include the perturbations in both the scalar field as well as the gravitational field. We would like the terms contributing to the background to all appear at the same order in  $\kappa$ . For this reason, we define the rescaled momentum  $P^{ij}$  by<sup>7</sup>

$$\pi^{ij} = \frac{1}{\kappa^2} P^{ij} . \quad (2.28)$$

Then, the constraints (2.3) and boundary term (2.4) become

$$\begin{aligned} \mathcal{H}_{\perp} &= \frac{1}{\kappa^2} \left( \frac{1}{\sqrt{g}}(P^{ij}P_{ij} - \frac{1}{d-1}P^2) - \sqrt{g}(R - 2\Lambda) \right) + \frac{\pi_{\phi}^2}{2\sqrt{g}} + \sqrt{g}(\frac{1}{2}g^{ij}\partial_i\phi\partial_j\phi + V(\phi)) , \\ \mathcal{H}^i &= -\frac{1}{\kappa^2} 2D_j P^{ij} + g^{ij}\pi_{\phi}\partial_j\phi , \quad \mathcal{B} = -\frac{2}{\kappa^2} N\sqrt{\sigma}k + \frac{2}{\kappa^2} r_i N_j P^{ij} . \end{aligned} \quad (2.29)$$

---

<sup>7</sup>In this paper, we consider a scalar field on the maximally sliced BTZ solution background below. Since the maximal slicing solution is time dependent, it has  $\pi^{ij}$  non-zero. This rescaling is then necessary for all terms from the background to appear at the same order in  $\kappa$ .

### 2.5.1 The perturbation expansion

As noted earlier, the scalar field appears at  $\mathcal{O}(\kappa^0)$  in the Hamiltonian. The fluctuations in the metric degrees of freedom must appear at the same order. To achieve this, let us expand the metric, momentum, lapse and shift as

$$g_{ij} = \hat{g}_{ij} + \kappa h_{ij} , \quad P^{ij} = \hat{P}^{ij} + \kappa p^{ij} , \quad N_i = \hat{N}_i + \kappa \beta_i , \quad N = \hat{N}(1 + \kappa \alpha) , \quad (2.30)$$

where the hatted quantities correspond to the background solution. It is important to note that the fluctuations in  $g$  and  $\pi$  should not change background solution. We consider fluctuations with compact support since these will not change the background solution. This can be relaxed to include fluctuations with a fast enough fall-off near the boundaries.

The details of the perturbation analysis are relegated to Appendix B. The quadratic Hamiltonian does not mix the metric and scalar fluctuations. The expression for the Hamiltonian up to  $\mathcal{O}(\kappa^0)$  is

$$H_2 = \int_{\Sigma} d^d x \left( \alpha \mathcal{C}_{\perp}(h, p) + \beta_i \mathcal{C}^i(h, p) + \mathcal{H}_{\text{grav}}(h, p) + \mathcal{H}_s(\phi, \pi_{\phi}) \right) + \text{boundary terms} , \quad (2.31)$$

where  $\mathcal{C}_{\perp}$  and  $\mathcal{C}^i$  are the linearized Hamiltonian and momentum constraints that depend only on the gravity fluctuations:

$$\begin{aligned} \mathcal{C}_{\perp} &= \hat{N} \left( 2\hat{P}^{ij} p_{ij} + 2h_{ik} \hat{P}^k{}_j \hat{P}^{ij} - h \hat{P}^{ij} \hat{P}_{ij} - \hat{g}(\hat{D}^a \hat{D}^b h_{ab} - \hat{D}^2 h - h^{ac} \hat{R}_{ac}) \right) , \\ \mathcal{C}^l &= 2\hat{D}_i p^{il} + \hat{P}^{ij} (\hat{D}_i h^l{}_j + \hat{D}_j h^l{}_i - \hat{D}^l h_{ij}) , \end{aligned} \quad (2.32)$$

and  $\mathcal{H}_{\text{grav}}(h, p)$  and  $\mathcal{H}_s(\phi, \pi_{\phi})$  are the dynamical, non-constraint, quadratic Hamiltonians for the metric and scalar degrees of freedom respectively:

$$\begin{aligned} \mathcal{H}_{\text{grav}}(h, p) &= \frac{\hat{N}}{\sqrt{\hat{g}}} \left( -\frac{1}{2} h (2\hat{P}^{ij} p_{ij} + 2h_{ik} \hat{P}^k{}_j \hat{P}^{ij}) + \frac{1}{4} (h^{ij} h_{ij} + \frac{1}{2} h^2) \hat{P}^{ij} \hat{P}_{ij} \right. \\ &\quad \left. + p^{ij} p_{ij} + 2p^{ij} h_{ik} \hat{P}^k{}_j + \hat{P}^{ij} \hat{P}^{kl} h_{ik} h_{jl} + 2\hat{P}^{ij} h_{ik} p^k{}_j \right) \\ &\quad - \hat{N} \sqrt{\hat{g}} \left( \frac{1}{4} (\frac{1}{2} h^2 - h_{ij} h^{ij}) (\hat{R} - 2\Lambda) \right. \\ &\quad \left. + \frac{1}{2} h (\hat{D}^a \hat{D}^b h_{ab} - \hat{D}^2 h - h^{ac} \hat{R}_{ac}) \right. \\ &\quad \left. + \frac{3}{4} \hat{D}^a h^{bc} \hat{D}_a h_{bc} + h^{ab} \hat{D}^2 h_{ab} - \hat{D}_b h^{bc} \hat{D}^a h_{ac} - h^{bc} \hat{D}_b \hat{D}^a h_{ac} \right. \\ &\quad \left. + h^{ab} \hat{D}_a \hat{D}_b h + \hat{D}_a h^{ac} \hat{D}_c h - \frac{1}{2} \hat{D}_b h^{ac} \hat{D}_a h^b{}_c - \frac{1}{4} \hat{D}^a h \hat{D}_a h \right. \\ &\quad \left. - h^{ac} \hat{D}_b \hat{D}_a h^b{}_c + h^{ae} h_e{}^c \hat{R}_{ac} \right) \\ &\quad - (\hat{N}^l p^{ij} - \hat{N}_k h^{kl} \hat{P}^{ij}) C_{ijl} , \end{aligned} \quad (2.33)$$

$$\mathcal{H}_s(\phi, \pi_{\phi}) = \hat{N} \left( \frac{1}{2\sqrt{\hat{g}}} \pi_{\phi}^2 + \sqrt{\hat{g}} (\frac{1}{2} \hat{g}^{ij} \partial_i \phi \partial_j \phi + V(\phi)) \right) - \hat{N}_i \hat{g}^{ij} \pi_{\phi} \partial_j \phi . \quad (2.34)$$

Note that the gravity fluctuations  $h_{ij}$ ,  $p^{ij}$  and the scalar fluctuations  $\phi$ ,  $\pi_{\phi}$  are decoupled at this order in perturbation theory. Hence, we can consider the scalar field as a probe on the background geometry without turning on the metric fluctuations. In  $d = 2$ , since there are no

local fluctuating gravitational degrees of freedom, the quadratic Hamiltonian  $H_2$  (2.31) involves only the gauge invariant scalar perturbations.

### 2.5.2 Gauge fixing the linearized constraints

The fluctuations  $\alpha$  and  $\beta_i$  in the lapse and shift are Lagrange multipliers, and their equations of motion give the linearized constraints  $\mathcal{C}_\perp = \mathcal{C}^i = 0$  (2.32) on the fluctuations. It is important to note that the constraints only involve the gravity fluctuations and not the scalar fields. The issue of gauge fixing was discussed non-perturbatively in  $\kappa$  in the previous subsections and the results of that discussion also hold order by order in  $\kappa$ . Thus, if we can manage to fix small diffeomorphism redundancy in pure gravity non-perturbatively by a suitable choice of gauge conditions, then it will be fixed at the linearized order as well. In Section 3, we demonstrate this for pure gravity in  $d = 2$  in the maximal slicing and Dirac gauge when the spatial hypersurface is a cylinder  $\Sigma = \mathbf{R} \times \mathbf{S}^1$ .

For completeness, we give the linearized version of the maximal slicing and Dirac gauge conditions

$$g_{ij}\pi^{ij} = 0, \quad \partial_i(g^{1/d}g^{ij}) = 0. \quad (2.35)$$

Expanding the above to  $\mathcal{O}(\kappa)$ , we get

$$\hat{g}_{ij}\hat{P}^{ij} + \kappa(\hat{g}_{ij}p^{ij} + h_{ij}\hat{P}^{ij}) = 0, \quad \partial_i(\hat{g}^{1/d}\hat{g}^{ij}) + \kappa\partial_i(\hat{g}^{1/d}(\frac{1}{d}h\hat{g}^{ij} - h^{ij})) = 0. \quad (2.36)$$

The leading order gauge conditions  $\hat{g}_{ij}\hat{P}^{ij} = 0$ ,  $\partial_i(\hat{g}^{1/d}\hat{g}^{ij}) = 0$  are satisfied by the background fields. Thus, the gauge fixing conditions at  $\mathcal{O}(\kappa)$  are on the trace part  $p = \hat{g}_{ij}p^{ij}$  and the traceless part  $\bar{h}_{ij} = h_{ij} - \frac{1}{d}\hat{g}_{ij}h$  of  $h^{ij}$ :

$$p + \bar{h}_{ij}\hat{P}^{ij} = 0, \quad \partial_i(\hat{g}^{1/d}\bar{h}^{ij}) = 0. \quad (2.37)$$

Note that only the traceless part of  $h_{ij}$  appears in the first constraint since  $\hat{P}^{ij}$  is traceless. These linearized gauge conditions can be used to independently study gauge fixing for the linearized constraints by Dirac's method.

### 2.5.3 Diffeomorphism invariance of the scalar field

Note that the above constraints do not involve the canonical variables of the scalar field, and hence the scalar field degrees of freedom are gauge invariant under these  $\mathcal{O}(\kappa)$  diffeomorphisms. Since we have also fixed the gauge for the background diffeomorphisms completely, the scalar field is truly gauge invariant to this order  $\mathcal{O}(\kappa^0)$  in perturbation theory.

## 3 Hamiltonian formulation in 2 + 1 dimensional AAdS spacetimes

We are interested in describing the 2 + 1 dimensional BTZ black hole in the maximal slicing gauge. Hence, we consider the maximal slicing gauge for  $d = 2$ , and choose our manifold  $\Sigma$  to be the cylinder  $\mathbf{R} \times \mathbf{S}^1$  which corresponds to the wormhole slices of the fully extended BTZ black hole. Through the gauge fixing procedure, we recover the well-known fact that there are

no propagating degrees of freedom in Einstein gravity in  $2 + 1$  dimensions. The dimension of the reduced phase space is finite, and equal to two in the case of  $\Sigma$  being the cylinder.

The gauge fixing procedure for gravity in  $d = 2$  for compact  $\Sigma$  (which does not include the AAdS<sub>3</sub> case of the current paper) has been studied by many authors [11, 12]. Also see the recent paper [13] for general results on solving the constraint equations in the AAdS<sub>3</sub> case.

### 3.1 The maximal slicing gauge condition in $d = 2$

We continue to work with the  $\pi = 0$  gauge fixing condition for the Hamiltonian constraint. The  $\pi = 0$  slice intersects the  $\mathcal{H}_\perp = 0$  slice transversally since the operator on the right hand side of  $\{\mathcal{H}_\perp, \pi\}$  in (2.9) is invertible for  $d = 2$  as well. Decomposing the spatial metric and momentum as  $g_{ij} = e^{2\lambda}\tilde{g}_{ij}$ ,  $\pi^{ij} = e^{-2\lambda}\tilde{\pi}^{ij}$  and plugging it into the Hamiltonian constraint, we get

$$\tilde{D}^2\lambda = \frac{\tilde{R} - \frac{1}{2}\tilde{g}^{ij}\partial_i\phi\partial_j\phi}{2} - \frac{\tilde{g}_{ik}\tilde{g}_{jl}\tilde{\pi}^{ij}\tilde{\pi}^{kl} + \frac{1}{2}\pi_\phi^2}{2\tilde{g}}e^{-2\lambda} - \frac{2\Lambda + V(\phi)}{2}e^{2\lambda}. \quad (3.1)$$

We can take  $\tilde{g}_{ij}$  in the Lichnerowicz equation to satisfy  $\tilde{R} = 2\Lambda$ , since is always possible to uniquely Weyl transform any metric  $g'_{ij}$  to a metric  $\tilde{g}_{ij} = e^{2\varphi}g'_{ij}$  of constant negative scalar curvature  $\tilde{R} = 2\Lambda$ . This is because the  $d = 2$  Yamabe equation  $D'^2\varphi = \frac{R'}{2} - \Lambda e^{2\varphi}$  has a unique solution for a given  $g'_{ij}$ . In Appendix A we review the argument that shows that the Lichnerowicz equation (3.1) has a unique solution provided the scalar field potential satisfies  $V(\phi) \leq 0$ .

### 3.2 Spatial harmonic gauge for the momentum constraints

Recall that we specialize to  $\Sigma$  being a cylinder  $\mathbf{R} \times \mathbf{S}^1$  which describes a wormhole connecting two asymptotic AdS regions. Recall that  $\tilde{g}_{ij}$  has constant negative curvature  $2\Lambda$ . It is well known that any constant negative curvature metric on  $\mathbf{R} \times \mathbf{S}^1$  which approaches the AdS metric asymptotically can be put in the form

$$\tilde{g}_{ij}dx^i dx^j = \frac{\ell^2}{\cos^2\theta}(d\theta^2 + m d\varphi^2), \quad \theta \in \left[-\frac{\pi}{2}, \frac{\pi}{2}\right], \quad \varphi \in [0, 2\pi), \quad (3.2)$$

where  $m$  is a positive real number.<sup>8</sup> It is easy to see that the metric  $\tilde{g}_{ij}$  satisfies the harmonic gauge condition in these coordinates:

$$\partial_i(\sqrt{\tilde{g}}\tilde{g}^{ij}) = 0. \quad (3.3)$$

---

<sup>8</sup>This can be reasoned as follows (see [51], and the recent work [13] for a nice review). Any non-compact two dimensional surface with constant negative curvature can be obtained as the quotient of the hyperbolic plane by a particular Fuchsian group, i.e., a discrete subgroup of  $\text{PSL}(2, \mathbf{R})$ . In particular, the non-compact cylinder with constant negative curvature  $-2$  is obtained by considering the cyclic group generated by a hyperbolic transformation with length  $2\pi\sqrt{m}$  for some positive number  $m$ . By conjugation by an appropriate  $\text{PSL}(2, \mathbf{R})$  element, this hyperbolic transformation can be taken to be the Möbius transformation

$$T = \begin{pmatrix} e^{\pi\sqrt{m}} & 0 \\ 0 & e^{-\pi\sqrt{m}} \end{pmatrix},$$

and the corresponding Fuchsian group is the cyclic group  $\langle T \rangle$  generated by  $T$ . The fundamental domain for this action in the hyperbolic upper-half plane is the strip  $1 \leq |z| < e^{2\pi\sqrt{m}}$ . Under the identification by the cyclic



Further, as noted in Section 2.2, this is the same as the Dirac gauge condition in  $d = 2$  and is conformally invariant. Thus, the above argument shows that choosing the coordinate system  $(\theta, \varphi)$  completely fixes the spatially harmonic gauge / Dirac gauge.

In the next subsection, we describe the solution of the Hamiltonian and momentum constraint equations in the  $\pi = 0$ , spatially harmonic gauge. Before doing that, we present several alternate coordinate systems on the cylinder which might be useful in different contexts.

**Alternate coordinate systems** A coordinate system in which the non-compactness of  $\mathbf{R} \times \mathbf{S}^1$  is more manifest is obtained by setting  $\tan \theta = \sinh u$  so that the metric becomes

$$d\tilde{s}^2 = \tilde{g}_{ij} dx^i dx^j = \ell^2 (du^2 + m \cosh^2 u d\varphi^2), \quad u \in (-\infty, \infty), \quad \varphi \in [0, 2\pi), \quad (3.4)$$

A more suggestive coordinate system, which covers only half the cylinder  $u > 0$  or  $u \leq 0$ , is the areal radial coordinate,  $r = \ell\sqrt{m} \cosh u$ , in which the metric becomes

$$d\tilde{s}^2 = \frac{dr^2}{\frac{r^2}{\ell^2} - m} + r^2 d\varphi^2, \quad (3.5)$$

which we recognize to be the exterior metric on a constant time slice of the BTZ black hole [14, 15]. Starting from here, one can obtain wormhole-like coordinates which cover the entire cylinder [52, 53] by writing  $w^2 = r^2 - \ell^2 m = \ell^2 m \sinh^2 u$ :

$$d\tilde{s}^2 = \ell^2 \left( \frac{dw^2}{w^2 + \ell^2 m} + (w^2 + \ell^2 m) d\varphi^2 \right). \quad (3.6)$$

### 3.3 Solving the constraint equations

Recall that the Hamiltonian constraint in the  $\pi = 0$  gauge becomes the Lichnerowicz equation (3.1) for the Weyl factor  $e^{2\lambda}$ :

$$\tilde{D}^2 \lambda = \frac{\tilde{R} - \frac{1}{2} \tilde{g}^{ij} \partial_i \phi \partial_j \phi}{2} - \frac{\tilde{g}_{ik} \tilde{g}_{jl} \tilde{\pi}^{ij} \tilde{\pi}^{kl} + \frac{1}{2} \pi_\phi^2}{2\tilde{g}} e^{-2\lambda} - \frac{2\Lambda + V(\phi)}{2} e^{2\lambda}, \quad (3.7)$$

where  $\tilde{R} = 2\Lambda$ . As discussed in Section 2.1, solving the Hamiltonian constraint in the  $\pi = 0$  gauge reduces the metric degrees of freedom to the space of Weyl orbits  $\text{Conf} = \text{Met}/\text{Weyl}$ . The further quotient by the spatial diffeomorphisms is equivalent to fixing the spatial harmonic gauge discussed above. The metric  $\tilde{g}_{ij}$  assumes a simple form (3.2) in the spatially harmonic gauge, with one free parameter  $m > 0$ . Thus, after gauge fixing the spatial diffeomorphisms by choosing the spatial harmonic gauge, the space of conformal classes of metrics modulo spatial diffeomorphisms is  $\text{Conf}/\text{Diff} = \mathbf{R}_+$ .

---

group, (1) the two semi-circles are mapped to each other, (2) the arcs  $-e^{2\pi\sqrt{m}} < x \leq -1$  and  $1 \leq x < e^{2\pi\sqrt{m}}$  on the real line become the boundary circles, and (3) the segment  $1 \leq y < e^{2\pi\sqrt{m}}$  on the positive  $y$  axis becomes the closed geodesic of length  $2\pi\sqrt{m}$  as measured by the hyperbolic metric  $y^{-2}(dx^2 + dy^2)$ .

The induced metric (3.2) is obtained by first performing the coordinate transformation  $x = r \sin \theta$ ,  $y = r \cos \theta$ , with  $\theta \in [-\frac{\pi}{2}, \frac{\pi}{2}]$  so that we get  $y^{-2}(dx^2 + dy^2) = \cos^{-2} \theta (d\theta^2 + r^{-2} dr^2)$ . Next, we write  $r = e^{\sqrt{m}\varphi}$  so that the metric becomes  $\cos^{-2} \theta (d\theta^2 + m d\varphi^2)$ . The identification of  $r = 1$  and  $r = e^{2\pi\sqrt{m}}$  implies that  $\varphi$  is an angular coordinate with period  $2\pi$ .

We next obtain simple expressions for  $\tilde{\pi}^{ij}$  as well, by solving the momentum constraints. It suffices to solve the momentum constraints  $-2\tilde{D}_i\tilde{\pi}^{ij} + \tilde{g}^{ij}\pi_\phi\partial_i\phi = 0$  for  $(\tilde{g}_{ij}, \tilde{\pi}^{ij}; \phi, \pi_\phi)$  since it is equivalent to Weyl rescaled  $(g_{ij}, \pi^{ij}; \phi, \pi_\phi)$  satisfying *their* momentum constraints  $-2D_i\pi^{ij} + g^{ij}\pi_\phi\partial_i\phi = 0$ . It is easier to work with the extrinsic curvature

$$K^{ij} = g^{-1/2}(\pi^{ij} - g^{ij}\pi) , \quad (3.8)$$

as opposed to the tensor density  $\pi^{ij}$ , and the scalar  $K_\phi = g^{-1/2}\pi_\phi$  instead of the density  $\pi_\phi$ . The momentum constraints in terms of  $K^{ij}$  and  $K_\phi$  are

$$\mathcal{H}^j = -2D_iK^{ij} + g^{ij}K_\phi\partial_i\phi = 0 . \quad (3.9)$$

**Pure gravity** We describe the solutions of the constraint equations for pure gravity without the scalar field, and outline the procedure for the case with scalar fields. The momentum constraints  $\mathcal{H}^\theta$  and  $\mathcal{H}^\varphi$  are given by

$$\begin{aligned} -\frac{1}{2}\mathcal{H}^\theta : \quad & \tilde{D}_\theta\tilde{K}^{\theta\theta} + \tilde{D}_\varphi\tilde{K}^{\varphi\theta} = -m\partial_\theta\tilde{K}^{\varphi\varphi} - 4m\tan\theta\tilde{K}^{\varphi\varphi} + \partial_\varphi\tilde{K}^{\varphi\theta} , \\ -\frac{1}{2}\mathcal{H}^\varphi : \quad & \tilde{D}_\theta\tilde{K}^{\theta\varphi} + \tilde{D}_\varphi\tilde{K}^{\varphi\varphi} = \partial_\theta\tilde{K}^{\theta\varphi} + \partial_\varphi\tilde{K}^{\varphi\varphi} + 4\tan\theta\tilde{K}^{\theta\varphi} , \end{aligned} \quad (3.10)$$

where we have eliminated  $\tilde{K}^{\theta\theta}$  using the maximal slicing gauge condition  $\tilde{g}_{ij}\tilde{K}^{ij} = 0$ :

$$\frac{\ell^2}{\cos^2\theta}(\tilde{K}^{\theta\theta} + m\tilde{K}^{\varphi\varphi}) = 0 . \quad (3.11)$$

Writing everything in terms of  $\tilde{K}_{ij}$ , we get the simple coupled equations

$$\partial_\theta\tilde{K}_{\theta\varphi} + \frac{1}{m}\partial_\varphi\tilde{K}_{\varphi\varphi} = 0 , \quad \partial_\varphi\tilde{K}_{\theta\varphi} - \partial_\theta\tilde{K}_{\varphi\varphi} = 0 , \quad (3.12)$$

which can be rewritten as decoupled second order equations for each of  $\tilde{K}_{\theta\varphi}$  and  $\tilde{K}_{\varphi\varphi}$ :

$$\left(\partial_\theta^2 + \frac{1}{m}\partial_\varphi^2\right)\tilde{K}_{\varphi\varphi} = 0 , \quad \left(\partial_\theta^2 + \frac{1}{m}\partial_\varphi^2\right)\tilde{K}_{\theta\varphi} = 0 . \quad (3.13)$$

The differential operator above is simply the scalar Laplacian for the metric (3.2),  $\tilde{D}^2 = \frac{1}{\ell^2}(\partial_\theta^2 + \frac{1}{m}\partial_\varphi^2)$ . We now have to impose appropriate boundary conditions on  $\tilde{K}_{ij}$ . Requiring  $\tilde{K}_{ij} = 0$  for all  $i, j$  at the boundaries  $\theta = \pm\frac{\pi}{2}$  is too strong: a solution of the Laplace equation which is zero at the boundaries is zero everywhere. To mimic AdS<sub>3</sub> as much as possible, we can set the off-diagonal part  $\tilde{K}_{\theta\varphi} = 0$  at both boundaries  $\theta = \pm\frac{\pi}{2}$ . Then, the unique solution to the Laplace equation  $\tilde{D}^2\tilde{K}_{\theta\varphi} = 0$  is  $\tilde{K}_{\theta\varphi} = 0$  everywhere. The equations (3.12) then imply that the unique solution for  $\tilde{K}_{\varphi\varphi}$  is a constant:

$$\tilde{K}_{\varphi\varphi} = c . \quad (3.14)$$

Thus, the solution for the momentum constraints  $\tilde{D}_i \tilde{K}^{ij} = 0$  in the pure gravity case in the maximal slicing and spatially harmonic gauge is

$$\tilde{K}_{\theta\theta} = -\frac{c}{m}, \quad \tilde{K}_{\varphi\varphi} = c, \quad \tilde{K}_{\theta\varphi} = 0. \quad (3.15)$$

The result of solving the momentum constraints is that there is one real number that specifies the momenta in the reduced phase space. The pair  $(m, c)$  can be thought of as coordinates on the reduced phase space which is the cotangent bundle  $T^*(\text{Conf}/\text{Diff}) = T^*\mathbf{R}_+$ .

Plugging in the expressions (3.15) into the Lichnerowicz equation (3.7) (without the scalar field contributions), we get

$$\tilde{D}^2 \lambda = -\frac{1}{\ell^2} - \frac{c^2 \cos^4 \theta}{m^2 \ell^4} e^{-2\lambda} + \frac{1}{\ell^2} e^{2\lambda}. \quad (3.16)$$

Since the above equation can be consistently truncated to the space of  $\lambda$  that are independent of the  $\varphi$  coordinate, and the solution to the equation is unique provided  $\lambda \rightarrow 0$  at the boundary, it is clear the unique solution  $\lambda$  is independent of  $\varphi$ .

**Gravity coupled to matter fields** The momentum constraints for the situation with a scalar field, or any other matter field or source, can be solved analogously after including the appropriate contributions to the right hand sides given in the Hamiltonian (2.2). For a scalar field, the requirement that  $V(\phi) \leq 0$  is required for the corresponding Lichnerowicz equation to have a unique solution. In this case, the reduced phase space consists of the scalar degrees of freedom  $(\phi, \pi_\phi)$  and  $(m, c)$  from the gravity sector.

In summary, we have shown that the small diffeomorphism invariance can be completely gauge fixed in the AAdS<sub>3</sub> case with two AAdS boundaries. This was done by choosing the maximal slicing, spatially harmonic gauge conditions for the Hamiltonian and momentum constraints respectively. The degrees of freedom that remain after gauge fixing in the pure gravity case are the variables  $m$  and  $c$  which are gauge invariant.

In the next section, we use a different spatial coordinate system which can be related to the spatially harmonic coordinates by a smooth diffeomorphism, and solve Einstein's equations explicitly in the maximal slicing gauge. We obtain an explicit solution for the Hamiltonian equations of motion which turns out to be a maximally sliced foliation of the fully extended, non-rotating BTZ black hole.

## 4 The BTZ black hole in the maximal slicing gauge

In this section, we solve the Einstein equations in the maximal slicing gauge  $\pi = 0$  in 2 + 1 dimensions with two asymptotically AdS boundaries. This solution turns out to be the fully extended BTZ black hole in the foliation with maximal slices. The maximally sliced foliation has the following properties: 1) the leaves or slices of the foliation are maximal (renormalized) volume surfaces, 2) the slices smoothly cut across the black hole horizons and stretch between the two asymptotic boundaries, and 3) the foliation does not include the singularities of the BTZ solution. These properties of the maximal slicing foliation were first observed in the 3 + 1

dimensional asymptotically flat Schwarzschild black hole [54, 55]. In Appendix D, we obtain the same maximal slicing solution by a variational principle using the property that maximal slices maximize the spatial volume.

We choose to work with the areal radial coordinate  $r$  and the angular coordinate  $\varphi$  on a given spatial slice. The maximal slicing foliation in areal radial coordinates requires two coordinate charts, the left and right ‘areal’ charts, to cover the region between the two asymptotic boundaries. Each chart is connected to only one of the two boundaries. The charts are combined smoothly by defining a new ‘wormhole’ coordinate  $x$  which exists globally and reduces to the areal radial coordinate in each chart.

We now summarize the construction of the maximal slicing foliation steps in the following subsections. More details and calculations can be found in Appendix C.

#### 4.1 A review of the BTZ black hole solution

The BTZ black hole metric is given by

$$-f(r)dt^2 + f(r)^{-1}dr^2 + r^2d\varphi^2, \quad f(r) = \frac{r^2}{\ell^2} - 8G_N M, \quad (4.1)$$

where  $\varphi$  is an angular coordinate with range  $[0, 2\pi)$ ,  $M$  is the mass of the black hole, and  $\ell$  is the AdS<sub>3</sub> radius which is related to the cosmological constant as  $\ell^2 = -1/\Lambda$ . The horizon is at  $r = r_h \equiv \ell\sqrt{8G_N M}$ . For convenience, we give a separate symbol for the surface gravity  $\eta = r_h/\ell^2 = \sqrt{8G_N M}/\ell$  so that the temperature of the black hole is  $\eta/2\pi$  and  $\beta = 2\pi/\eta = 2\pi\ell^2/r_h = 2\pi\ell/\sqrt{8G_N M}$ .

**Units** In the current and subsequent sections, we restore Newton’s constant  $G_N$ . This is in contrast with the previous Sections 2 and 3 where we set  $16\pi G_N = 1$ .

#### Kruskal-Szekeres coordinates and the fully extended two-sided BTZ spacetime

The metric (4.1) has a coordinate singularity at  $r = r_h$  and is valid for the range of coordinates  $-\infty < t < \infty$ ,  $r > r_h$ ,  $0 \leq \varphi < 2\pi$ . We designate this as Region I of the BTZ black hole spacetime. To go to values of  $r$  below  $r_h$  while avoiding the coordinate singularity, we can use Kruskal-Szekeres coordinates. Define the tortoise coordinate  $r_*$  in Region I with  $r > r_h$ :

$$r_* = \frac{1}{2\eta} \log \frac{r - r_h}{r + r_h}, \quad r = -r_h \coth \eta r_*. \quad (4.2)$$

The horizon  $r = r_h$  is at  $r_* = -\infty$ , and the boundary  $r = \infty$  is at  $r_* = 0$ . The null event horizon has two parts: the future and past horizons which are reached in the limits  $r_* \rightarrow -\infty$  and  $t \rightarrow \pm\infty$  respectively. The Kruskal-Szekeres coordinates are defined as

$$\text{Region I: } U = -\eta^{-1} \left( \frac{r - r_h}{r + r_h} \right)^{1/2} e^{-\eta t}, \quad V = \eta^{-1} \left( \frac{r - r_h}{r + r_h} \right)^{1/2} e^{\eta t}. \quad (4.3)$$

The metric (4.1) in terms of the null Kruskal coordinates  $U, V$  is

$$ds^2 = -4\frac{r_h^2}{\ell^2} \frac{dUdV}{(1+\eta^2UV)^2} + r_h^2 \left( \frac{1-\eta^2UV}{1+\eta^2UV} \right)^2 d\varphi^2. \quad (4.4)$$

The coordinate range for Region I  $-\infty < t < \infty$ ,  $r > r_h$ ,  $0 \leq \varphi < 2\pi$  maps to  $U < 0$ ,  $V > 0$ ,  $0 \leq \varphi < 2\pi$ . The future and past horizons are characterized by  $U = 0$  and  $V = 0$  respectively. The metric (4.4) can be continued past the horizons  $UV = 0$  to the other ranges of  $U$  and  $V$ . In total, we have four regions in the maximally BTZ extended spacetime:

1. Region I:  $U < 0$ ,  $V > 0$
2. Region F:  $U > 0$ ,  $V > 0$
3. Region II:  $U > 0$ ,  $V < 0$
4. Region P:  $U < 0$ ,  $V < 0$

These regions are shown in the Kruskal diagram in Figure 1.

Each of the Regions above have their own BTZ-type coordinates which can be mapped to the Kruskal-Szekeres coordinates in their appropriate ranges. For instance, in Region F, the black hole metric takes the same form as (4.1), but with  $r < r_h$ , and another ‘time’ coordinate  $t_F$  with range  $-\infty < t_F < \infty$ :

$$\text{Region F : } ds^2 = -f(r)dt_F^2 + f(r)^{-1}dr^2 + r^2d\varphi^2. \quad (4.5)$$

Since  $r < r_h$  in Region F,  $t_F$  actually works like a spatial coordinate. The Kruskal coordinates are related to these as

$$\text{Region F : } U = \eta^{-1} \left( \frac{r_h - r}{r_h + r} \right)^{1/2} e^{-\eta t_F}, \quad V = \eta^{-1} \left( \frac{r_h - r}{r_h + r} \right)^{1/2} e^{\eta t_F}. \quad (4.6)$$

Note the difference in signs on the right hand sides of (4.6) and (4.3).

We use one radial coordinate  $\tilde{r}$  to cover both Regions II and P with  $\tilde{r} > r_h$  in Region II and  $\tilde{r} < r_h$  in Region P. The time coordinate in Regions II and P are  $\tilde{t}$  and  $t_P$  respectively. We choose the time coordinate  $\tilde{t}$  in Region II to run in the opposite sense compared to the coordinate  $t$  in Region I. With this convention, the slice  $t = \tilde{t} = \text{constant}$  slices are constant Killing time slices of the fully extended BTZ black hole.

The black hole metric has the same form as in (4.1) but in terms of the coordinates  $(\tilde{r}, \tilde{t})$  in Region II and  $(\tilde{r}, t_P)$  in Region P:

$$\begin{aligned} \text{Region II : } ds^2 &= -f(\tilde{r})d\tilde{t}^2 + f(\tilde{r})^{-1}d\tilde{r}^2 + \tilde{r}^2d\varphi^2, \quad \tilde{r} > r_h, \\ \text{Region P : } ds^2 &= -f(\tilde{r})dt_P^2 + f(\tilde{r})^{-1}d\tilde{r}^2 + \tilde{r}^2d\varphi^2, \quad \tilde{r} < r_h. \end{aligned} \quad (4.7)$$

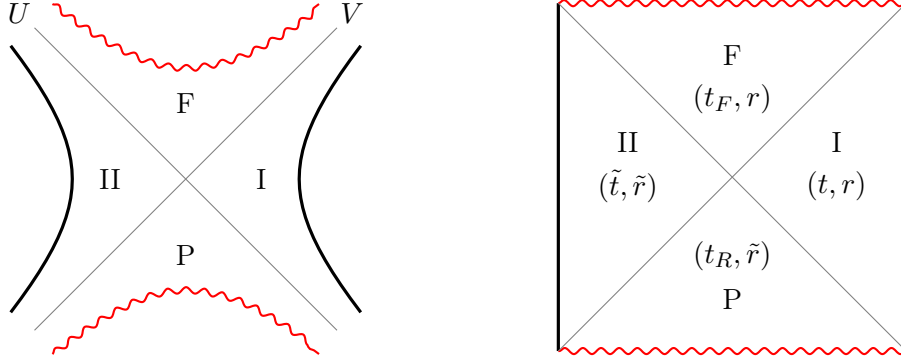


Figure 1: The four regions of the maximally extended BTZ black hole shown in the Kruskal and Penrose diagrams. The local BTZ-type coordinates in each Region are shown in the Penrose diagram, with  $r > r_h$  in Region I,  $r < r_h$  in Region F,  $\tilde{r} > r_h$  in Region II and  $\tilde{r} < r_h$  in Region P.

The Kruskal coordinates in Regions II and P are related to the local coordinates as

$$\begin{aligned}
 \text{Region II : } U &= \eta^{-1} \left( \frac{\tilde{r} - r_h}{\tilde{r} + r_h} \right)^{1/2} e^{-\eta \tilde{t}}, & V &= -\eta^{-1} \left( \frac{\tilde{r} - r_h}{\tilde{r} + r_h} \right)^{1/2} e^{\eta \tilde{t}}, \\
 \text{Region P : } U &= -\eta^{-1} \left( \frac{r_h - \tilde{r}}{r_h + \tilde{r}} \right)^{1/2} e^{-\eta t_P}, & V &= -\eta^{-1} \left( \frac{r_h - \tilde{r}}{r_h + \tilde{r}} \right)^{1/2} e^{\eta t_P}.
 \end{aligned} \tag{4.8}$$

We also define time and space Kruskal coordinates  $(\tau, \chi)$  as

$$\tau = \eta(V + U)/2, \quad \chi = \eta(V - U)/2, \quad \eta U = \tau - \chi, \quad \eta V = \tau + \chi. \tag{4.9}$$

**Penrose coordinates** We also consider Penrose coordinates  $p, q \in [-\pi/2, \pi/2]$  for the conformal compactification of the fully extended BTZ black hole. These are defined by

$$V = \eta^{-1} \tan \left( \frac{p + q}{2} \right), \quad U = -\eta^{-1} \tan \left( \frac{p - q}{2} \right), \tag{4.10}$$

or equivalently

$$p = \arctan(\eta V) + \arctan(-\eta U), \quad q = \arctan(\eta V) - \arctan(-\eta U). \tag{4.11}$$

The Penrose diagram of the BTZ black hole is given in Figure 1.

## 4.2 Solving Einstein's equations in the maximal slicing gauge using the areal radial coordinate

This part closely follows [55] who maximally sliced the Schwarzschild black hole in asymptotically flat spacetime in  $3 + 1$  dimensions.<sup>9</sup> We begin with the ADM form of the slicing in  $2 + 1$

<sup>9</sup>See also the textbook [56] for a detailed discussion.

dimensions:

$$\begin{aligned} ds^2 &= - \left( \alpha(r, \bar{t})^2 - \frac{\beta(r, \bar{t})^2}{A(r, \bar{t})} \right) d\bar{t}^2 + 2\beta(r, \bar{t})d\bar{t}dr + A(r, \bar{t})dr^2 + r^2d\varphi^2 \\ &= -\alpha(r, \bar{t})^2 d\bar{t}^2 + A(r, \bar{t}) \left( dr + \frac{\beta(r, \bar{t})}{A(r, \bar{t})} d\bar{t} \right)^2 + r^2 d\varphi^2. \end{aligned} \quad (4.12)$$

Note that the above ansatz does not have a  $d\bar{t}d\varphi$  component – this implies that rotating solutions are not included. The time  $\bar{t}$  can be identified with the formula for time presented in [57], where it was shown that the notion of time derived from the Einstein-Hamilton-Jacobi equation in terms of the configuration space data precisely matches with the time in ADM decomposition of the spacetime metric.

The spatial coordinate  $r$  is the areal radial coordinate since it measures the ‘area’ (in the present case, the circumference) of the constant  $r$  spatial surface. The coordinate system  $(r, \varphi)$  is different from the harmonic coordinate system  $(\theta, \varphi)$  used in the previous section. However, it is always possible to smoothly transform between the two by comparing the spatial metric in the two coordinate systems.<sup>10</sup> Plugging in the ansatz (4.12) into the Hamiltonian and radial momentum constraints, and the maximal slicing gauge condition, we get the following non-trivial equations:<sup>11</sup>

$$\text{Hamiltonian constraint } \mathcal{H}_\perp : \quad r\partial_r \log A - 2\Lambda r^2 A - 2\frac{\beta^2}{A\alpha^2} = 0, \quad (4.13a)$$

$$\text{Momentum constraint } \mathcal{H}^r : \quad \partial_r \log \left[ \frac{r\beta}{A\alpha} \right] = 0, \quad (4.13b)$$

$$K = 0 : \quad \partial_{\bar{t}} A - \beta\partial_r \log \left( \frac{r^2\beta^2}{A} \right) = 0. \quad (4.13c)$$

The asymptotic AdS boundary is obtained by taking  $r \rightarrow \infty$ . We impose the boundary condition  $\alpha \sim cr/\ell$  for some positive constant  $c$  on the lapse. We analyze the equations (4.13) with the above boundary condition in detail in Appendix C. Let us look at the solution for the metric component  $g_{rr} = A(r)$  for a moment:

$$A(r) = \left( \frac{r^2}{\ell^2} - 8G_N M + \frac{T(\bar{t})^2}{r^2} \right)^{-1}. \quad (4.14)$$

where  $M$  is a constant by virtue of the Einstein equations and is identified with the ADM mass of the BTZ solution, and  $T(\bar{t})$  is a known function of  $\bar{t}$  which we describe below (see equation (4.20)). It is immediately clear that the above component has coordinate singularities at the

<sup>10</sup>The spatial metric in the areal radial coordinate and in the harmonic coordinates is

$$ds^2 = A(r)dr^2 + r^2d\varphi^2 = e^{2\lambda(\theta; m, c)} \frac{\ell^2}{\cos^2 \theta} (d\theta^2 + md\varphi^2),$$

where  $\lambda(\theta; m, c)$  is the unique solution of the Lichnerowicz equation (3.7) for a given  $m$  and  $c$  which are coordinates on the reduced phase space. The coordinate transformation is then

$$r = e^{\lambda(\theta)} \frac{\ell\sqrt{m}}{\cos \theta}, \quad \frac{dr}{d\theta} = \ell\sqrt{m} \frac{d}{d\theta} (e^\lambda \sec \theta).$$

<sup>11</sup>We also need the equation  $\dot{K} = 0$  to ensure that maximal slicing is preserved at all times. However, it turns

positive roots  $r = R_{\pm}$  of the equation

$$r^4 - 8G_N M \ell^2 r^2 + \ell^2 T(\bar{t})^2 = 0, \quad (4.15)$$

given by

$$R_{\pm}(T) = \ell \sqrt{4G_N M} \left[ 1 \pm \sqrt{1 - \left( \frac{T(\bar{t})}{4G_N M \ell} \right)^2} \right]^{1/2}. \quad (4.16)$$

The radial coordinate  $r$  is identified with that of the BTZ black hole (4.1) in region I, so that one approaches the right boundary as  $r \rightarrow \infty$ . It is easy to see that  $R_{\pm} < r_h = \ell \sqrt{8G_N M}$ , and hence the above solution extends into Region F as well. However, due to the coordinate singularity at  $r = R_+$ , the chart cannot extend for  $r < R_+$ . This is why we need to describe the rest of the maximal slice that extends into Region II by a second copy of the maximal slicing solution.

We now present the two copies of the maximal slicing solution that describe the parts of the maximal slices connected to the right and left asymptotic boundaries. We call these the ‘right areal chart’ and the ‘left areal chart’. These slices are in the upper half of the Kruskal diagram that contains the  $t > 0$  part of Region I, the entire Region F, and the  $\tilde{t} < 0$  part of Region II.

**The right areal chart** The solution for  $R_+(T) < r < \infty$  is

$$ds^2 = -\alpha(r, \bar{t})^2 d\bar{t}^2 + A(r, \bar{t}) \left( dr + \frac{\alpha(r, \bar{t}) T(\bar{t})}{r} d\bar{t} \right)^2 + r^2 d\varphi^2, \quad (4.17a)$$

$$A(r, \bar{t}) = \left( \frac{r^2}{\ell^2} - 8G_N M + \frac{T(\bar{t})^2}{r^2} \right)^{-1}, \quad (4.17b)$$

$$\alpha(r, \bar{t}) = A(r, \bar{t})^{-1/2} \left[ c - \partial_{\bar{t}} T(\bar{t}) \int_{\infty}^r \frac{d\rho}{\rho} \left( \frac{\rho^2}{\ell^2} - 8G_N M + \frac{T(\bar{t})^2}{\rho^2} \right)^{-3/2} \right]. \quad (4.17c)$$

The lapse  $\alpha$  approaches the asymptotic AdS boundary condition  $cr/\ell$  as  $r \rightarrow \infty$ . Here  $M(\bar{t})$  and  $T(\bar{t})$  appear as two integration constants in the solving radial differential equations obtained from the Hamiltonian and radial momentum constraints respectively. The integration constant  $M(\bar{t})$  and can be shown to be independent of time using the  $\dot{K}_{rr}$  Einstein equation. The ADM mass at the right boundary turns out to be  $cM$ . These results are derived in Appendix C.

**The left areal chart** The solution in the second chart is similar but can have different boundary conditions for the lapse. Keeping in mind that this solution maps to Region II of the fully extended BTZ black hole, we use the radial coordinate  $\tilde{r}$  that appears in the BTZ metric in

---

out that the solution of the three equations presented above automatically satisfied  $\dot{K} = 0$ .



Region II (4.7) to describe this chart. The solution is

$$ds^2 = -\tilde{\alpha}(\tilde{r}, \bar{t})^2 d\bar{t}^2 + \tilde{A}(\tilde{r}, \bar{t}) \left( d\tilde{r} + \frac{\tilde{\alpha}(\tilde{r}, \bar{t})T(\bar{t})}{\tilde{r}} d\bar{t} \right)^2 + \tilde{r}^2 d\varphi^2, \quad (4.18a)$$

$$A(\tilde{r}, \bar{t}) = \left( \frac{\tilde{r}^2}{\ell^2} - 8G_N M + \frac{T(\bar{t})^2}{\tilde{r}^2} \right)^{-1}, \quad (4.18b)$$

$$\tilde{\alpha}(\tilde{r}, \bar{t}) = A(\tilde{r}, \bar{t})^{-1/2} \left[ \tilde{c} - \partial_{\bar{t}} T(\bar{t}) \int_{\infty}^{\tilde{r}} \frac{d\rho}{\rho} \left( \frac{\rho^2}{\ell^2} - 8G_N M + \frac{T(\bar{t})^2}{\rho^2} \right)^{-3/2} \right]. \quad (4.18c)$$

This is valid for the following range of  $\tilde{r}$ :

$$R_+(T) < \tilde{r} < \infty, \quad (4.19)$$

and describes the rest of the maximal slice that starts from  $r = R_+$  in Region F extends into Region II up to the left boundary. Note that the lapse  $\tilde{\alpha}$  approaches  $\tilde{c}\tilde{r}/\ell$  as  $\tilde{r} \rightarrow \infty$  for some constant  $\tilde{c}$  that could be different from  $c$ .

The only quantity we have not yet specified is the function  $T(\bar{t})$ . This is determined by the following implicit function:

$$(c + \tilde{c})\bar{t} + t_0 + \tilde{t}_0 = -2T \int_{R_+(T)}^{\infty} \frac{d\rho}{\rho} \left( \frac{\rho^2}{\ell^2} - 8G_N M \right)^{-1} \left( \frac{\rho^2}{\ell^2} - 8G_N M + \frac{T^2}{\rho^2} \right)^{-1/2}, \quad (4.20)$$

where  $c$  and  $\tilde{c}$  are the constants that determine the lapse at the right and left boundaries, and  $t_0$ ,  $\tilde{t}_0$  are arbitrary real constants that specify the origin of time on the right and left boundaries respectively. The Cauchy principal value prescription must be used to evaluate integral (4.20) due to the pole at  $\rho = \ell\sqrt{8G_N M}$ .

For completeness, we give the diffeomorphism to the standard BTZ metric in Regions I, F and II below. This is described in detail in Appendix C. The diffeomorphism is completely specified by giving the local time coordinate  $-t$  in Region I,  $t_F$  in Region F – in terms of  $\bar{t}$  and  $r$ , and the local coordinate  $\tilde{t}$  in Region II in terms of  $\bar{t}$  and  $\tilde{r}$ . We have

$$t(r, \bar{t}) - \hat{t}_F(R_+) = -T(\bar{t}) \int_{R_+(T)}^r \frac{d\rho}{\rho} \left( \frac{\rho^2}{\ell^2} - 8G_N M \right)^{-1} \left( \frac{\rho^2}{\ell^2} - 8G_N M + \frac{T(\bar{t})^2}{\rho^2} \right)^{-1/2}, \quad (4.21)$$

$$t_F(r, \bar{t}) - \hat{t}_F(R_+) = -T(\bar{t}) \int_{R_+(T)}^r \frac{d\rho}{\rho} \left( \frac{\rho^2}{\ell^2} - 8G_N M \right)^{-1} \left( \frac{\rho^2}{\ell^2} - 8G_N M + \frac{T(\bar{t})^2}{\rho^2} \right)^{-1/2}, \quad (4.22)$$

$$\tilde{t}(\tilde{r}, \bar{t}) - \hat{t}_F(R_+) = T(\bar{t}) \int_{R_+(T)}^{\tilde{r}} \frac{d\rho}{\rho} \left( \frac{\rho^2}{\ell^2} - 8G_N M \right)^{-1} \left( \frac{\rho^2}{\ell^2} - 8G_N M + \frac{T(\bar{t})^2}{\rho^2} \right)^{-1/2}, \quad (4.23)$$

where  $\hat{t}_F(R_+)$  is the value of  $t_F$  in Region F at which  $r = R_+$  on the maximal slice labelled by  $\bar{t}$ :

$$\hat{t}_F(R_+(T(\bar{t}))) = \frac{1}{2}(c - \tilde{c})\bar{t} + \frac{1}{2}(t_0 - \tilde{t}_0). \quad (4.24)$$

### Some properties of the solution

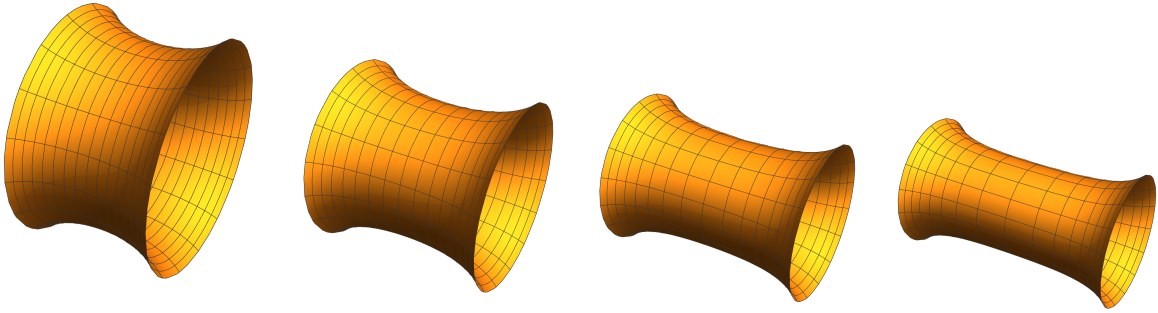


Figure 2: We plot the constant  $\bar{t}$  slices between the two null horizons, for various values of  $\bar{t}$ . The  $\varphi$  coordinate runs along the circle direction while the  $x$  coordinate runs along the length of the wormhole. As  $\bar{t}$  increases, the spatial wormhole stretches along the length and shrinks along the circle.

1. The function  $T(\bar{t})$  satisfies the inequality  $|T(\bar{t})| \leq 4G_N M \ell$ , since otherwise the roots  $R_{\pm}$  in (4.16) become complex.
2. At  $r = R_+(T(\bar{t}))$ , the root defined above in (4.16), the maximal slice is tangent to the constant  $r = R_+(T)$  hyperbola. Therefore  $r = R_+(T(\bar{t}))$  is the minimum radial value on a given  $\bar{t}$  maximal slice.
3. In spite of the failure of the above coordinate chart at  $r = R_+(T)$ , the lapse  $\alpha(r, \bar{t})$  remains finite and non-zero at  $r = R_+(T)$ ,

$$\alpha(r = R_+(T), \bar{t}) = \frac{\ell^2 \partial_{\bar{t}} T}{R_+^2 - R_-^2}. \quad (4.25)$$

4. The  $r = \ell\sqrt{4G_N M}$  hyperbola in Region F is itself a maximal slice.
5. As  $\bar{t} \rightarrow \infty$ , the slices approach the maximal slice  $r = \ell\sqrt{4G_N M}$ . The lapse goes to zero on this limit slice and time evolution grinds to a halt [55]. However, as mentioned in the Introduction, we will always restrict ourselves to times much smaller than the scrambling time  $t_*$  when studying the quantum dynamics of a scalar field on this solution.
6. The ADM masses can be computed at the left and right boundaries and are given by  $\tilde{c}M$  and  $cM$  respectively. See the calculation following (C.39) in Appendix C.

### 4.3 Wormhole coordinates

The metric components in the two charts diverge at the locus of points  $(t_F, r) = (\hat{t}_F(R_+), R_+)$  in Region F. We can remedy this by defining a new coordinate  $x$

$$x^2 = r^2 - R_+(T(\bar{t}))^2. \quad (4.26)$$

We call this the ‘wormhole’ coordinate since it covers the full spatial slice which has the topology of a wormhole, see Figure 2. The centre of the wormhole throat  $(t_F(R_+), R_+)$  always lies at

$x = 0$  for all  $\bar{t}$ , with  $x > 0$  covering the right chart and  $x < 0$  covering the left chart. In terms of these coordinates  $(\bar{t}, x, \varphi)$ , the metric is given by

$$ds^2 = -N^2 d\bar{t}^2 + g_{xx} (dx + N^x d\bar{t})^2 + (x^2 + R_+(\bar{t})^2) d\varphi^2, \quad (4.27)$$

with

$$N(\bar{t}, x) = \begin{cases} \frac{x\sqrt{x^2+R_+^2-R_-^2}}{\ell\sqrt{x^2+R_+^2}} \left[ c + \dot{T}\ell^3 \int_x^\infty \frac{dy}{y^2} \frac{\sqrt{y^2+R_+^2}}{(y^2+R_+^2-R_-^2)^{3/2}} \right] & x > 0 \\ -\frac{x\sqrt{x^2+R_+^2-R_-^2}}{\ell\sqrt{x^2+R_+^2}} \left[ \tilde{c} + \dot{T}\ell^3 \int_{-x}^\infty \frac{dy}{y^2} \frac{\sqrt{y^2+R_+^2}}{(y^2+R_+^2-R_-^2)^{3/2}} \right] & x < 0 \end{cases}, \quad (4.28a)$$

$$N^x(\bar{t}, x) = \frac{1}{x} \left( N(\bar{t}, x)T + R_+\dot{R}_+ \right), \quad (4.28b)$$

$$g_{xx}(\bar{t}, x) = \frac{\ell^2}{x^2 + R_+^2 - R_-^2}. \quad (4.28c)$$

In Appendix C, we show that the above solution is completely smooth except at the final limit slice  $\bar{t} \rightarrow \infty$  where  $g_{xx}$  has a coordinate singularity at  $x = 0$ . Thus we have constructed a smooth coordinate chart  $(\bar{t}, x, \varphi)$  for all finite  $\bar{t}$  with metric (4.27), whose constant time slices are maximal and go from the left asymptotic boundary to the right asymptotic boundary while smoothly cutting across the two horizons.

#### 4.4 Symmetric maximal slices

The solution we found above is labelled by 4 asymptotic parameters namely  $c$ ,  $\tilde{c}$ ,  $t_0$  and  $\tilde{t}_0$ . The parameters  $t_0$  and  $\tilde{t}_0$  correspond to a choice of origin of time at left and right boundaries, while  $c$  and  $\tilde{c}$  control how fast the two boundary clocks tick.

The ADM masses at the right and left asymptotic boundaries can be calculated and are found to be  $cM$  and  $\tilde{c}M$  respectively. Demanding that they be equal to each other and to the BTZ mass  $M$ , forces  $c = \tilde{c} = 1$ . This is physically motivated: *all observers* at each asymptotic boundary must agree with each other on the mass since they are describing the same black hole.

Together with  $c = \tilde{c} = 1$ , we also fix the origin of time on the two boundaries  $t_0 = \tilde{t}_0 = 0$ . The maximal slices then become symmetric. The spacetime metric for the symmetric maximal foliation is

$$ds^2 = -N^2 d\bar{t}^2 + g_{xx} (dx + N^x d\bar{t})^2 + (x^2 + R_+(\bar{t})^2) d\varphi^2, \quad (4.29a)$$

$$N(\bar{t}, x) = \frac{x\sqrt{x^2 + R_+^2 - R_-^2}}{\ell\sqrt{x^2 + R_+^2}} \left[ 1 + \dot{T}\ell^3 \int_x^\infty \frac{dy}{y^2} \frac{\sqrt{y^2 + R_+^2}}{(y^2 + R_+^2 - R_-^2)^{3/2}} \right], \quad (4.29b)$$

$$N^x(\bar{t}, x) = \frac{1}{x} \left( N(\bar{t}, x)T + R_+\dot{R}_+ \right), \quad g_{xx}(\bar{t}, x) = \frac{\ell^2}{x^2 + R_+^2 - R_-^2}. \quad (4.29c)$$

The function  $T(\bar{t})$  is determined by

$$\bar{t} = -T(\bar{t})\ell^3 \int_0^\infty \frac{dy}{(y^2 - R_-^2)\sqrt{(y^2 + R_+^2)(y^2 + R_+^2 - R_-^2)}}, \quad (4.30)$$

where we have rewritten the integral in (4.20) after a change of integration variable  $\rho^2 = y^2 + R_+(T)^2$ . The  $t = 0$  slice of the usual slicing of the BTZ black hole slice coincides with  $\bar{t} = 0$  slice of the symmetric foliation.

In Figures 3 and 4, we plot the symmetric maximal slices for  $\bar{t} > 0$  in the Kruskal and Penrose diagrams of the fully extended BTZ black hole. It will be useful to keep these Figures in mind while studying the properties listed below.

### Properties of the symmetric solution with $c = \bar{c} = 1$ and $t_0 = \bar{t}_0 = 0$

1. From (4.24) we see that  $t_F(R_+(T)) = 0$  for all  $\bar{t}$ . This means that the left and right areal charts meet exactly at the centre in the Kruskal and Penrose diagrams.
2. The right and left horizons are at  $x = \pm R_-(T(\bar{t}))$  respectively.
3. The final slice as  $\bar{t} \rightarrow \infty$  approaches  $r = \ell\sqrt{4G_N M}$ . Thus the maximal slices do not cover a portion of the black hole spacetime near the singularities. However a second family of maximal surfaces which lie completely inside the horizons cover this remaining portion. This family of maximal slices is briefly discussed in Section 4.5.
4. The lapse  $N$  is finite, positive (except at the final slice  $\bar{t} \rightarrow 0$  where it vanishes) and an even function of  $x$ . Its value and derivative at  $x = 0$  for all times  $\bar{t}$  is given by

$$N(x = 0, \bar{t}) = \frac{\partial_{\bar{t}} T \ell^2}{R_+^2 - R_-^2}, \quad \partial_x N(x = 0) = 0. \quad (4.31)$$

5. The standard BTZ coordinates  $t, r$  in Regions I and F are related to the wormhole coordinates  $\bar{t}, x$  in the range  $\bar{t} > 0, -R_- < x < \infty$  as follows:

$$r^2 = x^2 + R_+^2(\bar{t}), \quad (4.32a)$$

$$t = -T(\bar{t})\ell^3 \int_0^x \frac{dy}{(y^2 - R_-^2(\bar{t}))\sqrt{(y^2 + R_+^2(\bar{t}))(y^2 + R_+^2(\bar{t}) - R_-^2(\bar{t}))}}. \quad (4.32b)$$

The Region II coordinates  $(\tilde{t}, \tilde{r})$  are related to  $(\bar{t}, x)$  in the range  $\bar{t} > 0, -\infty < x < -R_-$  as

$$\tilde{r}^2 = x^2 + R_+^2(\bar{t}), \quad (4.33a)$$

$$\tilde{t} = -T(\bar{t})\ell^3 \int_0^x \frac{dy}{(y^2 - R_-^2(\bar{t}))\sqrt{(y^2 + R_+^2(\bar{t}))(y^2 + R_+^2(\bar{t}) - R_-^2(\bar{t}))}}. \quad (4.33b)$$

6. The coordinate transformation between the wormhole  $(\bar{t}, x)$  coordinates (collectively denoted below as  $x^\alpha$ ) and the Kruskal-Szekeres  $(U, V)$  coordinates (collectively denoted below as  $U^\mu$ ) is smooth and well-defined, even though we have not written it here explicitly. Since all the metric components are smooth and finite in the open spacetime region covered by the wormhole coordinates in both the coordinate systems, the Jacobian  $\partial U^\mu / \partial x^\alpha$  is finite and invertible. This is clear when we look at the transformation rule for the metric:

$$g_{\alpha\beta}(\bar{t}, x, \varphi) = \frac{\partial U^\mu}{\partial x^\alpha} \frac{\partial U^\nu}{\partial x^\beta} g_{\mu\nu}(U, V, \varphi) \longleftrightarrow g_{\mu\nu}(U, V, \varphi) = \frac{\partial x^\alpha}{\partial U^\mu} \frac{\partial x^\beta}{\partial U^\nu} g_{\alpha\beta}(\bar{t}, x, \varphi). \quad (4.34)$$

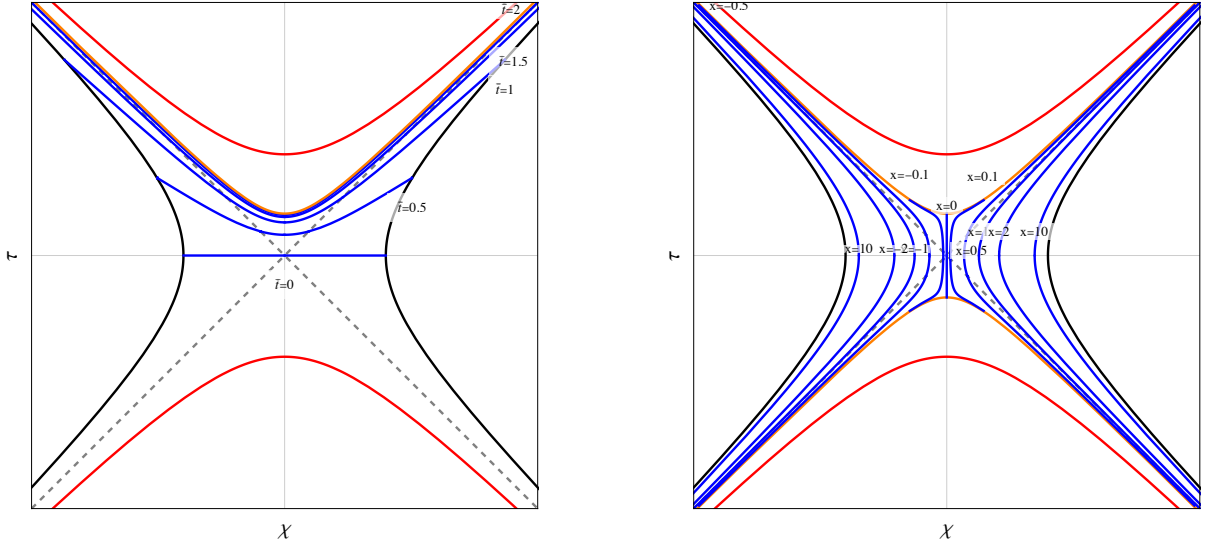


Figure 3: On the left panel we plot constant  $\bar{t}$  maximal slices (solid blue lines) in Kruskal-Szekeres diagram. The red curves are the singularities at  $r = 0$  while the black curves are the asymptotic boundaries at infinity. As  $\bar{t} \rightarrow \infty$ , the final slice approaches  $r_{\min} = \ell\sqrt{4G_N M}$  (orange curve) from below. Since these are symmetric slices, they intersect the  $\chi = 0$  line at right angles. On the right panel we plot the flow lines are generated by the vector field  $(N, N^x, 0)$ . These are simply the constant  $x$  trajectories in the diagram on the left.

**Flow Lines** We can also plot flow lines generated by the vector field  $(N, N^x, 0)$ . These flow lines are not orthogonal to maximal surfaces because of the non-zero shift and are simply given by constant  $x$  trajectories. Only for  $|x| < \ell\sqrt{4G_N M}$  do the flow lines go into the interior. For  $|x| > \ell\sqrt{4G_N M}$  they always remain in the exterior regions with  $|x| = \ell\sqrt{4G_N M}$  approaching the horizon as  $\bar{t} \rightarrow \infty$ . Flow lines are plotted in the second panel in Figures 3, 4.

In summary, we have solved the Einstein equations in the maximal slicing gauge and constructed a foliation that asymptotes to the two AAdS boundaries while cutting across the horizons and avoiding the singularity. There is a second family of maximal slices that do not reach the asymptotic boundaries and are contained entirely in the interior of the black hole. These slices are tethered to the singularity at  $r = 0$ . We describe this family below.

#### 4.5 A second family of maximal slices

Recall that the maximal slicing solution in the areal radial charts has coordinate singularities at the values  $r = R_{\pm}$  (4.16). The slices considered previously started from the boundary and encountered the larger root  $R_+$  first and stopped there to avoid the coordinate singularity. The maximal slices are tangential to the  $r = R_+(T(\bar{t}))$  hyperbolas.

If we choose maximal slices to be tangential to the  $r = R_-(T)$  hyperbola, then it is clear that they cannot be connected to the asymptotic boundaries. Instead, they remain inside the horizon and end on the singularity  $r = 0$ .

Just as for the first family, there will be two areal charts which would now be joined at  $r = R_-(T)$ . The spatial slices are sausage-like: they are cylindrical and cap off at the two ends at  $r = 0$ . We define the globally defined ‘sausage’ coordinate (analogous to the wormhole coordinate

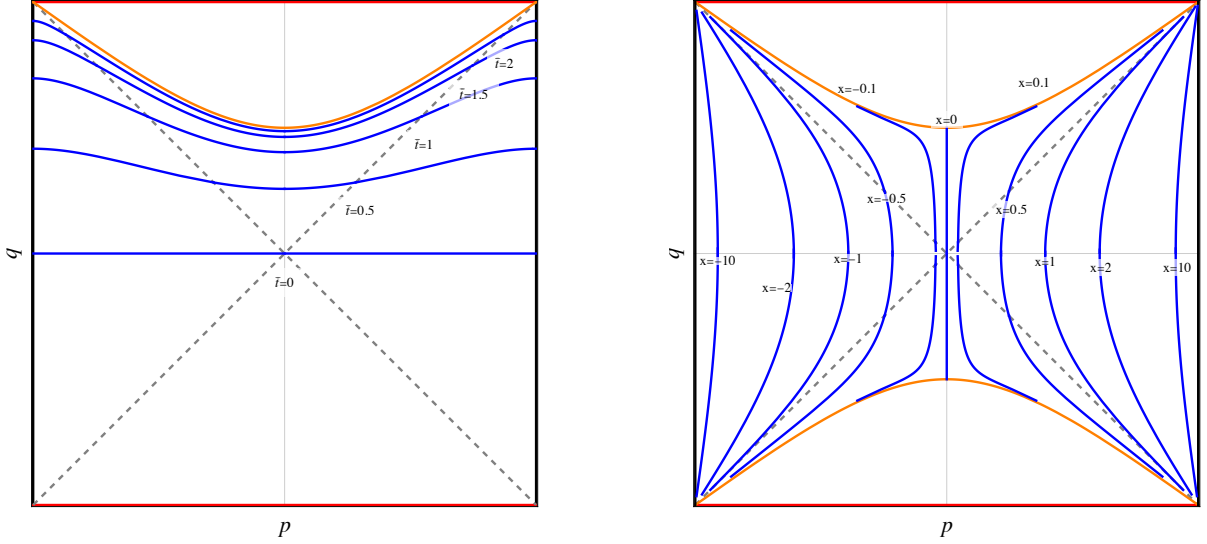


Figure 4: On the left panel we plot constant  $\bar{t}$  maximal slices (solid blue lines) in the Penrose diagram. The red curves are the singularities at  $r = 0$  while the black curves are the asymptotic boundaries at infinity. As  $\bar{t} \rightarrow \infty$ , the final slice approaches  $r_{\min} = \ell\sqrt{4G_N M}$  (orange curve) from below. On the right panel we plot the flow lines are generated by the vector field  $(N, N^x, 0)$ . These are simply the constant  $x$  trajectories in the diagram on the left.

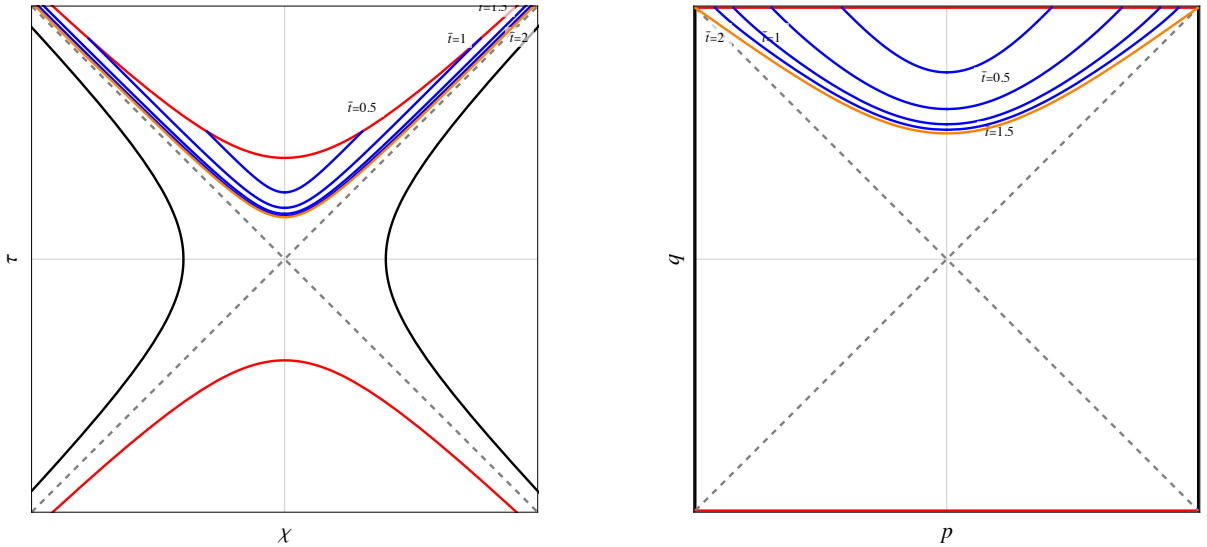


Figure 5: Constant  $\bar{t}$  slices of the second family are drawn in Kruskal-Szekeres diagram on the left and the Penrose diagram on the right. The red curves are the singularities at  $r = 0$  while the black curves are the asymptotic boundaries. The maximal slices are drawn in blue. These slices start at the singularity, grow outwards and end at the final slice at  $r_{\min} = \ell\sqrt{4G_N M}$  (orange curve) as  $\bar{t} \rightarrow \infty$ .

for the first family)

$$z^2 = R_-(T(\bar{t}))^2 - r^2, \quad z \in [-R_-(T), R_-(T)]. \quad (4.35)$$

We have  $z(r = R_-) = 0$ ,  $z(r = 0) = \pm R_-(T(\bar{t}))$ , and therefore the range of the sausage coordinate  $z$  is time dependent. For symmetric slices, the metric in these coordinates is given by

$$ds^2 = -N^2 d\bar{t}^2 + g_{zz} (dz + N^z d\bar{t})^2 + (R_-(\bar{t})^2 - z^2) d\varphi^2, \quad (4.36)$$

with

$$N(\bar{t}, z) = \frac{z\sqrt{z^2 + R_+^2 - R_-^2}}{\ell\sqrt{R_-^2 - z^2}} \left[ 1 + \dot{T}\ell^3 \int_{\sqrt{R_-^2 - z^2}}^{\infty} \frac{d\rho}{\rho} \left( \frac{\rho^2}{\ell^2} - 8G_N M + \frac{T(\bar{t})^2}{\rho^2} \right)^{-3/2} \right], \quad (4.37a)$$

$$N^z(\bar{t}, z) = -\frac{1}{z} \left( N(\bar{t}, z)T + R_- \dot{R}_- \right), \quad (4.37b)$$

$$g_{zz}(\bar{t}, z) = \frac{\ell^2}{z^2 + R_+^2 - R_-^2}. \quad (4.37c)$$

The coordinate transformation to the BTZ coordinates  $(t_F, r, \varphi)$  in Region F is given by

$$r^2 = R_-(T(\bar{t}))^2 - z^2, \quad (4.38a)$$

$$t_F = -T(\bar{t}) \int_{R_-(T)}^{\sqrt{R_-^2 - z^2}} \frac{d\rho}{\rho} \left( \frac{\rho^2}{\ell^2} - 8G_N M \right)^{-1} \left( \frac{\rho^2}{\ell^2} - 8G_N M + \frac{T^2}{\rho^2} \right)^{-1/2}. \quad (4.38b)$$

These second family of slices are plotted in Figure 5. They start from  $r = 0$  and cover the interior of the black hole up to a final limit slice at constant radial value  $r = \ell\sqrt{4G_N M}$ . The first family of maximal slices reached the same final slice but from the exterior (see Figures 3 and 4). Together the two families foliate the entire black hole spacetime.

We emphasize that the second family of maximal surfaces never reach the asymptotic boundaries. They can perhaps be of interest for questions involving the singularity but we do not study them further in this paper.

## 4.6 Large diffeomorphisms

In Section 2.4, we discussed large diffeomorphisms in the maximal slicing and Dirac gauge. For a given non-trivial boundary condition on the lapse and shift that corresponds to a given asymptotic symmetry, we showed that there is a unique solution that preserves the maximal slicing and Dirac gauge conditions. This is because the small diffeomorphism redundancy that can spoil the uniqueness is completely gauge-fixed by the gauge conditions.

In Section 3, we have demonstrated complete gauge-fixing for  $d = 2$  in the maximal slicing and spatially harmonic gauge (which is the same as the Dirac gauge in  $d = 2$ ). Next, we solved the constraint equations in the maximal slicing gauge with areal radial coordinate, and subsequently transformed to the wormhole coordinate, both of which can be related to the spatially harmonic gauge by a smooth diffeomorphism.

The general solution in Sections 4.2 and 4.3, where the lapse was allowed to asymptote to

$cr/\ell$  and  $\tilde{c}r/\ell$  on the two boundaries are indeed examples of the unique large diffeomorphisms: they correspond to asymptotic time translation by  $c$  and  $\tilde{c}$  respectively on the two boundaries. The solution for general  $c, \tilde{c}$  in Section 4.3 gives the flow lines for this large diffeomorphism, with the parameter  $\bar{t}$  now treated as a parameter along the flow lines. Since  $\bar{t}$  is used for the time coordinate of the distinguished symmetric foliation, we label the flow line parameter for general  $c, \tilde{c}$  as  $u$ . Similarly, since  $N$  and  $N^i$  have been used in this section for the lapse and shift for the distinguished symmetric foliation, we label the large diffeomorphism as  $(\zeta_\perp, \zeta^i)$ . The solution in Section 4.3 rewritten in terms of these new labels is

$$\begin{aligned} \zeta_\perp(u, x) &= \begin{cases} \frac{x\sqrt{x^2+R_+^2-R_-^2}}{\ell\sqrt{x^2+R_+^2}} \left[ c + \ell^3 \partial_u T_{c,\tilde{c}} \int_x^\infty \frac{dy}{y^2} \frac{\sqrt{y^2+R_+^2}}{(y^2+R_+^2-R_-^2)^{3/2}} \right] & x > 0 \\ -\frac{x\sqrt{x^2+R_+^2-R_-^2}}{\ell\sqrt{x^2+R_+^2}} \left[ \tilde{c} + \ell^3 \partial_u T_{c,\tilde{c}} \int_{-x}^\infty \frac{dy}{y^2} \frac{\sqrt{y^2+R_+^2}}{(y^2+R_+^2-R_-^2)^{3/2}} \right] & x < 0 \end{cases}, \\ \zeta^x(u, x) &= \frac{1}{x} (\zeta_\perp(u, x) T_{c,\tilde{c}}(u) + R_+ \partial_u R_+) , \\ \zeta^\varphi(u, x) &= 0 , \end{aligned} \tag{4.39}$$

where  $R_\pm$  are functions of  $T_{c,\tilde{c}}$  with the function  $T_{c,\tilde{c}}(u)$  specified implicitly by

$$(c + \tilde{c})u = -2T_{c,\tilde{c}} \int_{R_+(T_{c,\tilde{c}})}^\infty \frac{d\rho}{\rho} \left( \frac{\rho^2}{\ell^2} - 8G_N M \right)^{-1} \left( \frac{\rho^2}{\ell^2} - 8G_N M + \frac{T_{c,\tilde{c}}^2}{\rho^2} \right)^{-1/2}. \tag{4.40}$$

The action of this diffeomorphism on the symmetric maximal foliation specified by  $N$  and  $N^i$  with time coordinate  $\bar{t}$  in Section 4.4 is obtained as follows. For a given  $\bar{t}$ , we find out the value of  $u$  such that  $T_{c,\tilde{c}}(u) = T(\bar{t})$ . This gives  $u$  as a function of  $\bar{t}$ . The spacetime diffeomorphism  $\underline{\zeta}^\mu$  is then given by

$$\zeta_\perp(u(\bar{t}), x) = N(\bar{t}, x) \underline{\zeta}^{\bar{t}}(\bar{t}, x) , \quad \zeta^i(u(\bar{t}), x) = \underline{\zeta}^i(\bar{t}, x) + N^i(\bar{t}, x) \underline{\zeta}^{\bar{t}}(\bar{t}, x) , \tag{4.41}$$

where  $N$  and  $N^i$  are the lapse and shift of the symmetric foliation.

In Figure 6, we display the action of the large diffeomorphism corresponding to time translation only on the right boundary:  $c = 1, \tilde{c} = 0$ .

## 5 A probe scalar field in the maximally sliced BTZ black hole

We have shown in Section 2.5 that a probe scalar field in a fixed pure gravity background is *gauge invariant* under small diffeomorphisms at quadratic order in perturbation theory in  $\kappa$ . This is because (1) the metric and scalar degrees of freedom are decoupled at quadratic order in perturbation theory, and (2) the background diffeomorphisms are completely fixed by working in the maximal slicing - spatially harmonic gauge, and diffeomorphisms at  $\mathcal{O}(\kappa)$  are fixed purely in the metric fluctuation sector without involving the scalar field.

In the rest of the paper, we consider a free scalar field  $\phi$  of mass  $m$  in maximally sliced BTZ black hole background obtained in the previous section. This scalar field is dual to a generalized free field scalar operator  $\mathcal{O}$  with dimension  $\Delta_+ = 1 + \sqrt{1 + \ell^2 m^2}$  in the dual CFT.



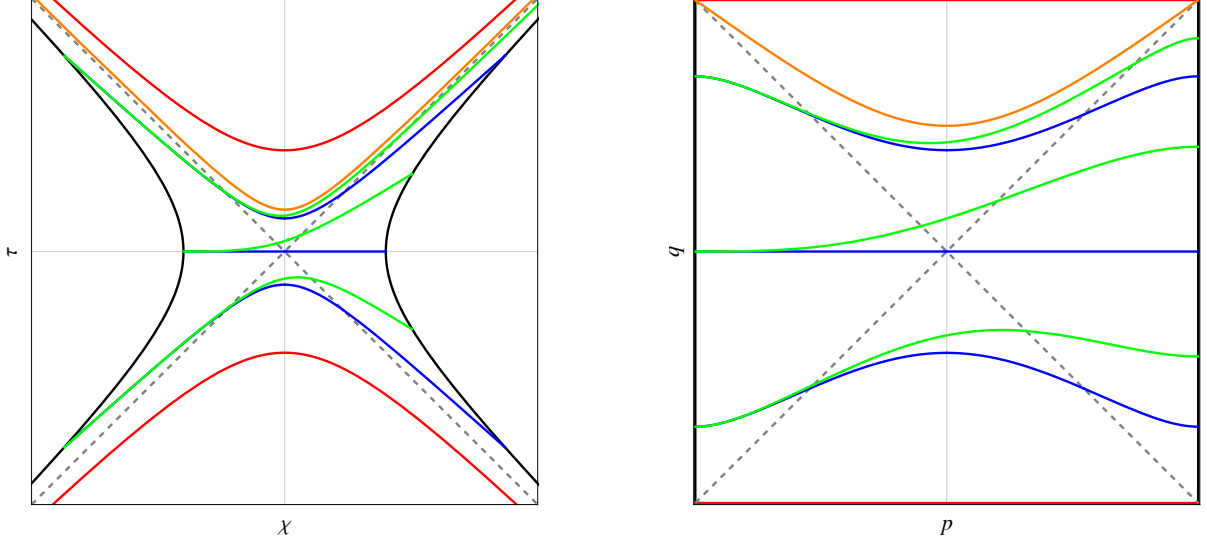


Figure 6: The action of the large diffeomorphism corresponding to translations only on the right boundary. The blue curves are the slices of the symmetric foliation and the green curves attached to the blue curves on the left boundary are their images under the large diffeomorphism.

Let us write the background geometry in the ADM split:

$$ds^2 = -N^2 dt^2 + g_{ij}(dx^i + N^i dt)(dx^j + N^j dt) . \quad (5.1)$$

The Hamiltonian of the massive scalar field in the above background is (2.33)

$$H = \int d^2x \left( N \left( \frac{\pi_\phi^2}{2\sqrt{g}} + \frac{1}{2}\sqrt{g} g^{ij} (\partial_i \phi \partial_j \phi + m^2 \phi^2) \right) + N^i \pi_\phi \partial_i \phi \right) . \quad (5.2)$$

The Hamiltonian equations of motion are

$$\partial_t \phi = \frac{N}{\sqrt{g}} \pi_\phi + N^i \partial_i \phi . \quad (5.3)$$

$$\partial_t \pi_\phi = \partial_i (N \sqrt{g} g^{ij} \partial_j \phi) - N \sqrt{g} m^2 \phi + \partial_i (N^i \pi_\phi) . \quad (5.4)$$

Plugging in the expression for  $\pi_\phi$  in terms of  $\dot{\phi}$ , we get the Klein-Gordon equation

$$\begin{aligned} \partial_t (-N^{-1} \sqrt{g} (\partial_t \phi - N^i \partial_i \phi)) + \partial_i (N^{-1} \sqrt{g} N^i \partial_t \phi) \\ + \partial_i (N \sqrt{g} (g^{ij} - N^{-2} N^i N^j) \partial_j \phi) - N \sqrt{g} m^2 \phi = 0 . \end{aligned} \quad (5.5)$$

It is expected that the initial value problem is well-posed for the above linear hyperbolic differential equation when suitable normalizable boundary conditions are imposed on the scalar field [9, 20, 58–67]. Thus, the general solution of the Klein-Gordon equation can be expanded in terms of a complete set of mode solutions  $L_I(x)$  (for instance, see the textbook [68]) where  $I$  is a formal index which can be discrete or continuous:

$$\phi(x) = \sum_I (a_I L_I(x) + a_I^\dagger L_I^*(x)) , \quad (5.6)$$

with the following Klein-Gordon inner products:

$$(L_I, L_J)_{\text{KG}} = \delta_{IJ} , \quad (L_I^*, L_J^*)_{\text{KG}} = -\delta_{IJ} , \quad (L_I, L_J^*)_{\text{KG}} = 0 . \quad (5.7)$$

These imply that the ladder operators  $a_I$  satisfy

$$[a_I, a_J^\dagger] = \delta_{IJ} , \quad [a_I, a_J] = 0 , \quad [a_I^\dagger, a_J^\dagger] = 0 . \quad (5.8)$$

In the present case of AAdS spacetimes, since the metric diverges as one approaches an AAdS boundary, the effective potential for the scalar field also diverges and the modes are expected to be discrete. It is important that the lapse remains non-zero on the full spatial slice for the modes to be discrete. For the Killing slices (corresponding to evolution in Killing time), the lapse vanishes at the bifurcate horizon which effectively decouples the two exteriors by pushing the horizon exponentially far away in each exterior region. A single exterior region no longer behaves like a box and the modes are continuous. However when the lapse remains non-zero everywhere, like in the wormhole coordinates, the potential on the full spatial slice acts like a box and we expect the modes to be discrete.

As is well-known, there is typically no preferred set of mode functions in a general curved spacetime due a lack of time translation symmetry. However, depending on the context, we can choose to expand the scalar field in an appropriate complete set of mode functions. Here, we are interested in the AdS/CFT interpretation of scalar field propagation in the maximally sliced BTZ black hole. Hence, it is useful to have an expansion of the scalar field in terms of modes which are relevant for AdS/CFT.

These mode functions are obtained by quantizing the scalar field separately in the two exterior regions of the BTZ black hole, and analytically continuing them to the interior regions [69] (see also [27] for a more recent discussion). The quantization is carried out in the Schwarzschild-like coordinate system which possesses a Killing time symmetry. These Killing time slices are different from the maximal slices which symmetrically interpolate between the two AAdS boundaries. Thus, to get a solution of the Klein-Gordon equation in maximal slicing coordinates, we perform a diffeomorphism from the BTZ-Schwarzschild coordinates to the maximal slicing coordinates.

One important point is that the mode functions obtained in the Killing time slicing oscillate infinitely rapidly as one approaches the horizon, and hence their derivatives are singular at the horizon. This will present a problem when we pull back the scalar field onto the maximal slices since they cut across the horizon. We show that smearing the Killing time mode with Hermite functions  $\psi_n(\omega/\eta)$  in the frequency domain smoothens out these singularities. The smeared modes are labelled by the discrete index  $n$  of the Hermite functions. This discreteness also is natural from point of view of quantization of scalar field in AAdS spacetimes since the scalar field is effectively in a gravitational box.

We then plug in the smooth scalar field into the quadratic Hamiltonian and obtain a well-defined Hamiltonian operator which evolves the scalar field along the maximal slices. This operator in particular describes the evolution of wavepackets which cross the horizon and hence describes infalling observers.

## 5.1 The scalar field mode expansion

Recall that the Kruskal diagram of the fully extended BTZ spacetime, Figure 1, contains four regions, each with its own BTZ-type coordinates. The Klein-Gordon equation for the scalar field in Region I with metric (4.1) is

$$-f^{-1}\partial_t^2\phi + r^{-1}\partial_r(rf\partial_r\phi) + r^{-2}\partial_\varphi^2\phi - m^2\phi = 0. \quad (5.9)$$

There is an analogous solution in each Region in terms of its local BTZ coordinates. The solutions in each Region are matched across the horizons to obtain a global solution [27]. The solutions of the Klein-Gordon equation and the matching of solutions across the horizons is discussed in detail in Appendix E and we present the results here.

### 5.1.1 Mode expansion in Region I

The scalar field mode expansion in Region I is

$$\phi(t, r, \varphi) = \sum_{q \in \mathbb{Z}} \int_0^\infty \frac{d\omega}{\sqrt{4\pi\omega}} \left( a_{\omega q} F_{\omega q}(t, r, \varphi) + \text{c.c.} \right), \quad (5.10)$$

The modes  $F_{\omega q}(t, r, \varphi)$  are normalizable with respect to the Klein-Gordon norm, and are given in terms of hypergeometric functions:

$$F_{\omega q}(t, r, \varphi) = \frac{1}{\sqrt{2\pi}} e^{-i\omega t - iq\varphi} C_{\omega q} (\rho - 1)^\alpha \rho^{\gamma - a} {}_2F_1 \left( a, a - c + 1; a - b + 1; \frac{1}{\rho} \right), \quad (5.11)$$

where the coordinate  $\rho$  is defined as

$$\rho = \frac{r^2}{r_h^2}, \quad (5.12)$$

and the constants  $\alpha$ ,  $\gamma$ ,  $a$ ,  $b$ , and  $c$ , are given by

$$\alpha = -i\frac{\omega}{2\eta} = -i\frac{\beta\omega}{4\pi}, \quad \gamma = i\frac{q\ell}{2r_h}, \quad (5.13)$$

$$c = 2\gamma + 1, \quad a = \alpha + \gamma + \frac{1}{2}\Delta_+, \quad b = \alpha + \gamma + \frac{1}{2}\Delta_-, \quad \Delta_\pm = 1 \pm \sqrt{1 + \ell^2 m^2}, \quad (5.14)$$

and the normalization constant is

$$C_{\omega q} = \frac{1}{N_{\omega q} \sqrt{2\pi r_h}}, \quad \text{with} \quad N_{\omega q} = \left| \frac{\Gamma(a - b + 1) \Gamma(c - a - b)}{\Gamma(1 - b) \Gamma(c - b)} \right|. \quad (5.15)$$

The ladder operators  $a_{\omega q}$ ,  $a_{\omega q}^\dagger$  satisfy the usual commutation relations

$$[a_{\omega q}, a_{\omega' q'}^\dagger] = \delta(\omega - \omega') \delta_{qq'}, \quad [a_{\omega q}, a_{\omega' q'}] = [a_{\omega q}^\dagger, a_{\omega' q'}^\dagger] = 0. \quad (5.16)$$

By the AdS/CFT extrapolate dictionary [19, 20], the corresponding boundary operator is obtained by multiplying by  $r^{\Delta_+}$  and taking the boundary limit  $r \rightarrow \infty$ . The solution  $F_{\omega q}$  behaves in the

limit  $r \rightarrow \infty$  as (see (E.87) in Appendix E):

$$F_{\omega q}(t, r, \varphi) \sim e^{-i\omega t} e^{-iq\varphi} \frac{1}{N_{\omega q} \sqrt{2\pi r r_h}} \left( \frac{r}{r_h} \right)^{-\Delta_+} + \mathcal{O}(r^{-\Delta_+-2}). \quad (5.17)$$

Thus, the boundary operator  $\mathcal{O}$  in the dual CFT is

$$\mathcal{O}(t, \varphi) = \frac{r_h^{\Delta_+-\frac{1}{2}}}{\sqrt{2\pi}} \sum_{q \in \mathbb{Z}} \int_0^\infty \frac{d\omega}{\sqrt{4\pi\omega}} \frac{1}{N_{\omega q}} (a_{\omega q} e^{-i\omega t} e^{-iq\varphi} + \text{c.c.}). \quad (5.18)$$

The modes  $F_{\omega q}$  as written in (5.11) have a convergent series expansion near infinity. It is useful to write the mode expansion in terms of modes which have a convergent series expansion near the horizon  $r = r_h$ :

$$\phi(t, r, \varphi) = \frac{1}{\sqrt{2\pi r r_h}} \sum_{q \in \mathbb{Z}} \int_0^\infty \frac{d\omega}{\sqrt{4\pi\omega}} (a_{\omega q} (F_{\omega q}^1 + F_{\omega q}^2) + \text{c.c.}), \quad (5.19)$$

where the functions  $F_{\omega q}^1$  and  $F_{\omega q}^2$  are given by

$$\begin{aligned} F_{\omega q}^1 &= e^{-i\omega t - iq\varphi} e^{i\delta_{\omega q}} (\rho - 1)^\alpha \rho^\gamma {}_2F_1(a, b; a + b - c + 1; 1 - \rho), \\ F_{\omega q}^2 &= e^{-i\omega t - iq\varphi} e^{-i\delta_{\omega q}} (\rho - 1)^{-\alpha} \rho^\gamma {}_2F_1(c - a, c - b; c - a - b + 1; 1 - \rho), \end{aligned} \quad (5.20)$$

with  $e^{i\delta_{\omega q}}$  being the phase of the particular ratio of  $\Gamma$  functions given in (5.15):

$$N_{\omega q} e^{i\delta_{\omega q}} = \frac{\Gamma(a - b + 1) \Gamma(c - a - b)}{\Gamma(1 - b) \Gamma(c - b)} = \frac{\Gamma(\Delta_+) \Gamma(i\omega/\eta)}{\Gamma\left(\frac{1}{2}(\Delta_+ + \frac{i\omega}{\eta} - \frac{iq\ell}{r_h})\right) \Gamma\left(\frac{1}{2}(\Delta_+ + \frac{i\omega}{\eta} + \frac{iq\ell}{r_h})\right)}. \quad (5.21)$$

The Boulware vacuum  $|B\rangle$  is defined as the state in the Fock space which is annihilated by the  $a_{\omega q}$ :

$$a_{\omega q} |B\rangle = 0, \quad \text{for all } \omega > 0, q \in \mathbb{Z}. \quad (5.22)$$

### 5.1.2 Mode expansion in Region II

An analogous computation can be done in Region II where the BTZ metric is given by

$$ds^2 = -f(\tilde{r}) d\tilde{t}^2 + f(\tilde{r})^{-1} d\tilde{r}^2 + \tilde{r}^2 d\varphi^2, \quad -\infty < \tilde{t} < \infty, \quad r_h < \tilde{r}. \quad (5.23)$$

The Klein-Gordon equation has the exact same form as in Region I in terms of the local coordinates  $(\tilde{t}, \tilde{r}, \varphi)$ . However, it is convenient to define the mode functions in Region II as the complex conjugates of those in Region I:

$$\tilde{F}_{\omega q}(\tilde{t}, \tilde{r}, \varphi) \equiv F_{\omega q}^*(\tilde{t}, \tilde{r}, \varphi). \quad (5.24)$$

The mode expansion of the scalar field in Region II is then

$$\phi(\tilde{t}, \tilde{r}, \varphi) = \sum_{q \in \mathbb{Z}} \int_0^\infty \frac{d\omega}{\sqrt{4\pi\omega}} (\tilde{a}_{\omega q} \tilde{F}_{\omega q}(\tilde{t}, \tilde{r}, \varphi) + \text{c.c.}). \quad (5.25)$$

The quantum operators  $\tilde{a}_{\omega q}$ ,  $\tilde{a}_{\omega q}^\dagger$  satisfy the canonical commutation relations:

$$[\tilde{a}_{\omega q}, \tilde{a}_{\omega' q'}^\dagger] = \delta(\omega - \omega') \delta_{qq'} , \quad [\tilde{a}_{\omega q}, \tilde{a}_{\omega' q'}] = [\tilde{a}_{\omega q}^\dagger, \tilde{a}_{\omega' q'}^\dagger] = 0 . \quad (5.26)$$

The corresponding operator in the CFT associated to the second boundary  $\tilde{r} \rightarrow \infty$  is

$$\tilde{\mathcal{O}}(\tilde{t}, \varphi) = \frac{r_h^{\Delta_+ - \frac{1}{2}}}{\sqrt{2\pi}} \sum_{q \in \mathbb{Z}} \int_0^\infty \frac{d\omega}{\sqrt{4\pi\omega}} \frac{1}{c_{\omega q}} (\tilde{a}_{\omega q} e^{i\omega\tilde{t}} e^{iq\varphi} + \text{c.c.}) . \quad (5.27)$$

The mode expansion in terms of functions which have a convergent series near the horizon is

$$\phi(\tilde{t}, \tilde{r}, \varphi) = \frac{1}{\sqrt{2\pi r h}} \sum_{q \in \mathbb{Z}} \int_0^\infty \frac{d\omega}{\sqrt{4\pi\omega}} (\tilde{a}_{\omega q} (F_{\omega q}^{1*} + F_{\omega q}^{2*}) + \text{c.c.}) . \quad (5.28)$$

The  $\tilde{a}_{\omega q}$  commute with the operators from Region I:

$$[\tilde{a}_{\omega q}, a_{\omega q}] = [\tilde{a}_{\omega q}, a_{\omega q}^\dagger] = 0 . \quad (5.29)$$

There is an analogous Boulware vacuum  $|\tilde{B}\rangle$  which is annihilated by the  $\tilde{a}_{\omega q}$ :

$$\tilde{a}_{\omega q} |\tilde{B}\rangle = 0 , \quad \text{for all } \omega > 0, q \in \mathbb{Z} . \quad (5.30)$$

The total vacuum for the union of Regions I and II is the tensor product of the Boulware vacua:

$$|B\rangle \otimes |\tilde{B}\rangle , \quad (5.31)$$

and the full Fock space is built upon this by using the creation operators  $a_{\omega q}^\dagger$  and  $\tilde{a}_{\omega q}^\dagger$ .

### 5.1.3 Mode expansions in Regions F and P

The solutions of the Klein-Gordon equation in Regions F and P are naturally written in terms of functions which have a convergent series near the horizon. They are then matched with the solutions in Regions I and II across the respective horizons which separate them. The final expressions are

$$\begin{aligned} \text{Region F : } \phi(t_F, r, \varphi) &= \frac{1}{\sqrt{2\pi r h}} \sum_{q \in \mathbb{Z}} \int_0^\infty \frac{d\omega}{\sqrt{4\pi\omega}} (a_{\omega q} G_{\omega q}^1 + \tilde{a}_{\omega q}^\dagger G_{\omega q}^2 + \text{c.c.}) , \\ \text{Region P : } \phi(t_P, \tilde{r}, \varphi) &= \frac{1}{\sqrt{2\pi r h}} \sum_{q \in \mathbb{Z}} \int_0^\infty \frac{d\omega}{\sqrt{4\pi\omega}} (\tilde{a}_{\omega q} G_{\omega q}^{1*} + a_{\omega q}^\dagger G_{\omega q}^{2*} + \text{c.c.}) . \end{aligned} \quad (5.32)$$

where  $G_{\omega q}^1$  and  $G_{\omega q}^2$  are analytic continuations of  $F_{\omega q}^1$  and  $F_{\omega q}^2$  respectively to behind the horizon, and are given by

$$\begin{aligned} G_{\omega q}^1 &= e^{i\delta_{\omega q}} e^{-i\omega t_F - iq\varphi} (1 - \rho)^\alpha \rho^\gamma {}_2F_1(a, b; a + b - c + 1; 1 - \rho) , \\ G_{\omega q}^2 &= e^{-i\delta_{\omega q}} e^{-i\omega t_F - iq\varphi} (1 - \rho)^{-\alpha} \rho^\gamma {}_2F_1(c - a, c - b; c - a - b + 1; 1 - \rho) . \end{aligned} \quad (5.33)$$

## 5.2 A smooth, global expression for the scalar field

Though we have obtained a globally defined expression for the scalar field, they are defined in terms of mode functions which are well-defined only in the individual four Regions of the maximally extended spacetime. For instance, the mode functions  $F_{\omega q}^i(t, r, \varphi)$  are valid only in Region I, and are analytic in the lower-half  $t$  plane. It is desirable to express the scalar field in terms of modes which are functions of the globally defined Kruskal coordinates  $U, V$ . In this subsection, we describe the mode expansion of the scalar field in terms of such modes.

### 5.2.1 The Hartle-Hawking modes

Following Unruh [69], one can obtain mode functions which are analytic in the lower half  $U$  and  $V$  planes. We review the construction of these modes in Appendix E and present the final expressions here. The mode functions which are analytic in the lower-half  $U$  and  $V$  planes are  $h_{\omega q}(U, V, \varphi)$  for both signs of  $\omega$ :

$$h_{\omega}(U, V, \varphi) = \frac{1}{\sqrt{4\pi\omega}\sqrt{2\sinh(\pi\omega/\eta)}} \begin{cases} e^{\pi\omega/2\eta}(F_{\omega q}^1 + F_{\omega q}^2) & \text{Region I} \\ e^{\pi\omega/2\eta}G_{\omega q}^1 + e^{-\pi\omega/2\eta}G_{\omega q}^2 & \text{Region F} \\ e^{-\pi\omega/2\eta}G_{\omega q}^1 + e^{\pi\omega/2\eta}G_{\omega q}^2 & \text{Region P} \\ e^{-\pi\omega/2\eta}(F_{\omega q}^1 + F_{\omega q}^2) & \text{Region II} . \end{cases} \quad (5.34)$$

These are the Hartle-Hawking mode functions. They form a complete set of functions only when we include both signs of  $\omega$ . The scalar field is then expanded as

$$\phi(U, V, \varphi) = \frac{1}{\sqrt{2\pi r h}} \sum_{q \in \mathbb{Z}} \int_{-\infty}^{\infty} d\omega \left( c_{\omega q} h_{\omega q}(U, V, \varphi) + \text{c.c.} \right) . \quad (5.35)$$

The operators  $c_{\omega q}$  for  $\omega < 0$  are sometimes written as  $\tilde{c}_{\omega q}$ :

$$\tilde{c}_{\omega q} = c_{-\omega q} , \quad \text{for } \omega > 0 . \quad (5.36)$$

The state annihilated by the  $c_{\omega q}, \tilde{c}_{\omega q}$ , for  $\omega > 0$ , is called the Hartle-Hawking vacuum:

$$c_{\omega q}|\text{HH}\rangle = \tilde{c}_{\omega q}|\text{HH}\rangle = 0 , \quad \text{for } \omega > 0, q \in \mathbb{Z} . \quad (5.37)$$

The  $c_{\omega q}$  and  $\tilde{c}_{\omega q}$  operators are related to the  $a_{\omega q}$  and  $\tilde{a}_{\omega q}$  operators since they are different expansions of the same scalar field. The relation can be obtained by comparing (5.35) with the mode expansions (5.10), (5.25) in Region I and II (see Appendix E):

$$c_{\omega q} = \frac{a_{\omega q} e^{\pi\omega/2\eta} - \tilde{a}_{\omega q}^{\dagger} e^{-\pi\omega/2\eta}}{\sqrt{2\sinh(\pi\omega/\eta)}} , \quad \tilde{c}_{\omega q} = \frac{\tilde{a}_{\omega q} e^{\pi\omega/2\eta} - a_{\omega q}^{\dagger} e^{-\pi\omega/2\eta}}{\sqrt{2\sinh(\pi\omega/\eta)}} . \quad (5.38)$$

The commutation relations for the  $c_{\omega q}$  and  $\tilde{c}_{\omega q}$  can be inferred from those of the  $a_{\omega q}$  and  $\tilde{a}_{\omega q}$ :

$$[c_{\omega q}, c_{\omega' q'}^{\dagger}] = [\tilde{c}_{\omega q}, \tilde{c}_{\omega' q'}^{\dagger}] = \delta(\omega - \omega') \delta_{qq'} , \quad [c_{\omega q}, \tilde{c}_{\omega' q'}] = [c_{\omega q}, c_{\omega' q'}] = [\tilde{c}_{\omega q}, \tilde{c}_{\omega' q'}] = 0 . \quad (5.39)$$

It is easy to see that the Hartle-Hawking vacuum is a thermal state for the Boulware excitations: the expectation value of the number operator  $a_{\omega q}^\dagger a_{\omega q}$  in  $|\text{HH}\rangle$  is

$$\langle \text{HH} | a_{\omega q}^\dagger a_{\omega q} | \text{HH} \rangle = \frac{1}{e^{2\pi\omega/\eta} - 1} \delta(\omega - \omega) , \quad (5.40)$$

where the  $\delta(0)$  is the total volume of the Region I. Note that the temperature is that of the black hole,  $\eta/2\pi$ .

### 5.2.2 Divergences in the derivatives of the Hartle-Hawking modes

While mode functions  $h_{\omega q}$  are analytic in the lower-half  $U$  and  $V$  planes by construction, they have the undesirable feature that their derivatives diverge at the horizons  $UV = 0$ . The near-horizon behaviour of  $h_{\omega q}$  is (see formulas (E.26) and (E.40) in Appendix E)

$$\frac{e^{-iq\varphi}}{\sqrt{4\pi\omega}\sqrt{2\sinh(\pi\omega/\eta)}} \begin{cases} e^{\pi\omega/2\eta} e^{i\delta_{\omega q}} (2\eta V)^{-i\omega/\eta} + e^{\pi\omega/2\eta} e^{-i\delta_{\omega q}} (-2\eta U)^{i\omega/\eta} & \text{Region I} \\ e^{\pi\omega/2\eta} e^{i\delta_{\omega q}} (2\eta V)^{-i\omega/\eta} + e^{-\pi\omega/2\eta} e^{-i\delta_{\omega q}} (2\eta U)^{i\omega/\eta} & \text{Region F} \\ e^{-\pi\omega/2\eta} e^{i\delta_{\omega q}} (-2\eta V)^{-i\omega/\eta} + e^{\pi\omega/2\eta} e^{-i\delta_{\omega q}} (-2\eta U)^{i\omega/\eta} & \text{Region P} \\ e^{-\pi\omega/2\eta} e^{i\delta_{\omega q}} (-2\eta V)^{-i\omega/\eta} + e^{-\pi\omega/2\eta} e^{-i\delta_{\omega q}} (2\eta U)^{i\omega/\eta} & \text{Region II} . \end{cases} \quad (5.41)$$

Clearly, its  $U$  and  $V$  derivatives diverge as  $1/U$  (resp.  $1/V$ ) as one approaches the horizon  $U \rightarrow 0$  (resp.  $V \rightarrow 0$ ). This results in a divergent expression for the Hamiltonian on a maximal slice since (1) the Hamiltonian involves derivatives of the scalar field, (2) the spatial integral on a maximal slice includes points on the horizons, (3) derivatives of the scalar field expanded in terms of  $h_{\omega q}$  are divergent at the horizons.

This means that the above mode expansion cannot be used in computing the Hamiltonian on a maximal slice. What we need is a mode expansion for the scalar field which is smooth everywhere, including the near-horizon region. We obtain such an expression next.

Though we have demonstrated the divergences for the BTZ black hole, this behaviour occurs for the Hartle-Hawking type mode functions associated to any black hole horizon, and, in fact, for Rindler horizons as well since they describe essential features of the near-horizon physics of black holes. This fact was already noted by Unruh [69].

### 5.2.3 Smoothing the divergences at the horizons

The derivatives of  $h_{\omega q} \sim e^{i\frac{\omega}{\eta} \log(-2\eta U)}$  go as a power of  $1/U$  near the horizon  $U = 0$ . To remove such a divergence, one can take superpositions over different  $\omega$  such that the resulting function of  $U$  decays to zero fast enough to suppress the power-law divergence in its derivatives. For example, smearing with a Gaussian  $e^{-c\omega^2}$  gives  $e^{-c'(\log U)^2}$  whose derivatives are indeed suppressed exponentially as  $U \rightarrow 0$ . Since the  $h_{\omega q}$  form a complete set of modes, it is desirable to have a complete set of smeared modes as well. For concreteness, we choose the complete set of Hermite

functions  $\psi_n(\omega/\eta)$  which contain the Gaussian factor  $e^{-\omega^2/\eta^2}$ .<sup>12 13</sup> Define

$$g_{nq}(U, V, \varphi) = \int_{-\infty}^{\infty} \frac{d\omega}{\eta} h_{\omega q}(U, V, \varphi) \psi_n(\omega/\eta) . \quad (5.42)$$

The integral over  $\omega$  has to be regulated by giving a infinitesimal imaginary part to  $\omega$ , since  $h_{\omega q}$  has a pole at  $\omega = 0$ . To see that the  $g_{nq}$  has finite derivatives with respect to  $U$  and  $V$ , let us further write  $h_{\omega q}$  in terms of its Fourier transform  $\widehat{h}_{\vartheta q}$  with respect to  $\omega$ :

$$h_{\omega q}(U, V, \varphi) = \int_{-\infty}^{\infty} d\vartheta e^{-i\omega\vartheta/\eta} \widehat{h}_{\vartheta q}(U, V, \varphi) . \quad (5.43)$$

We then have

$$\begin{aligned} g_{nq}(U, V, \varphi) &= \int_{-\infty}^{\infty} \frac{d\omega}{\eta} \psi_n(\omega/\eta) \int_{-\infty}^{\infty} d\vartheta e^{-i\omega\vartheta/\eta} \widehat{h}_{\vartheta q}(U, V, \varphi) , \\ &= \int_{-\infty}^{\infty} d\vartheta \widehat{h}_{\vartheta q}(U, V, \varphi) \int_{-\infty}^{\infty} \frac{d\omega}{\eta} \psi_n(\omega/\eta) e^{-i\omega\vartheta/\eta} , \\ &= (-i)^n \int_{-\infty}^{\infty} d\vartheta \widehat{h}_{\vartheta q}(U, V, \varphi) \psi_n(\vartheta) , \end{aligned} \quad (5.44)$$

where, in the second step we have interchanged the  $\omega$  and  $\vartheta$  integrals, and in the last step we have used the fact the Fourier transform of a Hermite function is another Hermite function.

To show that the derivatives of  $g_{nq}$  are smooth across the horizons, it is sufficient to obtain an expression for  $\widehat{h}_{\vartheta q}$  near the horizons  $UV = 0$ . This computation is complicated by the fact that the phase  $e^{i\delta_{\omega q}}$  in (5.41) arises as the phase of the following ratio of  $\Gamma$ -functions which is hard to manipulate:

$$\frac{\Gamma(\Delta_+) \Gamma(i\omega/\eta)}{\Gamma\left(\frac{1}{2}(\Delta_+ + \frac{i\omega}{\eta} - \frac{iq\ell}{r_h})\right) \Gamma\left(\frac{1}{2}(\Delta_+ + \frac{i\omega}{\eta} + \frac{iq\ell}{r_h})\right)} . \quad (5.45)$$

In the large mass limit  $m^2 \gg 1/\ell^2$ , the conformal dimension  $\Delta_+ = 1 + \sqrt{1 + \ell^2 m^2}$  is large, and the phase of the denominator in (5.45) can be neglected. In this limit,  $e^{i\delta_{\omega q}}$  is simply the phase of  $\Gamma(i\omega/\eta)$ . Note that it does not depend on any other feature of the black hole except its temperature, and is even independent of the angular momentum of the mode. This same phase in fact appears in the quantization of a scalar field in Rindler spacetime with acceleration parameter  $\eta$ . The appearance of the universal factor  $\Gamma(i\omega/\eta)$  in the phase  $e^{i\delta_{\omega q}}$  is another reflection of the fact that Rindler spacetime captures the essential features of near-horizon physics.

<sup>12</sup>There may be other choices for the smearing functions which achieve similar results. For instance, we can take Hermite functions  $\psi_n(\omega/\alpha)$  for any positive real parameter  $\alpha$ .

<sup>13</sup> The Hermite functions  $\psi_n(z)$  are defined in terms of the Hermite polynomials  $H_n(z)$  as

$$\psi_n(z) = \frac{1}{(\sqrt{\pi} 2^n n!)^{1/2}} e^{-z^2/2} H_n(z) , \quad H_n(z) = (-1)^n e^{z^2} \frac{d^n}{dz^n} e^{-z^2} .$$

They satisfy the orthogonality and completeness relations

$$\int_{-\infty}^{\infty} dz \psi_n(z) \psi_m(z) = \delta_{nm} , \quad \sum_{n=0}^{\infty} \psi_n(z) \psi_n(z') = \delta(z - z') .$$



In the large mass limit,  $\widehat{h}_{\vartheta q}(U, V, \varphi)$  takes the following form near the horizon:

$$\widehat{h}_{\vartheta q}(U, V, \varphi) \sim \frac{1}{2\pi\sqrt{2\eta}} e^{-iq\varphi} (e^{2i\eta V e^{-\vartheta}} + e^{-2i\eta U e^{\vartheta}}). \quad (5.46)$$

We derive this at the end of this subsection. Plugging this into (5.44), the smeared modes become, near the horizon,

$$g_{nq}(U, V, \varphi) \sim e^{-iq\varphi} \frac{(-i)^n}{2\pi\sqrt{2\eta}} \int_{-\infty}^{\infty} d\vartheta (e^{2i\eta V e^{-\vartheta}} + e^{-2i\eta U e^{\vartheta}}) \psi_n(\vartheta). \quad (5.47)$$

It is now manifest that the  $U$  or  $V$  derivatives of  $g_{nq}(U, V, \varphi)$  are finite in the near horizon limit: a  $U$  or  $V$  derivative brings down a  $e^{\pm\vartheta}$  but this is suppressed by the  $e^{-\vartheta^2}$  that is present in the Hermite function  $\psi_n(\vartheta)$  so that the integral is well-defined and finite.

Since the Gaussian suppression of  $\psi_n(\vartheta)$  for large  $\vartheta$  is ultimately responsible for the finiteness of the derivatives of  $g_{nq}(U, V, \varphi)$ , the finiteness of derivatives is expected to valid for general  $m^2$  as well, though the technical details will be more complicated.

**The large mass limit  $m^2 \gg 1/\ell^2$**  In the large mass limit, it was argued above that the phase  $e^{i\delta\omega q}$  receives contribution only from  $\Gamma(i\omega/\eta)$ . Using the well-known formula for  $|\Gamma(i\omega/\eta)|$ ,

$$|\Gamma(i\omega/\eta)| = \sqrt{\frac{\pi\eta}{\omega \sinh(\pi\omega/\eta)}}, \quad (5.48)$$

the near-horizon expressions for  $h_{\omega q}$  in (5.41) can be simplified in the large mass limit:

$$h_{\omega q} \sim \frac{e^{-iq\varphi}}{2\pi\sqrt{2\eta}} \begin{cases} e^{\pi\omega/2\eta}\Gamma(i\omega/\eta)(2\eta V)^{-i\omega/\eta} + e^{\pi\omega/2\eta}\Gamma(-i\omega/\eta)(-2\eta U)^{i\omega/\eta} & \text{Region I} \\ e^{\pi\omega/2\eta}\Gamma(i\omega/\eta)(2\eta V)^{-i\omega/\eta} + e^{-\pi\omega/2\eta}\Gamma(-i\omega/\eta)(2\eta U)^{i\omega/\eta} & \text{Region F} \\ e^{-\pi\omega/2\eta}\Gamma(i\omega/\eta)(-2\eta V)^{-i\omega/\eta} + e^{\pi\omega/2\eta}\Gamma(-i\omega/\eta)(-2\eta U)^{i\omega/\eta} & \text{Region P} \\ e^{-\pi\omega/2\eta}\Gamma(i\omega/\eta)(-2\eta V)^{-i\omega/\eta} + e^{-\pi\omega/2\eta}\Gamma(-i\omega/\eta)(2\eta U)^{i\omega/\eta} & \text{Region II} . \end{cases} \quad (5.49)$$

The above expressions for  $h_{\omega q}$  can be represented by a single integral:

$$h_{\omega q} \sim e^{-iq\varphi} \frac{1}{2\pi\sqrt{2\eta}} \int_{-\infty}^{\infty} d\vartheta e^{-i\omega\vartheta/\eta} (e^{2i\eta V e^{-\vartheta}} + e^{-2i\eta U e^{\vartheta}}). \quad (5.50)$$

It is easy to check that for the appropriate ranges of  $U$  and  $V$ , the above integral (after a suitable rotation of the contour to the imaginary axis) reduces to each of the four expressions in (5.49). From the above integral representation, we can extract the Fourier transform  $\widehat{h}_{\vartheta q}$  near the horizon:

$$\widehat{h}_{\vartheta q}(U, V, \varphi) \sim \frac{1}{2\pi\sqrt{2\eta}} e^{-iq\varphi} (e^{2i\eta V e^{-\vartheta}} + e^{-2i\eta U e^{\vartheta}}). \quad (5.51)$$

#### 5.2.4 The smeared modes

We have smeared the Hartle-Hawking modes  $h_{\omega q}(U, V, \varphi)$  with Hermite functions  $\psi_n(\omega/\eta)$  to obtain the smeared mode functions  $g_{nq}(U, V, \varphi)$  (5.42). Using the completeness of Hermite

functions, we can invert the relation (5.44) to get

$$h_{\omega q}(U, V, \varphi) = \sum_{n=0}^{\infty} g_{nq}(U, V, \varphi) \psi_n(\omega/\eta) . \quad (5.52)$$

Substituting the above into the mode expansion (5.35), we get a mode expansion for the scalar field in terms of the  $g_{nq}$  modes:

$$\phi(U, V, \varphi) = \frac{\sqrt{\eta}}{\sqrt{2\pi r_h}} \sum_{q \in \mathbb{Z}} \sum_{n=0}^{\infty} (e_{nq} g_{nq}(U, V, \varphi) + \text{c.c.}) , \quad (5.53)$$

where the operators  $e_{nq}$  are defined in terms of  $c_{\omega q}$  as

$$e_{nq} = \frac{1}{\sqrt{\eta}} \int_{-\infty}^{\infty} d\omega c_{\omega q} \psi_n(\omega/\eta) , \quad (5.54)$$

and satisfy the canonical commutation relations

$$[e_{mq}, e_{nq'}^\dagger] = \delta_{mn} \delta_{qq'} , \quad [e_{mq}, e_{nq'}] = [e_{mq}^\dagger, e_{nq'}^\dagger] = 0 . \quad (5.55)$$

Since  $e_{nq}$  only involve the  $c_{\omega q}$  and not the  $c_{\omega q}^\dagger$ , they also annihilate the Hartle-Hawking state  $|\text{HH}\rangle$ :

$$e_{nq} |\text{HH}\rangle = 0 , \quad n = 0, 1, \dots . \quad (5.56)$$

The mode expansion (5.53) is smooth across the horizons and globally defined in the fully extended BTZ spacetime. Once we have such an expansion, we can proceed to compute the Hamiltonian operator for the scalar field corresponding to the maximal slicing foliation. The finiteness of the derivatives of the scalar field mode expansion is important in such a computation especially because the slices of the foliation cut across the horizon.

The correlation functions of the scalar field in the Hartle-Hawking state are independent of the choice of expansion in terms of smooth mode functions, including the choice of smearing functions.

### 5.3 Hamiltonian for maximal slicing

The Hamiltonian for an arbitrary choice of lapse and shift is given by

$$H = \int d^2x \left( \frac{N}{2} \left( \frac{\pi_\phi^2}{\sqrt{g}} + \sqrt{g} g^{ij} \partial_i \phi \partial_j \phi + \sqrt{g} m^2 \phi^2 \right) + \pi_\phi N^i \partial_i \phi \right) . \quad (5.57)$$

This expression was derived classically but here we treat it as a quantum operator. From this we can also find Heisenberg equation of motion for  $\phi$  and  $\pi_\phi$ ,

$$\dot{\phi} = -i[\phi, H] = \frac{N}{\sqrt{g}} \pi_\phi + N^i \partial_i \phi \quad \longleftrightarrow \quad \pi_\phi = \sqrt{g} N^{-1} (\dot{\phi} - N^i \partial_i \phi) , \quad (5.58a)$$

$$\dot{\pi}_\phi = -i[\pi_\phi, H] = \partial_i (\sqrt{g} N g^{ij} \partial_j \phi) - \sqrt{g} N m^2 \phi + \partial_i (N^i \pi_\phi) . \quad (5.58b)$$

These agree with the classically derived equations of motion using Poisson brackets.

Recall the smooth mode expansion of the scalar field (5.53)

$$\phi = \frac{1}{\ell\sqrt{2\pi}} \sum_{q,n} (e_{nq} g_{nq}(U, V, \varphi) + \text{c.c.}) , \quad (5.59)$$

where the sum over the angular momentum quantum number  $q$  is over all integers and the sum over the mode number  $n$  is over all non-negative integers. We suppress the ranges for brevity. The conjugate momentum becomes

$$\pi_\phi = \frac{1}{\ell\sqrt{2\pi}} N^{-1} \sqrt{g} \sum_{q,n} e_{nq} (\dot{g}_{nq} - N^x g'_{nq}) + \text{c.c.} , \quad (5.60)$$

where the dot stands for  $\partial/\partial\bar{t}$  and the prime stands for  $\partial/\partial x$ .

We now evaluate the Hamiltonian for the scalar field on the maximally sliced BTZ black hole solution, presented in (4.29), Section 4.4. The Hamiltonian is then written in condensed form as

$$H = \sum_{q,q'} \sum_{n,n'} \begin{pmatrix} e_{n'q'}^\dagger & e_{n'q'} \end{pmatrix} \begin{pmatrix} A_{nn'qq'}(\bar{t}) & B_{nn'qq'}^*(\bar{t}) \\ B_{nn'qq'}(\bar{t}) & A_{nn'qq'}^*(\bar{t}) \end{pmatrix} \begin{pmatrix} e_{nq} \\ e_{nq}^\dagger \end{pmatrix} , \quad (5.61)$$

where the kernels  $A$  and  $B$  are defined as

$$A_{nn'qq'}(\bar{t}) = \frac{1}{2\pi\ell^2} \int dx d\varphi \sqrt{g} \left\{ \frac{N}{2} \left[ N^{-2} (\dot{g}_{n'q'}^* - N^x g_{n'q'}'^*) (\dot{g}_{nq} - N^x g'_{nq}) + g^{xx} g_{n'q'}'^* g'_{nq} + \right. \right. \\ \left. \left. (m^2 + qq' g^{\varphi\varphi}) g_{n'q'}^* g_{nq} \right] + N^{-1} N^x (\dot{g}_{n'q'}^* - N^x g_{n'q'}'^*) g'_{nq} \right\} . \quad (5.62)$$

and

$$B_{nn'qq'}(\bar{t}) = \frac{1}{2\pi\ell^2} \int dx d\varphi \sqrt{g} \left\{ \frac{N}{2} \left[ N^{-2} (\dot{g}_{n'q'} - N^x g_{n'q}'') (\dot{g}_{nq} - N^x g'_{nq}) + g^{xx} g_{n'q}' g'_{nq} + \right. \right. \\ \left. \left. (m^2 - qq' g^{\varphi\varphi}) g_{n'q}' g_{nq} \right] + N^{-1} N^x (\dot{g}_{n'q}' - N^x g_{n'q}'') g'_{nq} \right\} . \quad (5.63)$$

Since the mode functions  $g_{nq}$  are smooth across the horizons and fall-off at the boundary as  $x^{-\Delta_+}$ , with  $\Delta_+ > 1$ , the integrals in the above kernels  $A$  and  $B$  are finite. Note that the Hamiltonian operator is Hermitian by construction.

Since the Hamiltonian is time dependent, the evolution operator  $U(\bar{t})$  has to be constructed as the time-ordered exponential of  $H$ :

$$U(\bar{t}) = \mathcal{T} \exp \left( -i \int_0^{\bar{t}} d\bar{u} H(\bar{u}) \right) . \quad (5.64)$$

This is a *unitary* time-evolution operator which is constructed in terms of the smooth modes  $g_{nq}$  and describes the evolution of the quantum scalar field along the maximal slicing foliation.

In particular, the crossing of the horizon is described in a completely smooth manner without encountering any divergences.

The Hamiltonian (5.61) is written entirely in terms of the scalar field modes  $e_n$ . These are in fact operators on the product CFT of the two boundaries: they are smeared versions of the Hartle-Hawking modes  $c_{\omega q}$  which are related by the Bogoliubov transformations (5.38) to the Boulware operators  $a_{\omega q}, \tilde{a}_{\omega q}$ , which are themselves identified with the modes of the dual CFT operators via the extrapolate dictionary (5.18), (5.27). Hence, the Hamiltonian (5.61) serves as a time evolution operator in the dual product CFT on the two boundaries. Since the operators  $e_n$  involve a combination of both the left and right boundary operators, the evolution by this Hamiltonian in the CFT necessarily entangles the degrees of freedom in the two CFTs.

It would be interesting to explore the connection with the work of Leutheusser-Liu [24, 25] which proposes an evolution operator in the dual CFT which describes infalling observers using algebraic QFT techniques.

## Acknowledgments

We would like to thank Luis Alvarez-Gaume, Suresh Govindarajan, Alok Laddha, Raghu Mahajan, Gautam Mandal, Suvrat Raju, Ashoke Sen, Ronak Soni, Sandip Trivedi, Edward Witten, and especially Kyriakos Papadodimas for discussions. We also thank Hong Liu for a comment on an earlier draft. S. R. W. would like to thank the CERN Theory Division for hospitality, and the Infosys Foundation Homi Bhabha Chair at ICTS-TIFR for its support.

## A The Lichnerowicz equation

Here we review the proof of the existence and uniqueness of the solution to the Lichnerowicz solution in  $d = 2$  using the monotone iteration method [6–8, 44–46]. We write the equations in terms of the extrinsic curvature

$$\tilde{K}^{ij} = \tilde{g}^{-1/2}(\tilde{\pi}^{ij} - \tilde{g}^{ij}\pi) , \quad (\text{A.1})$$

and

$$\tilde{K}_\phi = \tilde{g}^{-1/2}\pi_\phi . \quad (\text{A.2})$$

The Lichnerowicz equation is

$$2\tilde{D}^2\lambda = \tilde{R} - \frac{1}{2}\tilde{g}^{ij}\partial_i\phi\partial_j\phi - (\tilde{g}_{ik}\tilde{g}_{jl}\tilde{K}^{ij}\tilde{K}^{kl} + \frac{1}{2}\tilde{K}_\phi^2)e^{-2\lambda} - (2\Lambda + V(\phi))e^{2\lambda} . \quad (\text{A.3})$$

Here,  $\tilde{g}_{ij}$  is a metric with Ricci scalar  $\tilde{R} = 2\Lambda$  (see the discussion after (3.1) in Section 3.1). Let us define

$$H(\lambda, x) \equiv \frac{1}{2}\left(\tilde{R} - \frac{1}{2}\tilde{g}^{ij}\partial_i\phi\partial_j\phi - (\tilde{g}_{ik}\tilde{g}_{jl}\tilde{K}^{ij}\tilde{K}^{kl} + \frac{1}{2}\tilde{K}_\phi^2)e^{-2\lambda} - (2\Lambda + V(\phi))e^{2\lambda}\right) . \quad (\text{A.4})$$

Let  $\lambda_\pm$  be some super- and sub-solutions respectively, i.e.,

$$\tilde{D}^2\lambda_- \geq H(\lambda_-, x) , \quad \tilde{D}^2\lambda_+ \leq H(\lambda_+, x) . \quad (\text{A.5})$$

What are appropriate sub- and super-solutions? When  $\lambda$  is large and negative, the  $e^{2\lambda}$  in (A.4) is negligible and the sum of the first two terms is large and negative. Thus,  $\lambda_- = C_-$  for a large and negative constant  $C_-$  is an appropriate sub-solution. Similarly, when  $\lambda$  is large and positive, the  $e^{2\lambda}$  term dominates if  $V(\phi) \leq 0$ ; hence, an appropriate super-solution is  $\lambda_+ = C_+$  for a large and positive constant  $C_+$ . Since the boundary condition on  $\lambda$  is that  $\lambda \rightarrow 0$  on the boundaries, we need to take  $\lambda = C_{\pm}$  till some cutoff near the boundaries and then smoothly, monotonically interpolate to zero as one approaches either boundary.

Next, define  $H_c(\lambda, x) = H(\lambda, x) - c\lambda$ . For a large and positive constant  $c$ ,  $H_c(\lambda, x)$  is a monotonically decreasing function in the interval  $[C_-, C_+]$ . Define a sequence of functions  $\lambda_0, \lambda_1, \dots$ , with  $\lambda_0 = \lambda_+$ , and

$$(\tilde{D}^2 - c)\lambda_n = H_c(\lambda_{n-1}, x), \quad \text{for } n \geq 1. \quad (\text{A.6})$$

The above equations have unique solutions since  $\tilde{D}^2 - c$  is negative definite. Suppose for some  $n$ ,  $\lambda_n \leq \lambda_+$ . This certainly true for  $n = 0$ . Then, we have

$$\begin{aligned} (\tilde{D}^2 - c)(\lambda_{n+1} - \lambda_+) &= H_c(\lambda_n, x) - \tilde{D}^2\lambda_+ + c\lambda_+ \\ &\geq H_c(\lambda_n, x) - H(\lambda_+, x) + c\lambda_+ = H_c(\lambda_n, x) - H_c(\lambda_+, x) \geq 0. \end{aligned} \quad (\text{A.7})$$

Suppose the maximum of  $\lambda_{n+1} - \lambda_+$  is positive, and is attained at some point  $x_0$ . Then, at  $x_0$ ,  $\tilde{D}^2(\lambda_{n+1} - \lambda_+)$  is negative, and  $-c(\lambda_{n+1} - \lambda_+)$  is negative as well. Thus,  $(\tilde{D}^2 - c)(\lambda_{n+1} - \lambda_+)$  is negative as well, and it contradicts the above inequality. Thus, the maximum of  $\lambda_{n+1} - \lambda_+$  is negative and hence  $\lambda_{n+1} \leq \lambda_+$ . Thus, by induction, for all  $n$ , we have  $\lambda_n \leq \lambda_+$ .

Similarly, suppose for some  $n$ , we have  $\lambda_- \leq \lambda_n$ . Then,

$$\begin{aligned} (\tilde{D}^2 - c)(\lambda_- - \lambda_{n+1}) &= \tilde{D}^2\lambda_- - c\lambda_- - H_c(\lambda_n, x) \\ &\geq H(\lambda_-, x) - c\lambda_- - H_c(\lambda_n, x) = H_c(\lambda_-, x) - H_c(\lambda_n, x) \geq 0. \end{aligned} \quad (\text{A.8})$$

If  $\lambda_- - \lambda_{n+1}$  has a maximum which is positive, and it is attained at some point  $x'_0$ , then  $\tilde{D}^2(\lambda_- - \lambda_{n+1}) < 0$  at that point, and so is  $-c(\lambda_- - \lambda_{n+1})$ . This contradicts the above inequality and hence  $\lambda_- - \lambda_{n+1} \leq 0$ . Thus, we have shown by induction in  $n$  that

$$\lambda_- \leq \lambda_n \leq \lambda_+, \quad \text{for all } n \geq 0. \quad (\text{A.9})$$

Next, suppose, for some  $n$ ,  $\lambda_n \leq \lambda_{n-1}$ . This certainly true for  $n = 1$ . Then,

$$(\tilde{D}^2 - c)(\lambda_{n+1} - \lambda_n) = H_c(\lambda_n, x) - H_c(\lambda_{n-1}, x) \geq 0. \quad (\text{A.10})$$

If the maximum of  $\lambda_{n+1} - \lambda_n$ , attained at a point  $x''_0$ , is positive, then  $(\tilde{D}^2 - c)(\lambda_{n+1} - \lambda_n) \leq 0$  at that point which is in contradiction with the above inequality. Thus,  $\lambda_{n+1} \leq \lambda_n$ . By induction, we have proved that

$$\lambda_{n+1} \leq \lambda_n, \quad \text{for all } n \geq 0. \quad (\text{A.11})$$

Since the sequence  $\{\lambda_n\}_{n \geq 0}$  is bounded and monotonically decreasing, it has a limit

$$\lim_{n \rightarrow \infty} \lambda_n \equiv \lambda ,$$

which satisfies the limit of the iterated equation

$$(\tilde{D}^2 - c)\lambda = H_c(\lambda, x) , \quad (\text{A.12})$$

which implies the Lichnerowicz equation  $\tilde{D}^2\lambda = H(\lambda, x)$ . Thus, a solution  $\lambda$  exists.

To show the uniqueness of the solution, let us first Weyl-transform back to  $g_{ij} = e^{2\lambda}\tilde{g}_{ij}$ ,  $K^{ij} = e^{-4\lambda}\tilde{K}^{ij}$ ,  $K_\phi = e^{-2\lambda}\tilde{K}_\phi$  using the solution  $\lambda$  which we know exists. Suppose there is another solution  $\lambda' \neq 0$ . Then, there is another configuration  $g'_{ij} = e^{2\lambda'}\tilde{g}_{ij}$ ,  $K'^{ij} = e^{-4\lambda'}\tilde{K}^{ij}$ ,  $\phi' = \phi$ ,  $K'_\phi = e^{-2\lambda'}\tilde{K}_\phi$ , which satisfies the Hamiltonian constraint. This implies that there is a Weyl transformation  $e^{2\hat{\lambda}} = e^{2(\lambda-\lambda')}$  such that  $g'_{ij} = e^{2\hat{\lambda}}g_{ij}$ ,  $K'^{ij} = e^{-4\hat{\lambda}}K^{ij}$ ,  $K'_\phi = e^{-2\hat{\lambda}}K_\phi$ . The Hamiltonian constraint for  $g'_{ij}, K'^{ij}, \phi, K'_\phi$  then gives the Lichnerowicz equation for  $\hat{\lambda}$ :

$$2\tilde{D}^2\hat{\lambda} = R - \frac{1}{2}g^{ij}\partial_i\phi\partial_j\phi - (g_{ik}g_{jl}K^{ij}K^{kl} + \frac{1}{2}K_\phi^2)e^{-2\hat{\lambda}} - ((2\Lambda + V(\phi))e^{2\hat{\lambda}}) . \quad (\text{A.13})$$

Here  $D_i$  is the covariant derivative compatible with  $g_{ij}$ . Since  $g_{ij}, K^{ij}, \phi, K_\phi$  satisfy the Hamiltonian constraint, we substitute it into the above equation to get

$$0 = 2D^2\hat{\lambda} + (g_{ik}g_{jl}K^{ij}K^{kl} + \frac{1}{2}K_\phi^2)(e^{-2\hat{\lambda}} - 1) + (2\Lambda + V(\phi))(e^{2\hat{\lambda}} - 1) . \quad (\text{A.14})$$

Note that  $\Lambda < 0$ . If the maximum of  $\hat{\lambda}$  is strictly positive, then at the maximum point, we have  $D^2\hat{\lambda} \leq 0$ , as well as  $e^{-2\hat{\lambda}} > 1$ , so that the right hand side is strictly negative which is a contradiction. Thus,  $\lambda \leq 0$ . Similarly, if the minimum of  $\hat{\lambda}$  is strictly negative, then the right hand side is  $> 0$  which is again a contradiction. Thus,  $\hat{\lambda} \geq 0$ . The only possibility is then  $\hat{\lambda} = 0$  so that  $\lambda = \lambda'$  and there is no other configuration  $g'_{ij}, K'^{ij}, \phi, K'_\phi$  that satisfies the Hamiltonian constraint starting from  $\tilde{g}_{ij}, \tilde{K}^{ij}, \phi, \tilde{K}_\phi$ .

## B Details of the perturbation theory analysis

To obtain the correct Hamiltonian up to  $\mathcal{O}(\kappa^0)$ , we start with the original action

$$\begin{aligned} \mathcal{S} &= \int dt \int_\Sigma d^d x \left( \pi^{ij}\dot{g}_{ij} - N\mathcal{H}_\perp - N_i\mathcal{H}^i \right) - \int dt \int_{\partial\Sigma} d^{d-1}\sigma \mathcal{B} , \\ &= \frac{1}{\kappa^2} \int dt \int_\Sigma d^d x \left( P^{ij}\dot{g}_{ij} - N \left( \frac{1}{\sqrt{g}}(P^{ij}P_{ij} - \frac{1}{d-1}P^2) - \sqrt{g}(R - 2\Lambda) \right) - 2D_i N_j P^{ij} \right) \\ &\quad + \int dt \int_\Sigma d^d x \left( \pi_\phi \dot{\phi} - N \left( \frac{1}{2\sqrt{g}}\pi_\phi^2 + \sqrt{g}(\frac{1}{2}g^{ij}\partial_i\phi\partial_j\phi + V(\phi)) \right) - N_i g^{ij} \pi_\phi \partial_j \phi \right) \\ &\quad - \frac{2}{\kappa^2} \int dt \int_{\partial\Sigma} d^{d-1}\sigma \left( -N\sqrt{\sigma}k + r_i N_j P^{ij} \right) . \end{aligned} \quad (\text{B.1})$$

The perturbation expansion of the various fields is

$$g_{ij} = \hat{g}_{ij} + \kappa h_{ij} , \quad P^{ij} = \hat{P}^{ij} + \kappa p^{ij} , \quad N_i = \hat{N}_i + \kappa \beta_i , \quad N = \hat{N}(1 + \kappa \alpha) . \quad (\text{B.2})$$

For convenience, we consider fluctuations with compact support so that the boundary terms do not contribute in the action and in any partial integrations below. As stated in the main text, one could allow slightly more general fluctuations which fall off sufficiently fast near the boundary.

Let us expand the above in a series in  $\kappa$  and retain terms from  $\mathcal{O}(\kappa^{-2})$  till  $\mathcal{O}(\kappa^0)$ . Foremost, note that since the scalar field is already at  $\mathcal{O}(\kappa^0)$ , the metric, lapse and shift that appear in the scalar field part of the action will just be the background values. Thus, at this order, the scalar and gravitational fluctuations are *not* coupled.

**Note:** The tensor indices are lowered and raised by the background metric  $\hat{g}_{ij}$  and its inverse  $\hat{g}^{ij}$ .

We give the expressions for various terms that appear in the Lagrangian from  $\mathcal{O}(\kappa^0)$  to  $\mathcal{O}\kappa^2$ , so that they contribute to the action from  $\mathcal{O}(\kappa^{-2})$  up to  $\mathcal{O}(\kappa^0)$ .

The expansion of  $\sqrt{g}$  and  $1/\sqrt{g}$ :

$$\sqrt{g} = \sqrt{\hat{g}} \left( 1 + \frac{\kappa}{2} h + \frac{\kappa^2}{4} (\frac{1}{2} h^2 - h^{ij} h_{ij}) \right), \quad \frac{1}{\sqrt{g}} = \frac{1}{\sqrt{\hat{g}}} \left( 1 - \frac{\kappa}{2} h + \frac{\kappa^2}{4} (h^{ij} h_{ij} + \frac{1}{2} h^2) \right). \quad (\text{B.3})$$

The covariant derivative  $D_i$  corresponding to  $g_{ij}$ , with  $\xi_i$  an arbitrary vector field:

$$D_i \xi_j - \hat{D}_i \xi_j = -\frac{1}{2} \xi_k g^{kl} \kappa C_{ijl} = -\frac{1}{2} \xi_k g^{kl} \kappa (\hat{D}_i h_{lj} + \hat{D}_j h_{il} - \hat{D}_l h_{ij}), \quad (\text{B.4})$$

The  $P^{ij} \dot{g}_{ij}$  term:

$$P^{ij} \dot{g}_{ij} = \hat{P}^{ij} \dot{\hat{g}}_{ij} + \kappa (p^{ij} \dot{\hat{g}}_{ij} + \hat{P}^{ij} \dot{h}_{ij}) + \kappa^2 p^{ij} \dot{h}_{ij}. \quad (\text{B.5})$$

The  $P^{ij} P_{ij} - \frac{1}{d-1} P^2$  term:

$$\begin{aligned} P^{ij} P_{ij} - \frac{1}{d-1} P^2 &= \hat{P}^{ij} \hat{P}_{ij} - \frac{1}{d-1} \hat{P}^2 + \kappa \left( 2 \hat{P}^{ij} p_{ij} + 2 h_{ik} \hat{P}^k{}_j \hat{P}^{ij} - \frac{1}{d-1} (2 \hat{P} p + 2 \hat{P} \hat{P}^{ij} h_{ij}) \right) \\ &\quad + \kappa^2 \left( p^{ij} p_{ij} + 2 p^{ij} h_{ik} \hat{P}^k{}_j + \hat{P}^{ij} \hat{P}^{kl} h_{ik} h_{jl} + 2 \hat{P}^{ij} h_{ik} p^k{}_j \right. \\ &\quad \left. - \frac{1}{d-1} (p^2 + 2 \hat{P}^{ij} h_{ij} p + (\hat{P}^{ij} h_{ij})^2 + 2 \hat{P} h_{ij} p^{ij}) \right). \end{aligned} \quad (\text{B.6})$$

The Ricci scalar:

$$\begin{aligned} R &= \hat{R} + \kappa (\hat{D}^a \hat{D}^b h_{ab} - \hat{D}^2 h - h^{ac} \hat{R}_{ac}) \\ &\quad + \kappa^2 \left( \frac{3}{4} \hat{D}^a h^{bc} \hat{D}_a h_{bc} + h^{ab} \hat{D}^2 h_{ab} - \hat{D}_b h^{bc} \hat{D}^a h_{ac} - h^{bc} \hat{D}_b \hat{D}^a h_{ac} \right. \\ &\quad + h^{ab} \hat{D}_a \hat{D}_b h + \hat{D}_a h^{ac} \hat{D}_c h - \frac{1}{2} \hat{D}_b h^{ac} \hat{D}_a h^b{}_c - \frac{1}{4} \hat{D}^a h \hat{D}_a h \\ &\quad \left. - h^{ac} \hat{D}_b \hat{D}_a h^b{}_c + h^{ae} h_e{}^c \hat{R}_{ac} \right). \end{aligned} \quad (\text{B.7})$$

The combinations  $N/\sqrt{g}$  and  $N\sqrt{g}$ :

$$\begin{aligned}\frac{N}{\sqrt{g}} &= \frac{\hat{N}}{\sqrt{\hat{g}}} \left( 1 + \kappa(\alpha - \frac{1}{2}h) + \kappa^2 \left( -\frac{1}{2}\alpha h + \frac{1}{4}(h^{ij}h_{ij} + \frac{1}{2}h^2) \right) \right), \\ N\sqrt{g} &= \hat{N}\sqrt{\hat{g}} \left( 1 + \kappa(\alpha + \frac{1}{2}h) + \kappa^2 \left( \frac{1}{2}\alpha h + \frac{1}{4}(\frac{1}{2}h^2 - h_{ij}h^{ij}) \right) \right).\end{aligned}\quad (\text{B.8})$$

The momentum part of the Hamiltonian constraint:

$$\begin{aligned}\frac{N}{\sqrt{g}} \left( P^{ij}P_{ij} - \frac{1}{d-1}P^2 \right) \\ = \frac{\hat{N}}{\sqrt{\hat{g}}} \left( \hat{P}^{ij}\hat{P}_{ij} - \frac{1}{d-1}\hat{P}^2 \right. \\ + \kappa \left( (\alpha - \frac{1}{2}h)(\hat{P}^{ij}\hat{P}_{ij} - \frac{1}{d-1}\hat{P}^2) + 2\hat{P}^{ij}p_{ij} + 2h_{ik}\hat{P}^k{}_j\hat{P}^{ij} - \frac{1}{d-1}(2\hat{P}p + 2\hat{P}\hat{P}^{ij}h_{ij}) \right) \\ + \kappa^2 \left( (\alpha - \frac{1}{2}h)(2\hat{P}^{ij}p_{ij} + 2h_{ik}\hat{P}^k{}_j\hat{P}^{ij} - \frac{1}{d-1}(2\hat{P}p + 2\hat{P}\hat{P}^{ij}h_{ij})) \right. \\ + \left( -\frac{1}{2}\alpha h + \frac{1}{4}(h^{ij}h_{ij} + \frac{1}{2}h^2) \right) (\hat{P}^{ij}\hat{P}_{ij} - \frac{1}{d-1}\hat{P}^2) \\ + p^{ij}p_{ij} + 2p^{ij}h_{ik}\hat{P}^k{}_j + \hat{P}^{ij}\hat{P}^{kl}h_{ik}h_{jl} + 2\hat{P}^{ij}h_{ik}p^k{}_j \\ \left. \left. - \frac{1}{d-1}(p^2 + 2\hat{P}^{ij}h_{ij}p + (\hat{P}^{ij}h_{ij})^2 + 2\hat{P}h_{ij}p^{ij}) \right) \right).\end{aligned}\quad (\text{B.9})$$

The Ricci scalar part of the Hamiltonian constraint:

$$\begin{aligned}N\sqrt{g}(R - 2\Lambda) &= \hat{N}\sqrt{\hat{g}} \left( \hat{R} - 2\Lambda + \kappa \left( (\alpha + \frac{1}{2}h)(\hat{R} - 2\Lambda) + \hat{D}^a\hat{D}^bh_{ab} - \hat{D}^2h - h^{ac}\hat{R}_{ac} \right) \right. \\ &+ \kappa^2 \left( (\frac{1}{2}\alpha h + \frac{1}{4}(\frac{1}{2}h^2 - h_{ij}h^{ij}))(\hat{R} - 2\Lambda) \right. \\ &+ (\alpha + \frac{1}{2}h)(\hat{D}^a\hat{D}^bh_{ab} - \hat{D}^2h - h^{ac}\hat{R}_{ac}) \\ &+ \frac{3}{4}\hat{D}^ah^{bc}\hat{D}_ah_{bc} + h^{ab}\hat{D}^2h_{ab} - \hat{D}_bh^{bc}\hat{D}^ah_{ac} - h^{bc}\hat{D}_b\hat{D}^ah_{ac} \\ &+ h^{ab}\hat{D}_a\hat{D}_bh + \hat{D}_ah^{ac}\hat{D}_ch - \frac{1}{2}\hat{D}_bh^{ac}\hat{D}_ah^b{}_c - \frac{1}{4}\hat{D}^ah\hat{D}_ah \\ &\left. \left. - h^{ac}\hat{D}_b\hat{D}_ah^b{}_c + h^{ae}h_e{}^c\hat{R}_{ac} \right) \right).\end{aligned}\quad (\text{B.10})$$

Thus, we can write the Hamiltonian constraint in a series in  $\kappa$ :

$$N\mathcal{H}_\perp = \hat{N}\hat{\mathcal{H}}_\perp + \kappa\mathcal{H}_{\perp 1} + \kappa^2\mathcal{H}_{\perp 2}, \quad (\text{B.11})$$

with

$$\hat{N}\hat{\mathcal{H}}_\perp = \hat{N} \left( \frac{1}{\sqrt{\hat{g}}} (\hat{P}^{ij}\hat{P}_{ij} - \frac{1}{d-1}\hat{P}^2) - \sqrt{\hat{g}}(\hat{R} - 2\Lambda) \right). \quad (\text{B.12})$$

$$\begin{aligned}\mathcal{H}_{\perp 1} &= \frac{\hat{N}}{\sqrt{\hat{g}}} \left( (\alpha - \frac{1}{2}h)(\hat{P}^{ij}\hat{P}_{ij} - \frac{1}{d-1}\hat{P}^2) + 2\hat{P}^{ij}p_{ij} + 2h_{ik}\hat{P}^k{}_j\hat{P}^{ij} - \frac{1}{d-1}(2\hat{P}p + 2\hat{P}\hat{P}^{ij}h_{ij}) \right) \\ &- \hat{N}\sqrt{\hat{g}} \left( (\alpha + \frac{1}{2}h)(\hat{R} - 2\Lambda) + \hat{D}^a\hat{D}^bh_{ab} - \hat{D}^2h - h^{ac}\hat{R}_{ac} \right),\end{aligned}\quad (\text{B.13})$$



and

$$\begin{aligned}
\mathcal{H}_{\perp 2} = & \frac{\hat{N}}{\sqrt{\hat{g}}} \left( (\alpha - \frac{1}{2}h)(2\hat{P}^{ij}p_{ij} + 2h_{ik}\hat{P}^k{}_j\hat{P}^{ij} - \frac{1}{d-1}(2\hat{P}p + 2\hat{P}\hat{P}^{ij}h_{ij})) \right. \\
& + (-\frac{1}{2}\alpha h + \frac{1}{4}(h^{ij}h_{ij} + \frac{1}{2}h^2))(\hat{P}^{ij}\hat{P}_{ij} - \frac{1}{d-1}\hat{P}^2) \\
& + p^{ij}p_{ij} + 2p^{ij}h_{ik}\hat{P}^k{}_j + \hat{P}^{ij}\hat{P}^{kl}h_{ik}h_{jl} + 2\hat{P}^{ij}h_{ik}p^k{}_j \\
& \left. - \frac{1}{d-1}(p^2 + 2\hat{P}^{ij}h_{ij}p + (\hat{P}^{ij}h_{ij})^2 + 2\hat{P}h_{ij}p^{ij}) \right) \\
& - \hat{N}\sqrt{\hat{g}} \left( (\frac{1}{2}\alpha h + \frac{1}{4}(\frac{1}{2}h^2 - h_{ij}h^{ij}))(\hat{R} - 2\Lambda) \right. \\
& + (\alpha + \frac{1}{2}h)(\hat{D}^a\hat{D}^bh_{ab} - \hat{D}^2h - h^{ac}\hat{R}_{ac}) \\
& + \frac{3}{4}\hat{D}^ah^{bc}\hat{D}_ah_{bc} + h^{ab}\hat{D}^2h_{ab} - \hat{D}_bh^{bc}\hat{D}^ah_{ac} - h^{bc}\hat{D}_b\hat{D}^ah_{ac} \\
& + h^{ab}\hat{D}_a\hat{D}_bh + \hat{D}_ah^{ac}\hat{D}_ch - \frac{1}{2}\hat{D}_bh^{ac}\hat{D}_ah^b{}_c - \frac{1}{4}\hat{D}^ah\hat{D}_ah \\
& \left. - h^{ac}\hat{D}_b\hat{D}_ah^b{}_c + h^{ae}h_e{}^c\hat{R}_{ac} \right). \tag{B.14}
\end{aligned}$$

The momentum constraint:

$$\begin{aligned}
2D_iN_jP^{ij} = & 2\left(\hat{D}_i\hat{N}_j + \kappa(\hat{D}_i\beta_j - \frac{1}{2}\hat{N}^lC_{ijl}) + \frac{\kappa^2}{2}(\hat{N}_kh^{kl}C_{ijl} - \beta^lC_{ijl})\right)(\hat{P}^{ij} + \kappa p^{ij}) \\
= & 2\hat{D}_i\hat{N}_j\hat{P}^{ij} + \kappa\left((2\hat{D}_i\beta_j - \hat{N}^lC_{ijl})\hat{P}^{ij} + 2\hat{D}_i\hat{N}_jp^{ij}\right) \\
& + \kappa^2\left((2\hat{D}_i\beta_j - \hat{N}^lC_{ijl})p^{ij} + (\hat{N}_kh^{kl} - \beta^l)C_{ijl}\hat{P}^{ij}\right). \tag{B.15}
\end{aligned}$$

The action can be written as

$$\mathcal{S} = \frac{1}{\kappa^2} \int dt \int_{\Sigma} d^d x (\hat{\mathcal{L}} + \kappa\mathcal{L}_1 + \kappa^2\mathcal{L}_2), \tag{B.16}$$

with

$$\hat{\mathcal{L}} = \hat{P}^{ij}\dot{\hat{g}}_{ij} - \hat{N}\left(\frac{1}{\sqrt{\hat{g}}}(\hat{P}^{ij}\hat{P}_{ij} - \frac{1}{d-1}\hat{P}^2) - \sqrt{\hat{g}}(\hat{R} - 2\Lambda)\right) - 2\hat{D}_i\hat{N}_j\hat{P}^{ij}, \tag{B.17}$$

$$\begin{aligned}
\mathcal{L}_1 = & p^{ij}\left(\dot{\hat{g}}_{ij} - \frac{\hat{N}}{\sqrt{\hat{g}}}(2\hat{P}_{ij} - \frac{1}{d-1}2\hat{P}\hat{g}_{ij}) - 2\hat{D}_{(i}\hat{N}_{j)}\right) \\
& + h_{ij}\left(-\dot{\hat{P}}^{ij} + \frac{1}{2}\frac{\hat{N}}{\sqrt{\hat{g}}}\hat{g}^{ij}(\hat{P}^{ab}\hat{P}_{ab} - \frac{1}{d-1}\hat{P}^2) - 2\frac{\hat{N}}{\sqrt{\hat{g}}}\hat{P}^j{}_a\hat{P}^{ai} + \frac{1}{d-1}\frac{\hat{N}}{\sqrt{\hat{g}}}2\hat{P}\hat{P}^{ij} \right. \\
& + \hat{N}\sqrt{\hat{g}}\frac{1}{2}\hat{g}^{ij}(\hat{R} - 2\Lambda) + \sqrt{\hat{g}}\hat{D}^i\hat{D}^j\hat{N} - \sqrt{\hat{g}}\hat{D}^2\hat{N} - \hat{N}\sqrt{\hat{g}}\hat{R}^{ij} \\
& \left. + \hat{D}_l(\hat{N}^l\hat{P}^{ij}) - \hat{D}_k(\hat{N}^j\hat{P}^{ik}) - \hat{D}_k(\hat{N}^i\hat{P}^{kj})\right) \\
& + \alpha\left(-\frac{\hat{N}}{\sqrt{\hat{g}}}(\hat{P}^{ij}\hat{P}_{ij} - \frac{1}{d-1}\hat{P}^2) + \hat{N}\sqrt{\hat{g}}(\hat{R} - 2\Lambda) \right. \\
& \left. - 2\hat{D}_i\beta_j\hat{P}^{ij}\right). \tag{B.18}
\end{aligned}$$

$$\begin{aligned}
\mathcal{L}_2 = & p^{ij} \dot{h}_{ij} \\
& + \alpha \left( -\frac{\hat{N}}{\sqrt{\hat{g}}} (2\hat{P}^{ij} p_{ij} + 2h_{ik} \hat{P}^k{}_j \hat{P}^{ij} - \frac{1}{d-1} (2\hat{P}p + 2\hat{P}\hat{P}^{ij} h_{ij})) \right. \\
& \quad + \frac{\hat{N}}{\sqrt{\hat{g}}} \frac{1}{2} h (\hat{P}^{ij} \hat{P}_{ij} - \frac{1}{d-1} \hat{P}^2) + \hat{N} \sqrt{\hat{g}} \frac{1}{2} h (\hat{R} - 2\Lambda) \\
& \quad \left. + \hat{N} \sqrt{\hat{g}} (\hat{D}^a \hat{D}^b h_{ab} - \hat{D}^2 h - h^{ac} \hat{R}_{ac}) \right) \\
& - 2\hat{D}_i \beta_j p^{ij} + \beta^l (\hat{D}_i h_{lj} + \hat{D}_j h_{il} - \hat{D}_l h_{ij}) \hat{P}^{ij} \\
& - \frac{\hat{N}}{\sqrt{\hat{g}}} \left( -\frac{1}{2} h (2\hat{P}^{ij} p_{ij} + 2h_{ik} \hat{P}^k{}_j \hat{P}^{ij} - \frac{1}{d-1} (2\hat{P}p + 2\hat{P}\hat{P}^{ij} h_{ij})) \right. \\
& \quad + \frac{1}{4} (h^{ij} h_{ij} + \frac{1}{2} h^2) (\hat{P}^{ij} \hat{P}_{ij} - \frac{1}{d-1} \hat{P}^2) \\
& \quad + p^{ij} p_{ij} + 2p^{ij} h_{ik} \hat{P}^k{}_j + \hat{P}^{ij} \hat{P}^{kl} h_{ik} h_{jl} + 2\hat{P}^{ij} h_{ik} p^k{}_j \\
& \quad \left. - \frac{1}{d-1} (p^2 + 2\hat{P}^{ij} h_{ij} p + (\hat{P}^{ij} h_{ij})^2 + 2\hat{P} h_{ij} p^{ij}) \right) \\
& + \hat{N} \sqrt{\hat{g}} \left( \frac{1}{4} (\frac{1}{2} h^2 - h_{ij} h^{ij}) (\hat{R} - 2\Lambda) \right. \\
& \quad + \frac{1}{2} h (\hat{D}^a \hat{D}^b h_{ab} - \hat{D}^2 h - h^{ac} \hat{R}_{ac}) \\
& \quad + \frac{3}{4} \hat{D}^a h^{bc} \hat{D}_a h_{bc} + h^{ab} \hat{D}^2 h_{ab} - \hat{D}_b h^{bc} \hat{D}^a h_{ac} - h^{bc} \hat{D}_b \hat{D}^a h_{ac} \\
& \quad + h^{ab} \hat{D}_a \hat{D}_b h + \hat{D}_a h^{ac} \hat{D}_c h - \frac{1}{2} \hat{D}_b h^{ac} \hat{D}_a h^b{}_c - \frac{1}{4} \hat{D}^a h \hat{D}_a h \\
& \quad \left. - h^{ac} \hat{D}_b \hat{D}_a h^b{}_c + h^{ae} h_e{}^c \hat{R}_{ac} \right), \\
& + \hat{N}^l C_{ijl} p^{ij} - \hat{N}_k h^{kl} C_{ijl} \hat{P}^{ij}. \tag{B.19}
\end{aligned}$$

Some important points about the Lagrangian above are as follows:

1. The piece  $\hat{\mathcal{L}}$  is the original Lagrangian evaluated on the background and is equal to  $\hat{P}^{ij} \dot{g}_{ij}$  since the background satisfies the Hamiltonian and momentum constraints.
2. In the piece  $\mathcal{L}_1$  which is linear in the perturbations, the coefficients of each of the perturbations  $\alpha$ ,  $\beta_i$ ,  $h_{ij}$  and  $p^{ij}$  are the background equations of motion in Hamiltonian form. Hence  $\mathcal{L}_1 = 0$  when the background quantities satisfy the equations of motion.
3. The quadratic piece  $\mathcal{L}_2$  involve the lapse and shift fluctuations,  $\alpha$  and  $\beta_i$  respectively, only linearly and without time derivatives. Thus, these are Lagrange multipliers and their equations of motion are constraints on the fluctuations  $h_{ij}$  and  $p^{ij}$ .
4. Most importantly, the quadratic piece  $\mathcal{L}_2$  also contains terms which are *not* constraints and specify the non-trivial dynamics on the phase space of fluctuating degrees of freedom.

## C More details of the maximally sliced BTZ black hole solution

We give details of the solution of the Einstein's equations in maximal slicing gauge in 2 + 1 dimensions. The general ADM ansatz for a non-rotating metric is

$$\begin{aligned}
ds^2 = & -\alpha(r, \bar{t})^2 d\bar{t}^2 + A(r, \bar{t}) \left( dr + \frac{\beta(r, \bar{t})}{A(r, \bar{t})} d\bar{t} \right)^2 + r^2 d\varphi^2, \\
= & - \left( \alpha(r, \bar{t})^2 - \frac{\beta(r, \bar{t})^2}{A(r, \bar{t})} \right) d\bar{t}^2 + 2\beta(r, \bar{t}) d\bar{t} dr + A(r, \bar{t}) dr^2 + r^2 d\varphi^2. \tag{C.1}
\end{aligned}$$

We use the notation  $\dot{\phantom{x}}$  to denote a derivative with respect to the time  $\bar{t}$ .

### C.1 Solving the constraint equations in maximal slicing gauge

Let us first solve the Hamiltonian constraint  $\mathcal{H}_\perp = K^{ij}K_{ij} - K^2 - R + 2\Lambda = 0$  and momentum constraints  $\mathcal{H}^j = -2D_i K^{ij}$ . The spatial metric is

$$ds^2 = g_{ij}dx^i dx^j = A(r)dr^2 + r^2 d\varphi^2 . \quad (\text{C.2})$$

The constraint equations simplify in the above spatial coordinate system with the maximal slicing gauge  $g^{ij}K_{ij} = 0$ . The maximal slicing condition is

$$A^{-1}K_{rr} + r^{-2}K_{\varphi\varphi} = 0 . \quad (\text{C.3})$$

The momentum constraint  $\mathcal{H}^\varphi$  is automatically satisfied due to the angular symmetry. The radial momentum constraint  $\mathcal{H}^r$  becomes the simple equation

$$\partial_r K_{\varphi\varphi} = 0 , \quad \text{with solution} \quad K_{\varphi\varphi} = -T . \quad (\text{C.4})$$

The Ricci scalar of  $g_{ij}$  is

$$R = \frac{\partial_r A}{rA^2} . \quad (\text{C.5})$$

The Hamiltonian constraint becomes the following first order equation for  $A$ :

$$2\frac{T^2}{r^4} - \frac{\partial_r A}{rA^2} + 2\Lambda = 0 , \quad (\text{C.6})$$

whose solution is

$$A(r) = \left( \frac{r^2}{\ell^2} - 8G_N M + \frac{T^2}{r^2} \right)^{-1} , \quad (\text{C.7})$$

where  $8G_N M$  is the integration constant. It turns out that  $M$  will be ADM mass of the solution, and we show below that it is a constant under time evolution using the  $\dot{K}_{rr}$  Einstein equation.

Thus, the phase space is characterized by the two variables  $M$  and  $T$  arising from the metric and extrinsic curvature respectively. Time evolution is represented as a trajectory in the two dimensional phase space  $(M(\bar{t}), T(\bar{t}))$  with time parameter  $\bar{t}$  that enters in the ADM ansatz (C.1). In fact, any large diffeomorphism can be represented as a transformation in  $(M, T)$  space.

### C.2 Solving for the lapse and shift

We next solve for the lapse and shift. With the ADM form of the metric (C.1), we compute the extrinsic curvature  $K_{ij} = \frac{1}{2N}(\dot{g}_{ij} - 2D_{(i}N_{j)})$  on a constant  $\bar{t}$  slice:<sup>14</sup>

$$K_{rr} = \frac{1}{2\alpha} \left( \partial_{\bar{t}} A + \beta \frac{\partial_r A}{A} - 2\partial_r \beta \right) , \quad K_{\varphi\varphi} = -\frac{r\beta}{A\alpha} . \quad (\text{C.8a})$$

---

<sup>14</sup>It is convenient to use a Mathematica package such as `diffgeo.m` by Matthew Headrick.

The Hamiltonian constraint, the radial momentum constraint and the maximal slicing condition become

$$\text{Hamiltonian constraint } \mathcal{H}_\perp : \quad r\partial_r \log A - 2\Lambda r^2 A - 2\frac{\beta^2}{A\alpha^2} = 0 , \quad (\text{C.9a})$$

$$\text{Momentum constraint } \mathcal{H}^r : \quad \partial_r \left( \frac{r\beta}{A\alpha} \right) = 0 , \quad (\text{C.9b})$$

$$K = 0 : \quad \partial_{\bar{t}} A - \beta \partial_r \log \left( \frac{r^2 \beta^2}{A} \right) = 0 , \quad (\text{C.9c})$$

$$\dot{K} = 0 : \quad \left( \partial_r^2 + \frac{1}{r} \partial_r - \frac{\partial_r A}{2A} \partial_r - \frac{\partial_r A}{rA} + 4\Lambda A \right) \alpha = 0 . \quad (\text{C.9d})$$

Recall that we have already solved the first two equations, with the solution

$$A(r, \bar{t}) = \left( \frac{r^2}{\ell^2} - 8G_N M + \frac{T(\bar{t})^2}{r^2} \right)^{-1} , \quad \frac{r\beta}{A\alpha} = T(\bar{t}) . \quad (\text{C.10})$$

The third equation  $K = 0$  can now be solved for  $\alpha$  to get

$$\alpha(r, \bar{t}) = A(r, \bar{t})^{-1/2} \left[ c - \partial_{\bar{t}} T \int_\infty^r \frac{d\rho}{\rho} \left( \frac{\rho^2}{\ell^2} - 8G_N M + \frac{T(\bar{t})^2}{\rho^2} \right)^{-3/2} \right] . \quad (\text{C.11})$$

The integration constant is  $c$ , and is imposed as a boundary condition on  $\alpha$  as  $r \rightarrow \infty$ :

$$\lim_{r \rightarrow \infty} \alpha = c \frac{r}{\ell} , \quad (\text{C.12})$$

which is the familiar asymptotic AdS boundary condition for the lapse. The last equation  $\dot{K} = 0$  is the statement that the maximal slicing condition is maintained under time evolution. One can check that the solution (C.11) for  $\alpha$  satisfies (C.9d). Note that  $T$  as a function of  $\bar{t}$  is still undetermined.

Now we show that  $M$  is a constant under time evolution by using the  $\dot{K}_{rr}$  Einstein equation for the metric (C.1)

$$\dot{K}_{rr} = D_r D_r \alpha + (R_{rr} + K K_{rr} - 2K_{rr}^2 g^{rr}) \alpha + \frac{\beta}{A} \partial_r K_{rr} + 2K_{rr} \partial_r \frac{\beta}{A} + 2\alpha \Lambda g_{rr} . \quad (\text{C.13})$$

We use the  $\dot{K} = 0$  equation (C.9d) to rewrite second derivative above in terms of only single derivatives, i.e.,

$$D_r D_r \alpha = -\frac{1}{r} \partial_r \alpha + \frac{\alpha}{r} \partial_r \log A - 4\alpha \Lambda A .$$

Now we plug in

$$K = 0 , \quad K_{rr} = -\frac{\beta}{r\alpha} , \quad \beta = \frac{\alpha A T}{r} , \quad g_{rr} = A = \frac{1}{g^{rr}} , \quad R_{rr} = \frac{1}{2r} \partial_r \log A ,$$

and use (C.9c) to replace every occurrence of  $\partial_r \alpha$  in terms of derivatives of  $A$ :

$$\partial_r \alpha = \frac{r}{2T} \partial_{\bar{t}} \log A - \frac{\alpha}{2} \partial_r A .$$

Finally using the expression (C.7) for  $A$ , we find that the equation (C.13) implies that  $\dot{M} = 0$ .

Thus, the solution to the Einstein's equations in maximal slicing gauge is

$$\begin{aligned} ds^2 &= -\alpha(r, \bar{t})^2 d\bar{t}^2 + A(r, \bar{t}) \left( dr + \frac{\alpha(r, \bar{t})T(\bar{t})}{r} d\bar{t} \right)^2 + r^2 d\varphi^2, \\ A(r, \bar{t}) &= \left( \frac{r^2}{\ell^2} - 8G_N M + \frac{T(\bar{t})^2}{r^2} \right)^{-1}, \\ \alpha(r, \bar{t}) &= A(r, \bar{t})^{-1/2} \left[ c - \partial_{\bar{t}} T(\bar{t}) \int_{\infty}^r \frac{d\rho}{\rho} \left( \frac{\rho^2}{\ell^2} - 8G_N M + \frac{T(\bar{t})^2}{\rho^2} \right)^{-3/2} \right]. \end{aligned} \quad (\text{C.14})$$

The above solution has a coordinate singularity at  $r = R_+(T)$  where  $R_+(T)$  is a root of the equation  $r^4 - 8G_N M \ell^2 r^2 + \ell^2 T^2 = 0$ , see below. Thus, a diffeomorphism to the fully extended BTZ black hole will only cover a portion of the Kruskal diagram that is connected to one of the two boundaries. We choose the above solution to be diffeomorphic to a region of the BTZ solution that includes the boundary Region I.

### C.3 Diffeomorphism to the BTZ black hole

Recall the standard BTZ metric in Region I:

$$ds^2 = -f(r)^2 dt^2 + f(r)^{-1} dr^2 + r^2 d\varphi^2; \quad f(r) = \frac{r^2}{\ell^2} - 8G_N M. \quad (\text{C.15})$$

The simplest diffeomorphism keeps the radial coordinate  $r$  and angle  $\varphi$  the same, and writing  $t = t(r, \bar{t})$ , i.e., considering the BTZ time  $t$  as a function of  $\bar{t}$  and  $r$ . Plugging this into (C.15) and comparing with (C.1), we get

$$\partial_{\bar{t}} t = \epsilon \alpha \sqrt{A}, \quad \partial_r t = -\epsilon \frac{T \sqrt{A}}{r f(r)}, \quad (\text{C.16})$$

where  $\epsilon$  is a sign. In Region I for  $t > 0$ , since  $t$  increases as  $r$  decreases along a putative maximal slice, we must choose  $\epsilon = +1$ . Similarly,  $\epsilon = -1$  for the  $t < 0$  part of Region I. This can be seen by tracking the change in  $r$  and  $t$  along a maximal slice in Figure 3.

Suppose we consider a maximal slice that starts at the boundary in the  $t > 0$  part of Region I. Then, the first equation in (C.16) gives

$$\lim_{r \rightarrow \infty} t = ct + t_0, \quad (\text{C.17})$$

where  $t_0$  is an arbitrary constant which sets the origin of time on the boundary in Region I. The diffeomorphism in Region F to the BTZ metric

$$ds^2 = -f(r)^2 dt_F^2 + f(r)^{-1} dr^2 + r^2 d\varphi^2, \quad r < \ell \sqrt{8G_N M}, \quad (\text{C.18})$$

is

$$\partial_{\bar{t}} t_F = \epsilon \alpha \sqrt{A}, \quad \partial_r t_F = -\epsilon \frac{T \sqrt{A}}{r f(r)}, \quad (\text{C.19})$$

where the sign  $\epsilon$  must be chosen to be  $+1$  for the  $t_F > 0$  part of Region F and  $-1$  in the  $t_F < 0$  part of Region F. Note that the derivative  $\partial t_F / \partial r$  blows up at the roots  $R_{\pm}(T)$  of the equation  $r^4 - 8G_N M \ell^2 r^2 + T^2 \ell^2 = 0$  which appears in the  $\sqrt{A}$  factor on the right hand side. The roots are

$$R_{\pm}(T) = \ell \sqrt{4G_N M} \left[ 1 \pm \sqrt{1 - \left( \frac{T(\bar{t})}{4G_N M \ell} \right)^2} \right]^{1/2}, \quad (\text{C.20})$$

and they are located behind the horizon  $R_- \leq R_+ \leq \ell \sqrt{8G_N M}$ . The metric component  $g_{rr} = A(r)$  also blows up at the same values of  $r$ , and hence these are coordinate singularities. Another implication of the divergence in  $\partial t_F / \partial r$  is that the constant  $\bar{t}$  slice becomes tangent to the constant  $r$  hyperbola at  $r = R_+$ . This fact that would be crucial when we match the two areal charts later.

Integrating the second equation in (C.19) for points on the maximal slice that are in the  $t_F > 0$  part of Region F, we get

$$t_F(r, \bar{t}) - \hat{t}_F(R_+) = -T(\bar{t}) \int_{R_+(T)}^r \frac{d\rho}{\rho} \left( \frac{\rho^2}{\ell^2} - 8G_N M \right)^{-1} \left( \frac{\rho^2}{\ell^2} - 8G_N M + \frac{T(\bar{t})^2}{\rho^2} \right)^{-1/2}, \quad (\text{C.21})$$

where we have chosen the lower limit of integration to be  $R_+$  where the solution has a coordinate singularity. The above diffeomorphism in Region F can be extended to Region I as well by taking  $r > \ell \sqrt{8G_N M}$  in (C.21); the integration range will now have a simple pole at the horizon which has to be dealt with the usual Cauchy principal-value prescription. After this, it is easy to see that it satisfies the second equation in (C.16). So, the diffeomorphism in Region I is

$$t(r, \bar{t}) - \hat{t}_F(R_+) = -T(\bar{t}) \int_{R_+(T)}^r \frac{d\rho}{\rho} \left( \frac{\rho^2}{\ell^2} - 8G_N M \right)^{-1} \left( \frac{\rho^2}{\ell^2} - 8G_N M + \frac{T(\bar{t})^2}{\rho^2} \right)^{-1/2}. \quad (\text{C.22})$$

Note that the reference time  $\hat{t}_F(R_+)$  is not yet fixed. We fix this later after we obtain maximal slices in Region II as well below.

The function  $T(\bar{t})$  is implicitly determined by using the boundary condition (C.17) on  $t$  as  $r \rightarrow \infty$ :

$$\bar{c}t + t_0 = \hat{t}_F(R_+) - T(\bar{t}) \int_{R_+(T)}^{\infty} \frac{d\rho}{\rho} \left( \frac{\rho^2}{\ell^2} - 8G_N M \right)^{-1} \left( \frac{\rho^2}{\ell^2} - 8G_N M + \frac{T(\bar{t})^2}{\rho^2} \right)^{-1/2}. \quad (\text{C.23})$$

We now describe the maximal slicing solution that is diffeomorphic to the portion of the fully extended BTZ black hole that includes the boundary in Region II. Recall the BTZ metric in Region II:

$$ds^2 = -f(\tilde{r})^2 d\tilde{t}^2 + f(\tilde{r})^{-1} d\tilde{r}^2 + \tilde{r}^2 d\varphi^2, \quad \tilde{r} > \ell \sqrt{8G_N M}. \quad (\text{C.24})$$

Note that  $\tilde{t}$  is chosen to increase in the opposite sense to the that of the time  $t$  in Region I. Thus, the  $\bar{t} > 0$  maximal slice actually starts from the boundary in the  $t > 0$  part of Region I, enters the  $t_F > 0$  part of Region F at the future horizon  $U = 0, V > 0$ , goes to the  $t_F < 0$  part of Region F and exits Region F at the past horizon  $U > 0, V = 0$  and reaches the boundary in Region II in the  $\tilde{t} < 0$  part.

To obtain maximal slices in the  $\tilde{t} < 0$  region map to Region II of the fully extended BTZ black

hole, we use the same radial coordinate  $\tilde{r}$  as in (C.24) for the maximal slicing ansatz (C.1). The solution in the maximal slicing gauge is the same as earlier, with obvious changes in notation:

$$\begin{aligned} ds^2 &= -\tilde{\alpha}(\tilde{r}, \tilde{t})^2 d\tilde{t}^2 + \tilde{A}(\tilde{r}, \tilde{t}) \left( d\tilde{r} + \frac{\tilde{\alpha}(\tilde{r}, \tilde{t}) \tilde{T}(\tilde{t})}{\tilde{r}} d\tilde{t} \right)^2 + \tilde{r}^2 d\varphi^2, \\ A(\tilde{r}, \tilde{t}) &= \left( \frac{\tilde{r}^2}{\ell^2} - 8G_N M + \frac{\tilde{T}(\tilde{t})^2}{\tilde{r}^2} \right)^{-1}, \\ \tilde{\alpha}(\tilde{r}, \tilde{t}) &= A(\tilde{r}, \tilde{t})^{-1/2} \left[ \tilde{c} - \partial_{\tilde{t}} \tilde{T}(\tilde{t}) \int_{\infty}^{\tilde{r}} \frac{d\rho}{\rho} \left( \frac{\rho^2}{\ell^2} - 8G_N M + \frac{\tilde{T}(\tilde{t})^2}{\rho^2} \right)^{-3/2} \right]. \end{aligned} \quad (\text{C.25})$$

Note that the boundary condition for  $\tilde{\alpha}$  as  $\tilde{r} \rightarrow \infty$  is  $\tilde{c}\tilde{r}/\ell$ , with  $\tilde{c}$  not necessarily equal to  $c$  from the previous solution that maps to Region I of the BTZ black hole. The diffeomorphism to the BTZ metric in Region II is

$$\partial_{\tilde{t}} \tilde{t} = \epsilon \tilde{\alpha} \sqrt{A(\tilde{r}, \tilde{t})}, \quad \partial_{\tilde{r}} \tilde{t} = -\epsilon \frac{\tilde{T} \sqrt{A(\tilde{r}, \tilde{t})}}{\tilde{r} f(\tilde{r})}, \quad (\text{C.26})$$

where the sign  $\epsilon$  must be chosen to be  $-1$  for the  $\tilde{t} < 0$  part of Region II and  $+1$  in the  $\tilde{t} > 0$  part of Region II. The first equation with  $\epsilon = -1$  gives the boundary condition

$$\lim_{\tilde{r} \rightarrow \infty} \tilde{t} = -\tilde{c}\tilde{t} - \tilde{t}_0. \quad (\text{C.27})$$

Following the same procedure as earlier, the coordinate transformation to BTZ coordinates in the  $\tilde{t} < 0$  part of Region II is

$$\tilde{t}(\tilde{r}, \tilde{t}) - \hat{t}_F(R_+(\tilde{T})) = \tilde{T} \int_{R_+(\tilde{T})}^{\tilde{r}} \frac{d\rho}{\rho} \left( \frac{\rho^2}{\ell^2} - 8G_N M \right)^{-1} \left( \frac{\rho^2}{\ell^2} - 8G_N M + \frac{\tilde{T}^2}{\rho^2} \right)^{-1/2}, \quad (\text{C.28})$$

where  $\hat{t}_F(R_+(\tilde{T}))$  is the  $t_F$  coordinate of the point  $\tilde{r} = R_+(\tilde{T})$  in Region F where the metric (C.25) has a coordinate singularity. The  $r \rightarrow \infty$  limit of (C.28) gives the following implicit expression for  $\tilde{T}(\tilde{t})$ :

$$-\tilde{c}\tilde{t} - \tilde{t}_0 = \hat{t}_F(R_+(\tilde{T})) + \tilde{T}(\tilde{t}) \int_{R_+(\tilde{T})}^{\infty} \frac{d\rho}{\rho} \left( \frac{\rho^2}{\ell^2} - 8G_N M \right)^{-1} \left( \frac{\rho^2}{\ell^2} - 8G_N M + \frac{\tilde{T}^2}{\rho^2} \right)^{-1/2}. \quad (\text{C.29})$$

**Matching left and right charts** We match the maximal slices from the left and right charts. Continuity in the radial coordinate forces the reference points  $\hat{t}(R_+(T))$  and  $\hat{t}_F(R_+(\tilde{T}))$  to be the same. This in turn requires the functions  $\tilde{T}(\tilde{t})$  and  $T(\tilde{t})$  to be the same, i.e.,  $\tilde{T}(\tilde{t}) = T(\tilde{t})$ . Since these slices are tangent to the same constant  $r$  hyperbola, they are guaranteed to be smooth at  $r = R_+(T(\tilde{t}))$ . Adding (C.23) and (C.29) we get

$$\hat{t}_F(R_+) = \frac{1}{2}(c - \tilde{c})\tilde{t} + \frac{1}{2}(t_0 - \tilde{t}_0). \quad (\text{C.30})$$

This determines  $\hat{t}_F(R_+)$  and now the maximal slicing coordinates are completely known. Taking the difference of (C.23) and (C.29) gives

$$(c + \tilde{c})\bar{t} + t_0 + \tilde{t}_0 = -2T \int_{R_+(T)}^{\infty} \frac{d\rho}{\rho} \left( \frac{\rho^2}{\ell^2} - 8G_N M \right)^{-1} \left( \frac{\rho^2}{\ell^2} - 8G_N M + \frac{T^2}{\rho^2} \right)^{-1/2}. \quad (\text{C.31})$$

This equation can be thought of as a more democratic definition of the function  $T(\bar{t})$ .

#### C.4 The wormhole coordinate

While we have matched the left and right charts, the metric component  $g_{rr} = A(r)$  still diverges at the locus of matching points. We can remedy this by defining a new coordinate by

$$x^2 = r^2 - R_+(T(\bar{t}))^2. \quad (\text{C.32})$$

In terms of these coordinates  $(\bar{t}, x, \varphi)$ , the metric is given by

$$ds^2 = -N^2 d\bar{t}^2 + g_{xx} (dx + N^x d\bar{t})^2 + (x^2 + R_+(\bar{t})^2) d\varphi^2, \quad (\text{C.33})$$

with

$$N(\bar{t}, x) = \begin{cases} \frac{x\sqrt{x^2+R_+^2-R_-^2}}{\ell\sqrt{x^2+R_+^2}} \left[ c + \dot{T}\ell^3 \int_x^{\infty} \frac{dy}{y^2} \frac{\sqrt{y^2+R_+^2}}{(y^2+R_+^2-R_-^2)^{3/2}} \right] & x > 0 \\ -\frac{x\sqrt{x^2+R_+^2-R_-^2}}{\ell\sqrt{x^2+R_+^2}} \left[ \tilde{c} + \dot{T}\ell^3 \int_{-x}^{\infty} \frac{dy}{y^2} \frac{\sqrt{y^2+R_+^2}}{(y^2+R_+^2-R_-^2)^{3/2}} \right] & x < 0 \end{cases}, \quad (\text{C.34a})$$

$$N^x(\bar{t}, x) = \frac{1}{x} \left( N(\bar{t}, x)T + R_+\dot{R}_+ \right), \quad (\text{C.34b})$$

$$g_{xx}(\bar{t}, x) = \frac{\ell^2}{x^2 + R_+^2 - R_-^2}. \quad (\text{C.34c})$$

One can check that the lapse is continuous and smooth at  $x = 0$ . The easiest way to see this is to Taylor-expand near  $x = 0$ :

$$\lim_{x \rightarrow 0^+} N = \frac{\dot{T}\ell^2}{R_+^2 - R_-^2} + \frac{x}{\ell} \sqrt{1 - R_-^2/R_+^2} (c + \dot{T}\ell^3 \mathcal{F}(\bar{t}, \infty)) + \dot{T}\ell^2 \frac{R_+^2 + R_-^2}{R_+^2(R_+^2 - R_-^2)} x^2 + \mathcal{O}(x^3), \quad (\text{C.35})$$

$$\lim_{x \rightarrow 0^-} N = \frac{\dot{T}\ell^2}{R_+^2 - R_-^2} - \frac{x}{\ell} \sqrt{1 - R_-^2/R_+^2} (\tilde{c} + \dot{T}\ell^3 \mathcal{F}(\bar{t}, \infty)) + \dot{T}\ell^2 \frac{R_+^2 + R_-^2}{R_+^2(R_+^2 - R_-^2)} x^2 + \mathcal{O}(x^3), \quad (\text{C.36})$$

where

$$\mathcal{F}(\bar{t}, x) = \int_0^x \frac{dy}{y^2} \frac{\sqrt{y^2 + R_+^2}}{(y^2 + R_+^2 - R_-^2)^{3/2}}. \quad (\text{C.37})$$



The value of lapse at  $x = 0$  is indeed the same. The first derivative matches provided

$$\dot{T} = -\frac{c + \tilde{c}}{2\ell^3 \mathcal{F}(\bar{t}, \infty)}. \quad (\text{C.38})$$

We can integrate this equation to get  $\bar{t}$  as a function of  $T$ , which matches with (C.31). This can be verified, for example numerically, for arbitrary  $c$  and  $\tilde{c}$ . In fact, all even powers match trivially, whereas higher odd powers (and therefore derivatives) in (C.35) and (C.36) match provided (C.38) is satisfied. Thus the lapse is a completely smooth function of  $x$ . The shift  $N^x$  is also continuous and smooth since it is defined in terms of the lapse function. In particular,

$$\begin{aligned} \lim_{x \rightarrow 0} N^x &= \partial_x N(x=0)T = \sqrt{1 - R_-^2/R_+^2} \frac{T}{2\ell} (c - \tilde{c}), \\ \lim_{x \rightarrow 0} \partial_x N^x &= \frac{T}{2} \partial_x^2 N(x=0) = T \dot{T} \ell^2 \frac{R_+^2 + R_-^2}{R_+^2(R_+^2 - R_-^2)}. \end{aligned}$$

Finally  $g_{xx}$  is also continuous and smooth. Thus we have constructed a coordinate chart  $(\bar{t}, x, \varphi)$  with metric (C.33), whose constant time slices are maximal, go from the left asymptotic boundary to the right asymptotic boundary while smoothly cutting across the two horizons.

## C.5 ADM masses

Let us calculate the asymptotic ADM masses for the right (C.14) and left (C.25) charts above. But first we recall the mass calculation for BTZ in standard coordinates (C.15). The ADM mass formula is given by

$$M_{\text{ADM}} = -\frac{1}{8\pi G_N} \lim_{S_t \rightarrow \infty} \int_{S_t} d\varphi \sqrt{\sigma} N \left( k - \frac{1}{\ell} \right). \quad (\text{C.39})$$

Here  $S_t$  is the asymptotic sphere ( $S^1$ ),  $\sigma_{AB}$  is the induced metric,  $k$  is the mean extrinsic curvature of  $S_t$  embedded in constant time slice  $\Sigma_t$ . The subtraction by  $1/\ell$  is a holographic counterterm [35–39] which removes the divergence in the first term arising from the AAdS boundary. Alternatively, one can interpret the  $1/\ell$  as arising from the mean extrinsic curvature of a boundary surface with the same intrinsic geometry as  $S_t$  but embedded in the  $M \rightarrow 0$  limit of the constant time surface in (C.39).

The unit normal to  $S_t$  is given by  $n^a = (\sqrt{f}, 0)$ , from which one finds the mean extrinsic curvature

$$k = D_a n^a = \frac{\sqrt{f}}{r}. \quad (\text{C.40})$$

The induced metric on  $S_t$  is just  $ds^2 = \sigma_{\varphi\varphi} d\varphi^2 = r^2 d\varphi^2$ , and therefore we find

$$M_{\text{ADM}} = -\frac{1}{8\pi G_N} \lim_{S_t \rightarrow \infty} \int_{S_t} d\varphi \sqrt{\sigma} N (k - \ell^{-1}) = M. \quad (\text{C.41})$$

Now we consider the right (and left) charts above and calculate the respective ADM masses. Note that the information about  $c$  or  $\tilde{c}$  is only in the lapse, since the mean extrinsic curvature  $k$  are calculated at constant  $\bar{t}$  and so do not know about  $c$  or  $\tilde{c}$ . The unit normal to  $S_t$  is given by

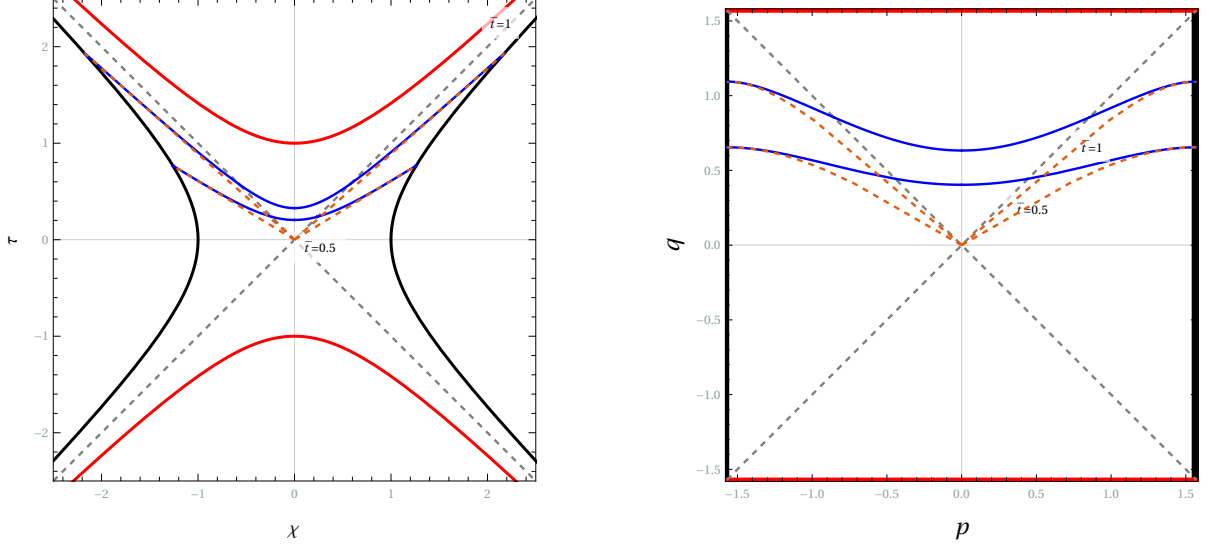


Figure 7: The Maximal slices (blue) approach the Killing slices (orange, dashed) at the asymptotic boundaries.

$n^a = (1/\sqrt{A}, 0)$ , from which one finds the mean extrinsic curvature to be

$$k = D_a n^a = \frac{1}{r\sqrt{A}} . \quad (\text{C.42})$$

Thus we find ADM mass at the right boundary

$$M_{\text{ADM}} = -\frac{1}{8\pi G_N} \lim_{S_t \rightarrow \infty} \int_{S_t} d\varphi \sqrt{\sigma} \alpha (k - \ell^{-1}) = cM , \quad (\text{C.43})$$

and

$$\tilde{M}_{\text{ADM}} = -\frac{1}{8\pi G_N} \lim_{S_t \rightarrow \infty} \int_{S_t} d\varphi \sqrt{\sigma} \tilde{\alpha} (k - \ell^{-1}) = \tilde{c}M . \quad (\text{C.44})$$

## C.6 Asymptotic falloff of the extrinsic curvature $K_{ij}$ and the boundary stress tensor

The maximal slices we constructed approach the Killing slices of the BTZ black hole. This is evident from the Figure 7. The metric itself asymptotically approaches the the AdS<sub>3</sub> metric in global coordinates. However the fall-offs of the extrinsic curvature naively disagrees with that of the original BTZ solution which has  $K_{ij} = 0$ . For example, in the right areal chart (4.17) we find  $K_{\varphi\varphi} = -T(\bar{t})$  which is not zero except on the  $\bar{t} = 0$  slice.

To see if there is any difference in the physics of the boundary dual, we compute the boundary stress tensor for the maximally sliced BTZ solution. We find that it is the same as that for the standard BTZ solution.

Following [35], first we rewrite the metric of the right areal chart (4.17) in ADM-like form

$$ds^2 = X^2 dr^2 + \gamma_{\mu\nu} (dz^\mu + Y^\mu dr) (dz^\nu + Y^\nu dr) , \quad (\text{C.45a})$$

$$\gamma_{\bar{t}\bar{t}} = -\alpha(r, \bar{t})^2 \left( 1 - \frac{A(r, \bar{t}) T(\bar{t})^2}{r^2} \right) , \quad \gamma_{\varphi\varphi} = r^2 , \quad \gamma_{\bar{t}\varphi} = 0 , \quad (\text{C.45b})$$

$$X^2 = \frac{r^2 A(r, \bar{t})}{r^2 - A(r, \bar{t}) T(\bar{t})^2} , \quad Y^{\bar{t}} = -\frac{r A(r, \bar{t}) T(\bar{t})}{\alpha(r, \bar{t}) (r^2 - A(r, \bar{t}) T(\bar{t})^2)} , \quad Y^\varphi = 0 . \quad (\text{C.45c})$$

The functions  $A(r, \bar{t})$  and  $\alpha(r, \bar{t})$  were already defined in (4.17b) and (4.17c). The renormalized stress-tensor is given by

$$T_{\mu\nu} = -\frac{1}{8\pi G_N} \left[ \Theta_{\mu\nu} - \Theta \gamma_{\mu\nu} + \frac{1}{\ell} \gamma_{\mu\nu} \right] . \quad (\text{C.46})$$

Let us denote  $\hat{n}$  the outward pointing unit vector normal to a constant large  $r$  surface, then  $\Theta_{\mu\nu}$  is the associated second fundamental form

$$\Theta_{\mu\nu} = \mathcal{D}_{(\mu} \hat{n}_{\nu)} . \quad (\text{C.47})$$

The non-zero components of  $\Theta$  are

$$\begin{aligned} \Theta_{\bar{t}\bar{t}} = & -\frac{\alpha}{2Ar^5 \sqrt{\frac{1}{A} - \frac{T^2}{r^2}}} \left( Ar (-rT^3 \partial_{\bar{t}} A + \alpha T^4 \partial_r A + 2rT^2 (\alpha - 2r \partial_r \alpha) + 2r^3 \partial_{\bar{t}} T) \right. \\ & \left. + r^3 (2rT \partial_{\bar{t}} A - \alpha T^2 \partial_r A + 2r^2 \partial_r \alpha) - 2A^2 T^4 (\alpha - r \partial_r \alpha) \right) \end{aligned} \quad (\text{C.48a})$$

$$\Theta_{\varphi\varphi} = \sqrt{\frac{r^2}{A} - T^2} . \quad (\text{C.48b})$$

From this we can find the stress tensor defined above (C.46),

$$8\pi G_N T_{\bar{t}\bar{t}} = \frac{\alpha^2 (r^2 - AT^2) \left( r^2 - \ell \sqrt{\frac{r^2}{A} - T^2} \right)}{\ell r^4} , \quad (\text{C.49})$$

$$\begin{aligned} 8\pi G_N T_{\varphi\varphi} = & \frac{-\alpha (r^2 - AT^2) (2r - T^2 \partial_r A) + rT \partial_{\bar{t}} A (AT^2 - 2r^2)}{2\alpha A (AT^2 - r^2) \sqrt{\frac{1}{A} - \frac{T^2}{r^2}}} \\ & + \frac{-2\partial_r \alpha (r^2 - AT^2)^2 - 2Ar^3 \partial_{\bar{t}} T}{2\alpha A (AT^2 - r^2) \sqrt{\frac{1}{A} - \frac{T^2}{r^2}}} - \sqrt{\frac{r^2}{A} - T^2} - \frac{r^2}{\ell} . \end{aligned} \quad (\text{C.50})$$

We expand this for large  $r$ ,

$$T_{\bar{t}\bar{t}} = \frac{M}{2\pi\ell} - \frac{3G_N M^2 \ell}{\pi r^2} + \frac{M\ell^2 (3R_+(T)^4 + R_-(T)^4 - 2R_+(T)^2 R_-(T)^2) \partial_{\bar{t}} T}{3\pi (R_+(T)^2 - R_-(T)^2)^2 r^3} + \mathcal{O}(1/r^4) , \quad (\text{C.51})$$

$$T_{\varphi\varphi} = \frac{M\ell}{2\pi} + \frac{3G_N M^2 \ell^3}{\pi r^2} + \frac{3\ell^2 (8G_N M\ell^2 - R_+(T)^2 - R_-(T)^2) \partial_{\bar{t}} T}{16\pi G_N r^3} + \mathcal{O}(1/r^4) . \quad (\text{C.52})$$

Taking the  $r \rightarrow \infty$  limit we get the same answer as in standard BTZ coordinates

$$T_{\bar{t}\bar{t}} = \frac{M}{2\pi\ell}, \quad T_{\varphi\varphi} = \frac{M\ell}{2\pi}, \quad (\text{C.53})$$

Note that  $T_{\bar{t}\bar{t}}$  is indeed proportional to the ADM mass of the black hole. In fact, the subleading  $\mathcal{O}(1/r^2)$  term is also the same as in BTZ  $(r, t, \varphi)$  coordinates; the deviation starts only at  $\mathcal{O}(1/r^3)$ .

## D Maximal slices in the BTZ black hole from a variational principle

Let us start with the fully extended BTZ black hole, with coordinates  $(t, r)$  with  $-\infty < t < \infty$ ,  $r > r_h$  in Region I,  $(t_F, r)$  with  $-\infty < t_F < \infty$ ,  $r < r_h$  in region F. Here  $r_h = \ell\sqrt{8G_N M}$  is the horizon radius. The metric in each of these regions is

$$\begin{aligned} \text{Region I:} \quad ds^2 &= -f(r)dt^2 + f(r)^{-1}dr^2 + r^2d\varphi^2, \quad f(r) = \frac{r^2}{\ell^2} - 8G_N M, \\ \text{Region F:} \quad ds^2 &= -f(r)dt_F^2 + f(r)^{-1}dr^2 + r^2d\varphi^2. \end{aligned} \quad (\text{D.1})$$

### D.1 The variational principle

Consider a spherically symmetric hypersurface in the BTZ spacetime described by the function

$$t = F(r), \quad r > r_h, \quad t_F = G(r), \quad r < r_h. \quad (\text{D.2})$$

We then have  $dt = F'(r)dr$ , so that the induced 2-metric  $g_{ab}$  on the hypersurface is

$$ds_2^2 = -f(r)F'(r)^2dr^2 + f(r)^{-1}dr^2 + r^2d\varphi^2. \quad (\text{D.3})$$

The volume of the hypersurface is obtained from the induced metric:

$$\mathcal{V} = \int drd\varphi \sqrt{g} = \int drd\varphi \sqrt{r^2(f(r)^{-1} - f(r)F'(r)^2)} = 2\pi \int dr \sqrt{r^2(f(r)^{-1} - f(r)F'(r)^2)}. \quad (\text{D.4})$$

The variation of  $\mathcal{V}$  with respect to variations in  $F(r)$  gives

$$\delta\mathcal{V} = \int drd\varphi g^{-1/2}\delta g = \int drd\varphi g^{-1/2}(-r^2 f 2F' \partial_r \delta F). \quad (\text{D.5})$$

The extremum of the volume is a maximum in Lorentzian signature. Thus, the equation of the maximal hypersurface is obtained by setting  $\delta\mathcal{V} = 0$ :

$$\partial_r(g^{-1/2}r^2 f F') = 0, \quad \text{that is} \quad \partial_r \left( \frac{r^2 f F'}{\sqrt{r^2(f(r)^{-1} - f(r)F'(r)^2)}} \right) = 0, \quad (\text{D.6})$$

which is satisfied by

$$\frac{r f F'}{\sqrt{f^{-1} - f F'^2}} = T, \quad (\text{D.7})$$

where  $T$  is an  $r$ -independent constant. This gives

$$F'(r) = \pm \frac{T}{rf\sqrt{f + \frac{T^2}{r^2}}} . \quad (\text{D.8})$$

The induced metric on the hypersurface is then

$$(-fF'^2 + f^{-1})dr^2 + r^2d\varphi^2 = \frac{1}{f + \frac{T^2}{r^2}}dr^2 + r^2d\varphi^2 . \quad (\text{D.9})$$

The main requirement is that the quantity inside the square root in (D.8) be positive. We can analyze this requirement as follows. Let  $R_{\pm}^2$  be the roots of the quadratic equation in  $r^2$ :

$$(r^2)^2 - 8G_N M \ell^2 r^2 + \ell^2 T^2 = 0 , \quad R_{\pm}^2 = 4G_N M \ell^2 \left( 1 \pm \sqrt{1 - \frac{T^2}{\ell^2 (4G_N M)^2}} \right) . \quad (\text{D.10})$$

Then,  $F'(r)$  can be written as

$$F'(r) = \pm \frac{\ell T}{f\sqrt{(r^2 - R_+^2)(r^2 - R_-^2)}} . \quad (\text{D.11})$$

Since  $R_+ \geq R_-$ , it is clear that the square root is real only when  $r > R_+$  or  $r < R_-$ . Let us focus on the first branch of solutions  $r > R_+$ . It is easy to see that  $R_+$  itself is smaller than the horizon radius  $r_h = \ell\sqrt{8G_N M}$ . Thus, the maximal hypersurface in Region I goes all the way up to the horizon.

The sign on the right hand side can be fixed by noting that, in the  $t > 0$  part of Region I, the  $t$  coordinate of a point on the surface increases as the  $r$  coordinate decreases. Since  $f > 0$  in Region I, the sign must be  $-$  for  $\frac{\partial t}{\partial r} < 0$ .

Thus, we get, in the  $t > 0$  part of Region I,

$$F(r) - \bar{t} = -\ell^3 T \int_{\infty}^r \frac{dr}{(r^2 - 8G_N M \ell^2) \sqrt{(r^2 - R_+^2(T))(r^2 - R_-^2(T))}} , \quad (\text{D.12})$$

where  $\bar{t}$  has the interpretation of the value of the coordinate  $t$  as  $r \rightarrow \infty$ . At this stage, for every  $\bar{t}$  and  $T$  we have a maximal hypersurface in Region I of the BTZ spacetime. We have exhibited the dependence of  $R_{\pm}$  on  $T$  explicitly to indicate that  $T$  is an independent parameter. We mostly suppress the dependence on  $T$  unless necessary.

In the same way, we have a maximal surface given by  $t_F = G(r)$  in Region F which satisfies the same differential equation as above:

$$G'(r) = \pm \frac{\ell T_F}{f\sqrt{(r^2 - R_+(T_F)^2)(r^2 - R_-(T_F)^2)}} . \quad (\text{D.13})$$

The integration constant  $T_F$  need not be the same as  $T$  from Region I a priori. However, when we connect the solutions in Region I and Region F across the horizon by analytic continuation, it will turn out that  $T_F = T$ . Thus, we replace  $T_F$  by  $T$  in the subsequent steps.

Since  $f < 0$  in Region F, the two signs  $\pm$  correspond to the parts of the maximal surface in

which  $t_F$  decreases as  $r$  increases (resp. decreases) along the hypersurface. The two parts meet at the minimum point  $r = R_+$  where the derivative  $\frac{\partial t_F}{\partial r} = G'(r)$  goes to infinity. The geometric interpretation of this is that the maximal hypersurface is tangential to the constant  $r = R_+$  hypersurface in Region F. Suppose the time coordinate of this point is  $t_F = \hat{t}_F$ . Then, on either side of this point the  $r$  coordinate increases along the hypersurface as one moves away from it. We then integrate the equation above to get

$$G(r) - \hat{t}_F = \pm \ell^3 T \int_{R_+(T)}^r \frac{dr}{(r^2 - 8G_N M \ell^2) \sqrt{(r^2 - R_+^2(T))(r^2 - R_-^2(T))}} , \quad (\text{D.14})$$

As explained earlier, the two parts of the maximal hypersurface in Region F  $t_F < \hat{t}_F$  and  $t_F > \hat{t}_F$  correspond to the two signs in (D.14) above. The right hand side can be extended beyond the horizon  $r = r_h = \ell\sqrt{8G_N M}$  provided the simple pole in the integrand at  $r_h$  is handled by the Cauchy principal value prescription. Then, it is easy to see that the analytically continued function satisfies the differential equation for  $F(r)$  in Region I.

The BTZ metric remains the same in Region II, with the time coordinate being  $\tilde{t}$  with  $-\infty < \tilde{t} < \infty$ , and radial coordinate  $\tilde{r}$ :

$$ds^2 = -f(\tilde{r})d\tilde{t}^2 + f^{-1}(\tilde{r})d\tilde{r}^2 + \tilde{r}^2 d\varphi^2 . \quad (\text{D.15})$$

The maximal surface  $\tilde{t} = \tilde{F}(\tilde{r})$  satisfies the same equation as earlier:

$$\tilde{F}'(\tilde{r}) = \pm \frac{\ell \tilde{T}}{f \sqrt{(\tilde{r}^2 - R_+(\tilde{T})^2)(\tilde{r}^2 - R_-(\tilde{T})^2)}} . \quad (\text{D.16})$$

Again, the integration constant  $\tilde{T}$  is a priori independent of the corresponding constants in the other regions. However, when we connect the surfaces across the horizon,  $\tilde{T}$  will coincide with  $T$  in the other regions. Thus, we take  $\tilde{T} = T$  in the following.

In the  $\tilde{t} < 0$  part of Region II,  $\tilde{t}$  decreases towards  $-\infty$  as  $r$  decreases towards  $r_h$ . Since  $f > 0$  in Region II, we have to choose the + sign in the above equation for a maximal hypersurface in the  $\tilde{t} < 0$  part of Region II. Then, we get

$$\tilde{F}(r) - \bar{\tilde{t}} = +\ell^3 T \int_{\infty}^r \frac{dr}{(r^2 - 8G_N M \ell^2) \sqrt{(r^2 - R_+^2(T))(r^2 - R_-^2(T))}} , \quad (\text{D.17})$$

where  $\bar{\tilde{t}}$  is the value of  $\tilde{t}$  on the maximal slice as one approaches the boundary  $r \rightarrow \infty$ .

For  $r > r_h$  in Region I, we have two definitions of the time function  $t(r)$ , (1) from the direct solution of the differential equation in Region I, and (2) from the analytic continuation of the solution in Region F. Equating the two expressions, we get

$$\begin{aligned} t(r) &= \bar{\tilde{t}} - \ell^3 T \int_{\infty}^r \frac{dr}{(r^2 - r_h^2) \sqrt{(r^2 - R_+^2(T))(r^2 - R_-^2(T))}} , \\ &= \hat{t}_F - \ell^3 T \int_{R_+(T)}^r \frac{dr}{(r^2 - r_h^2) \sqrt{(r^2 - R_+^2(T))(r^2 - R_-^2(T))}} , \end{aligned} \quad (\text{D.18})$$

which gives a relation between the three parameters  $T$ ,  $\hat{t}_F$  and  $\bar{t}$ :

$$\bar{t} - \hat{t}_F = \ell^3 T \int_{\infty}^{R_+(T)} \frac{dr}{(r^2 - r_h^2) \sqrt{(r^2 - R_+^2(T))(r^2 - R_-^2(T))}} . \quad (\text{D.19})$$

Similarly, one gets a relation between  $\bar{\bar{t}}$ ,  $\hat{t}_F$  and  $T$ :

$$\bar{\bar{t}} - \hat{t}_F = -\ell^3 T \int_{\infty}^{R_+(T)} \frac{dr}{(r^2 - r_h^2) \sqrt{(r^2 - R_+^2(T))(r^2 - R_-^2(T))}} . \quad (\text{D.20})$$

One can eliminate  $\hat{t}_F$  from the above expressions to get  $\hat{t}_F = \frac{1}{2}(\bar{t} + \bar{\bar{t}})$  and

$$\frac{1}{2}(\bar{t} - \bar{\bar{t}}) = \ell^3 T \int_{\infty}^{R_+(T)} \frac{dr}{(r^2 - r_h^2) \sqrt{(r^2 - R_+^2(T))(r^2 - R_-^2(T))}} . \quad (\text{D.21})$$

which determines the parameter  $T$  as a function of the two boundary parameters  $\bar{t}$  and  $\bar{\bar{t}}$ . Thus, we have two parameter set of maximal hypersurfaces in the BTZ black hole, with the two parameters specified by the time coordinates  $\bar{t}$  and  $\bar{\bar{t}}$  of the ends of the maximal hypersurface.

## D.2 The spacetime metric in maximal slicing coordinates

The BTZ metric in Region I is

$$ds^2 = -f dt^2 + f^{-1} dr^2 + r^2 d\varphi^2 . \quad (\text{D.22})$$

Recall the relation between the BTZ time  $t$  in region I and the parameter  $\bar{t}$  on the maximal slice:

$$t(\bar{t}, r) - \bar{t} = -\ell^3 T \int_{\infty}^r \frac{dr}{(r^2 - 8G_N M \ell^2) \sqrt{(r^2 - R_+^2(T))(r^2 - R_-^2(T))}} , \quad (\text{D.23})$$

We then have

$$dt = \frac{\partial t}{\partial \bar{t}} d\bar{t} + \frac{\partial t}{\partial r} dr , \quad (\text{D.24})$$

with

$$\frac{\partial t}{\partial r} = -\frac{\ell T}{f \sqrt{(r^2 - R_+^2(T))(r^2 - R_-^2(T))}} , \quad \frac{\partial t}{\partial \bar{t}} = 1 - \dot{T} \int_{\infty}^r \frac{dr}{r \left( \frac{r^2}{\ell^2} - 8G_N M + \frac{T^2}{r^2} \right)^{3/2}} . \quad (\text{D.25})$$

Plugging this back into the BTZ metric, we get

$$\begin{aligned} ds^2 &= -f \left( \frac{\partial t}{\partial \bar{t}} \right)^2 d\bar{t}^2 - 2f \frac{\partial t}{\partial \bar{t}} \frac{\partial t}{\partial r} d\bar{t} dr + \left( f^{-1} - f \left( \frac{\partial t}{\partial r} \right)^2 \right) dr^2 + r^2 d\varphi^2 , \\ &= -\alpha^2(r, \bar{t}) d\bar{t}^2 + A(r, \bar{t}) \left( dr + \frac{\alpha(r, \bar{t}) T(\bar{t})}{r} d\bar{t} \right)^2 + r^2 d\varphi^2 , \end{aligned} \quad (\text{D.26})$$

where

$$A(r, \bar{t}) = \frac{1}{\frac{r^2}{\ell^2} - 8G_N M + \frac{T(\bar{t})^2}{r^2}}, \quad \alpha(r, \bar{t}) = A(r, \bar{t})^{-1/2} \left( 1 - \dot{T} \int_{\infty}^r d\rho \rho^{-1} A(\rho, \bar{t})^{-3/2} \right). \quad (\text{D.27})$$

Note that this exactly matches the metric obtained by solving the Einstein equations in maximal slicing gauge with areal radial coordinate, and doing a diffeomorphism to the BTZ black hole.

## E Solutions of the Klein-Gordon equation in the BTZ spacetime

### E.1 Separation of variables

The 2 + 1 components of the BTZ black hole metric (4.1) are

$$N(r) = f(r)^{1/2}, \quad N_i = 0, \quad g_{rr} = f(r)^{-1}, \quad g_{\varphi\varphi} = r^2, \quad g_{r\varphi} = 0, \quad (\text{E.1})$$

which gives  $\sqrt{g} = r f(r)^{-1/2}$ . The wave equation takes the form

$$-f^{-1}\ddot{\phi} + r^{-1}\partial_r(r f \partial_r \phi) + r^{-1}\partial_\varphi(r^{-1}\partial_\varphi \phi) - m^2\phi = 0. \quad (\text{E.2})$$

Since  $\partial_t$  and  $\partial_\varphi$  are Killing vectors, we can separate variables and write a particular mode of the scalar field as

$$F_{\omega q}(t, r, \varphi) \equiv \frac{1}{\sqrt{2\pi}} e^{-i\omega t} e^{-iq\varphi} f_{\omega q}(r), \quad (\text{E.3})$$

where  $\omega, q$  are the frequency and angular momentum along the circle respectively. Changing variables to the dimensionless  $\rho = r^2/r_h^2$  and defining

$$f_{\omega q}(\rho) = (\rho - 1)^\alpha \rho^\gamma \chi(\rho), \quad \text{with} \quad \alpha = -i\frac{\omega}{2\eta} = -i\frac{\beta\omega}{4\pi}, \quad \gamma = i\frac{q\ell}{2r_h}, \quad (\text{E.4})$$

we see that  $\chi$  satisfies the hypergeometric equation:

$$\rho(1 - \rho)\chi''(\rho) + (c - (a + b + 1)\rho)\chi'(\rho) - ab\chi(\rho) = 0, \quad (\text{E.5})$$

with

$$c = 2\gamma + 1, \quad a = \alpha + \gamma + \frac{1}{2}\Delta_+, \quad b = \alpha + \gamma + \frac{1}{2}\Delta_-, \quad \Delta_\pm = 1 \pm \sqrt{1 + \ell^2 m^2}. \quad (\text{E.6})$$

Note that  $\Delta_+$  is the conformal dimension of the operator dual to  $\phi$  in the dual CFT. The hypergeometric equation has regular singular points at  $\rho = 0$ ,  $\rho = 1$  and  $\rho = \infty$ , corresponding to the origin (or inner horizon), the horizon (or the outer horizon), and infinity. There are solutions readily available (as a convergent series via the Frobenius method) in the neighbourhood of each of these points. This greatly facilitates further analysis. For instance, in the neighbourhood of  $z = 0$ ,

$${}_2F_1(a_1, a_2; b_1; z) = \sum_{n=0}^{\infty} \frac{(a_1)_n (a_2)_n}{(b_1)_n} \frac{z^n}{n!}, \quad \text{with} \quad (a)_n = a(a+1)\cdots(a+n-1), \quad (\text{E.7})$$



so that

$${}_2F_1(a_1, a_2; b_1; 0) = 1 . \quad (\text{E.8})$$

Below, we list the solutions  $\chi(\rho)$  that are regular in the neighbourhood of the three singular points  $\rho = \infty, 1, 0$ . We use the notation of DLMF [70, §15.10]. The solutions regular at  $\rho = 1$  are

$$\begin{aligned} w_3(\rho) &= {}_2F_1(a, b; a + b - c + 1; 1 - \rho) , \\ w_4(\rho) &= (1 - \rho)^{c-a-b} {}_2F_1(c - a, c - b; c - a - b + 1; 1 - \rho) , \end{aligned} \quad (\text{E.9})$$

the solutions regular at  $\rho = \infty$  are

$$\begin{aligned} w_5(\rho) &= e^{i\pi a} \rho^{-a} {}_2F_1\left(a, a - c + 1; a - b + 1; \frac{1}{\rho}\right) , \\ w_6(\rho) &= e^{i\pi b} \rho^{-b} {}_2F_1\left(b, b - c + 1; b - a + 1; \frac{1}{\rho}\right) , \end{aligned} \quad (\text{E.10})$$

and the solutions regular at  $\rho = 0$  are

$$\begin{aligned} w_1(\rho) &= {}_2F_1(a, b; c; \rho) , \\ w_2(\rho) &= \rho^{1-c} {}_2F_1(a - c + 1, b - c + 1; 2 - c; \rho) . \end{aligned} \quad (\text{E.11})$$

## E.2 Solution in Region I

Let us look at the solution in the exterior region I. Recalling that  $f_{\omega q}(\rho) = (\rho - 1)^\alpha \rho^\gamma \chi(\rho)$ , the general solution in the neighbourhood of  $\rho = \infty$  is a linear combination of  $(\rho - 1)^\alpha \rho^\gamma w_5$  and  $(\rho - 1)^\alpha \rho^\gamma w_6$  in (E.10):

$$\begin{aligned} f_{\omega q}(\rho) &= C_{\omega q} e^{-i\pi a} (\rho - 1)^\alpha \rho^\gamma w_5(\rho) + C'_{\omega q} e^{-i\pi b} (\rho - 1)^\alpha \rho^\gamma w_6(\rho) , \\ &= C_{\omega q} (\rho - 1)^\alpha \rho^{\gamma-a} {}_2F_1\left(a, a - c + 1; a - b + 1; \frac{1}{\rho}\right) \\ &\quad + C'_{\omega q} (\rho - 1)^\alpha \rho^{\gamma-b} {}_2F_1\left(b, b - c + 1; b - a + 1; \frac{1}{\rho}\right) , \end{aligned} \quad (\text{E.12})$$

for some constants  $C_{\omega q}$  and  $C'_{\omega q}$ . It can be shown that the normalizable component of  $f_{\omega q}(\rho)$  w.r.t. the Klein-Gordon inner product is proportional to  $w_5$  and is given by

$$f_{\omega q}(\rho) = C_{\omega q} (\rho - 1)^\alpha \rho^{\gamma-a} {}_2F_1\left(a, a - c + 1; a - b + 1; \frac{1}{\rho}\right) . \quad (\text{E.13})$$

The constant  $C_{\omega q}$  can be fixed by demanding that  $F_{\omega q} = \frac{1}{\sqrt{2\pi}} e^{-i\omega t} e^{-iq\varphi} f_{\omega q}$  satisfy the canonical Klein-Gordon inner product

$$(F_{\omega' q'}, F_{\omega q})_{\text{KG}} = 2\omega \delta(\omega - \omega') \delta_{qq'} . \quad (\text{E.14})$$

We do this in Appendix E.8 below and obtain

$$C_{\omega q} = \frac{1}{N_{\omega q} \sqrt{2\pi r_h}} , \quad \text{with} \quad N_{\omega q} = \left| \frac{\Gamma(a - b + 1) \Gamma(c - a - b)}{\Gamma(1 - b) \Gamma(c - b)} \right| . \quad (\text{E.15})$$

The mode expansion for the scalar field in Region I is then

$$\phi(t, r, \varphi) = \sum_{q \in \mathbb{Z}} \int_0^\infty \frac{d\omega}{\sqrt{4\pi\omega}} a_{\omega q} F_{\omega q}(t, r, \varphi) + \text{c.c.} . \quad (\text{E.16})$$

We then have

$$a_{\omega q} = \frac{1}{\sqrt{4\pi\omega}} (F_{\omega q}, \phi_I)_{\text{KG}} . \quad (\text{E.17})$$

Using that  $F_{\omega q}$  satisfy the canonical Klein-Gordon inner product (E.14), we get the commutation relations

$$[a_{\omega q}, a_{\omega' q'}^\dagger] = \delta(\omega - \omega') \delta_{qq'} , \quad [a_{\omega q}, a_{\omega' q'}] = [a_{\omega q}^\dagger, a_{\omega' q'}^\dagger] = 0 . \quad (\text{E.18})$$

**Solutions regular at the horizon** The mode functions (E.13) have a good Taylor series near  $\rho = \infty$ . To obtain an expression near the horizon for the mode function in Region I, we have to first use a connection formula to write  $w_5(\rho)$  in terms of hypergeometric functions that have a good expansion near  $\rho = 1$ :

$$w_5(\rho) = e^{i\pi a} \frac{\Gamma(a-b+1)\Gamma(c-a-b)}{\Gamma(1-b)\Gamma(c-b)} w_3(\rho) + e^{i\pi(c-b)} \frac{\Gamma(a-b+1)\Gamma(a+b-c)}{\Gamma(a)\Gamma(a-c+1)} w_4(\rho) . \quad (\text{E.19})$$

Plugging in the values of  $a, b, c$  (E.6) in the coefficients, we see that, when  $\omega$  and  $q$  are real,

$$\begin{aligned} \frac{\Gamma(a-b+1)\Gamma(c-a-b)}{\Gamma(1-b)\Gamma(c-b)} &= \left( \frac{\Gamma(a-b+1)\Gamma(a+b-c)}{\Gamma(a)\Gamma(a-c+1)} \right)^* \\ &= \frac{\Gamma(\Delta_+) \Gamma(i\omega/\eta)}{\Gamma\left(\frac{1}{2}(\Delta_+ + \frac{i\omega}{\eta} - \frac{iq\ell}{r_h})\right) \Gamma\left(\frac{1}{2}(\Delta_+ + \frac{i\omega}{\eta} + \frac{iq\ell}{r_h})\right)} . \end{aligned} \quad (\text{E.20})$$

Let

$$\frac{\Gamma(a-b+1)\Gamma(c-a-b)}{\Gamma(1-b)\Gamma(c-b)} = N_{\omega q} e^{i\delta_{\omega q}} , \quad (\text{E.21})$$

with  $N_{\omega q}$  the magnitude and  $\delta_{\omega q}$  the phase of the left-hand side. We have already encountered  $N_{\omega q}$  in the normalization of the mode function (E.13). We can then write

$$\begin{aligned} f_{\omega q} &= \frac{e^{-i\pi a}}{N_{\omega q} \sqrt{2\pi r_h}} (\rho - 1)^\alpha \rho^\gamma w_5(\rho) , \\ &= \frac{1}{\sqrt{2\pi r_h}} \left( e^{i\delta_{\omega q}} (\rho - 1)^\alpha \rho^\gamma w_3(\rho) + e^{i\pi(c-b-a)} e^{-i\delta_{\omega q}} (\rho - 1)^\alpha \rho^\gamma w_4(\rho) \right) , \end{aligned} \quad (\text{E.22})$$

which can be written more explicitly using (E.9) as<sup>15</sup>

$$\begin{aligned}
f_{\omega q} &= \frac{1}{\sqrt{2\pi r_h}} \left( e^{i\delta_{\omega q}} (\rho - 1)^\alpha \rho^\gamma {}_2F_1(a, b; a + b - c + 1; 1 - \rho) \right. \\
&\quad \left. + e^{-i\delta_{\omega q}} e^{-i\pi 2\alpha} (\rho - 1)^\alpha \rho^\gamma (1 - \rho)^{-2\alpha} {}_2F_1(c - a, c - b; c - a - b + 1; 1 - \rho) \right), \\
&= \frac{1}{\sqrt{2\pi r_h}} \left( e^{i\delta_{\omega q}} (\rho - 1)^\alpha \rho^\gamma {}_2F_1(a, b; a + b - c + 1; 1 - \rho) \right. \\
&\quad \left. + e^{-i\delta_{\omega q}} (\rho - 1)^{-\alpha} \rho^\gamma {}_2F_1(c - a, c - b; c - a - b + 1; 1 - \rho) \right). \tag{E.23}
\end{aligned}$$

It will be useful to write the mode function  $F_{\omega q}$  succinctly as

$$F_{\omega q} = e^{-i\omega t - iq\varphi} f_{\omega q} = \frac{1}{\sqrt{2\pi r_h}} (F_{\omega q}^1 + F_{\omega q}^2), \tag{E.24}$$

with

$$\begin{aligned}
F_{\omega q}^1 &= e^{-i\omega t - iq\varphi} e^{i\delta_{\omega q}} (\rho - 1)^\alpha \rho^\gamma {}_2F_1(a, b; a + b - c + 1; 1 - \rho), \\
F_{\omega q}^2 &= e^{-i\omega t - iq\varphi} e^{-i\delta_{\omega q}} (\rho - 1)^{-\alpha} \rho^\gamma {}_2F_1(c - a, c - b; c - a - b + 1; 1 - \rho). \tag{E.25}
\end{aligned}$$

Near the horizon  $\rho = 1$  in Region I, we have  $\rho - 1 \sim 4e^{2\eta r_*}$  (with  $r_*$  the tortoise coordinate in Region I) so that the above functions behave as

$$F_{\omega q}^1 \sim e^{-iq\varphi} e^{i\delta_{\omega q}} (2\eta V)^{-i\omega/\eta}, \quad F_{\omega q}^2 \sim e^{-iq\varphi} e^{-i\delta_{\omega q}} (-2\eta U)^{i\omega/\eta}. \tag{E.26}$$

Thus, the scalar field behaves as

$$\phi(U, V, \varphi) = \frac{1}{\sqrt{2\pi r_h}} \sum_{q \in \mathbb{Z}} \int_0^\infty \frac{d\omega}{\sqrt{4\pi\omega}} a_{\omega q} e^{-iq\varphi} \left( e^{i\delta_{\omega q}} (2\eta V)^{-i\omega/\eta} + e^{-i\delta_{\omega q}} (-2\eta U)^{i\omega/\eta} \right) + \text{c.c.} \tag{E.27}$$

### E.3 Solution in region II

We write the ansatz for a mode of the scalar field in Region II as

$$\tilde{F}_{\omega q}(\tilde{t}, \tilde{r}, \varphi) = \frac{1}{\sqrt{2\pi}} e^{i\omega \tilde{t}} e^{iq\varphi} \tilde{f}_{\omega q}(\tilde{r}). \tag{E.28}$$

The solution for  $\tilde{f}_{\omega q}$  that is normalizable has the same functional form as (E.13) above, but with the choices

$$\tilde{\alpha} = \alpha^* = \frac{i\omega}{2\eta}, \quad \tilde{\gamma} = \gamma^* = -\frac{iq\ell}{2r_h}, \tag{E.29}$$

$$\tilde{c} = 2\tilde{\gamma} + 1, \quad \tilde{a} = \tilde{\alpha} + \tilde{\gamma} + \frac{1}{2}\Delta_+, \quad \tilde{b} = \tilde{\alpha} + \tilde{\gamma} + \frac{1}{2}\Delta_-, \quad \Delta_\pm = 1 \pm \sqrt{1 + \ell^2 m^2}. \tag{E.30}$$

<sup>15</sup>In the last step, we have absorbed the phase  $e^{-i\pi 2\alpha}$  into  $(1 - \rho)^{-2\alpha}$  to obtain  $(\rho - 1)^{-2\alpha}$ :

$$e^{-i\pi 2\alpha} (1 - \rho)^{-2\alpha} = e^{-2\alpha \log((1-\rho)e^{-i\pi})} = (\rho - 1)^{-2\alpha}.$$

The mode function in region II is then

$$\tilde{f}_{\omega q}(\tilde{\rho}) = C_{\omega q} (\tilde{\rho} - 1)^{\tilde{\alpha}} \tilde{\rho}^{\tilde{\gamma} - \tilde{a}} {}_2F_1 \left( \tilde{a}, \tilde{a} - \tilde{c} + 1; \tilde{a} - \tilde{b} + 1; \frac{1}{\tilde{\rho}} \right). \quad (\text{E.31})$$

$\tilde{\alpha}$  and  $\tilde{\gamma}$  are chosen as above so that  $\tilde{f}_{\omega q}^*$  is exactly the same function of  $\rho$  as  $f_{\omega q}$  in Region I (E.13). This choice is useful when we define the Hartle-Hawking modes.

The mode expansion for the scalar field in Region II is then

$$\phi(\tilde{t}, \tilde{r}, \varphi) = \sum_{q \in \mathbb{Z}} \int_0^\infty \frac{d\omega}{\sqrt{4\pi\omega}} \tilde{a}_{\omega q} \tilde{F}_{\omega q}(\tilde{t}, \tilde{r}, \varphi) + \text{c.c.}, \quad (\text{E.32})$$

with the canonical commutation relations

$$[\tilde{a}_{\omega q}, \tilde{a}_{\omega' q'}^\dagger] = \delta(\omega - \omega'), \quad [\tilde{a}_{\omega q}, \tilde{a}_{\omega' q'}] = [\tilde{a}_{\omega q}^\dagger, \tilde{a}_{\omega' q'}^\dagger] = 0. \quad (\text{E.33})$$

We note the following property of  $\tilde{F}_{\omega q}$  under complex conjugation:

$$\tilde{F}_{-\omega, -q}^* = \tilde{F}_{\omega q} = F_{-\omega, -q}. \quad (\text{E.34})$$

We also record mode functions that are regular near the horizon  $\tilde{\rho} = 1$ . From the relations (E.34), it follows that

$$\tilde{F}_{\omega q} = \frac{1}{\sqrt{2\pi r_h}} (F_{\omega q}^{1*} + F_{\omega q}^{2*}). \quad (\text{E.35})$$

The near-horizon  $\tilde{\rho} \rightarrow 1$  behaviour of the scalar field is then

$$\phi(U, V, \varphi) \sim \frac{1}{\sqrt{2\pi r_h}} \sum_{q \in \mathbb{Z}} \int_0^\infty \frac{d\omega}{\sqrt{4\pi\omega}} \tilde{a}_{\omega q} e^{iq\varphi} \left( e^{-i\delta_{\omega q}} (-2\eta V)^{i\omega/\eta} + e^{i\delta_{\omega q}} (2\eta U)^{-i\omega/\eta} \right) + \text{c.c.} \quad (\text{E.36})$$

## E.4 Solution in Region F

The ansatz in Region F is

$$e^{-i\omega t_F} e^{-iq\varphi} f_{\omega q}^F(r). \quad (\text{E.37})$$

As usual, we write  $f^F(r) = (1 - \rho)^\alpha \rho^\gamma \chi(\rho)$  so that  $\chi$  satisfies the hypergeometric equation (E.5). There is no normalizability condition imposed on the solution in Region F. Hence, both linearly independent solutions to the Klein-Gordon equation are admitted. We write them in terms of hypergeometric functions  $w_3, w_4$  (E.9) which are defined in a neighbourhood of the horizon  $\rho = 1$ . The mode expansion of the scalar field is then

$$\phi(t_F, r, \varphi) = \frac{1}{\sqrt{2\pi r_h}} \sum_{q \in \mathbb{Z}} \int_0^\infty \frac{d\omega}{\sqrt{4\pi\omega}} \left( C_{\omega q}^F G^1(t_F, r, \varphi) + C_{\omega q}^{F'} G^2(t_F, r, \varphi) + \text{c.c.} \right), \quad (\text{E.38})$$

where  $C_{\omega q}^F$  and  $C_{\omega q}^{F'}$  are some constants, and  $G_{\omega q}^1$  and  $G_{\omega q}^2$  are defined as

$$\begin{aligned} G_{\omega q}^1 &= e^{i\delta_{\omega q}} e^{-i\omega t_F - iq\varphi} (1 - \rho)^\alpha \rho^\gamma {}_2F_1(a, b; a + b - c + 1; 1 - \rho), \\ G_{\omega q}^2 &= e^{-i\delta_{\omega q}} e^{-i\omega t_F - iq\varphi} (1 - \rho)^{-\alpha} \rho^\gamma {}_2F_1(c - a, c - b; c - a - b + 1; 1 - \rho). \end{aligned} \quad (\text{E.39})$$

We fix the constants  $C_{\omega q}^F$  and  $C_{\omega q}^{F'}$  by matching with the mode expansions in Regions I and II at the horizons.

The near horizon behaviour of the  $G^i$  can be obtained by writing  $1 - \rho \sim 4e^{2\eta r^* F}$ . Then,

$$G_{\omega q}^1 \sim e^{-iq\varphi} e^{i\delta_{\omega q}} (2\eta V)^{-i\omega/\eta}, \quad G_{\omega q}^2 \sim e^{-iq\varphi} e^{-i\delta_{\omega q}} (2\eta U)^{i\omega/\eta}, \quad (\text{E.40})$$

which implies

$$\begin{aligned} \phi(U, V, \varphi) \sim \frac{1}{\sqrt{2\pi r_h}} \sum_{q \in \mathbb{Z}} \int_0^\infty \frac{d\omega}{\sqrt{4\pi\omega}} & \left[ e^{-iq\varphi} (C_{\omega q}^F e^{i\delta_{\omega q}} (2\eta V)^{-i\omega/\eta} + C_{\omega q}^{F'} e^{-i\delta_{\omega q}} (2\eta U)^{i\omega/\eta}) \right. \\ & \left. + e^{iq\varphi} (C_{\omega q}^{F*} e^{-i\delta_{\omega q}} (2\eta V)^{i\omega/\eta} + C_{\omega q}^{F'^*} e^{i\delta_{\omega q}} (2\eta U)^{-i\omega/\eta}) \right]. \end{aligned} \quad (\text{E.41})$$

The above expression should match the expression from Region I at the future horizon  $U = 0$  and that from Region II at the past horizon  $V = 0$  so that the scalar field is continuous across the horizons [27]. As  $U \rightarrow 0$ , the  $U$  dependent part oscillates progressively faster and can be set to zero in all expressions (similarly for the  $V \rightarrow 0$  case). The near-horizon expression for the scalar field in Region I is

$$\begin{aligned} \phi(t, r, \varphi) = \frac{1}{\sqrt{2\pi r_h}} \sum_{q \in \mathbb{Z}} \int_0^\infty \frac{d\omega}{\sqrt{4\pi\omega}} & \left[ a_{\omega q} e^{-iq\varphi} (e^{i\delta_{\omega q}} (2\eta V)^{-i\omega/\eta} + e^{-i\delta_{\omega q}} (-2\eta U)^{i\omega/\eta}) \right. \\ & \left. + a_{\omega q}^\dagger e^{iq\varphi} (e^{-i\delta_{\omega q}} (2\eta V)^{i\omega/\eta} + e^{i\delta_{\omega q}} (-2\eta U)^{-i\omega/\eta}) \right]. \end{aligned} \quad (\text{E.42})$$

Similarly, the near-horizon expression for the scalar field in Region II is

$$\begin{aligned} \phi(\tilde{t}, \tilde{r}, \varphi) \sim \frac{1}{\sqrt{2\pi r_h}} \sum_{q \in \mathbb{Z}} \int_0^\infty \frac{d\omega}{\sqrt{4\pi\omega}} & \left[ \tilde{a}_{\omega q} e^{iq\varphi} (e^{-i\delta_{\omega q}} (-2\eta V)^{i\omega/\eta} + e^{i\delta_{\omega q}} (2\eta U)^{-i\omega/\eta}) \right. \\ & \left. + \tilde{a}_{\omega q}^\dagger e^{-iq\varphi} (e^{i\delta_{\omega q}} (-2\eta V)^{-i\omega/\eta} + e^{-i\delta_{\omega q}} (2\eta U)^{i\omega/\eta}) \right]. \end{aligned} \quad (\text{E.43})$$

Matching (E.41) with (E.42) and (E.43) at  $U = 0$  and  $V = 0$  respectively, we get

$$C_{\omega q}^F = a_{\omega q}, \quad C_{\omega q}^{F'} = \tilde{a}_{\omega q}^\dagger. \quad (\text{E.44})$$

Thus, the mode expansion in Region F is

$$\phi(t_F, r, \varphi) = \frac{1}{\sqrt{2\pi r_h}} \sum_{q \in \mathbb{Z}} \int_0^\infty \frac{d\omega}{\sqrt{4\pi\omega}} \left( a_{\omega q} G_{\omega q}^1 + \tilde{a}_{\omega q}^\dagger G_{\omega q}^2 + \text{c.c.} \right). \quad (\text{E.45})$$

## E.5 Solution in Region P

The ansatz in Region P is

$$\phi(t_P, \tilde{r}, \varphi) = e^{i\omega t_P} e^{iq\varphi} f_{\omega q}^P(\tilde{r}). \quad (\text{E.46})$$

with the solutions

$$\begin{aligned}
f_{\omega q}^P(\tilde{r}) &= C_{\omega q}^P (1 - \tilde{\rho})^{\tilde{\alpha}} \tilde{\rho}^{\tilde{\gamma}} w_3(\tilde{\rho}) + C_{\omega q}^{P'} (1 - \tilde{\rho})^{\tilde{\alpha}} \tilde{\rho}^{\tilde{\gamma}} w_4(\tilde{\rho}) , \\
&= C_{\omega q}^P (1 - \tilde{\rho})^{\tilde{\alpha}} \tilde{\rho}^{\tilde{\gamma}} {}_2F_1\left(\tilde{a}, \tilde{b}; \tilde{a} + \tilde{b} - \tilde{c} + 1; 1 - \tilde{\rho}\right) \\
&\quad + C_{\omega q}^{P'} (1 - \tilde{\rho})^{-\tilde{\alpha}} \tilde{\rho}^{\tilde{\gamma}} {}_2F_1\left(\tilde{c} - \tilde{a}, \tilde{c} - \tilde{b}; \tilde{c} - \tilde{a} - \tilde{b} + 1; 1 - \tilde{\rho}\right) , \tag{E.47}
\end{aligned}$$

for some constants  $C_{\omega q}^P$  and  $C_{\omega q}^{P'}$ . Note that the functions above are simply  $G^{1*}$  and  $G^{2*}$  respectively so that the scalar field in Region P has the mode expansion

$$\phi(t_P, \tilde{r}, \varphi) = \frac{1}{\sqrt{2\pi r_h}} \sum_{q \in \mathbb{Z}} \int_0^\infty \frac{d\omega}{\sqrt{4\pi\omega}} \left( C_{\omega q}^P G_{\omega q}^{1*}(t_P, \tilde{r}, \varphi) + C_{\omega q}^{P'} G_{\omega q}^{2*}(t_P, \tilde{r}, \varphi) + \text{c.c.} \right) . \tag{E.48}$$

The near horizon expression is

$$\begin{aligned}
\phi(t_P, \tilde{r}, \varphi) &\sim \frac{1}{\sqrt{2\pi r_h}} \sum_{q \in \mathbb{Z}} \int_0^\infty \frac{d\omega}{\sqrt{4\pi\omega}} \left[ e^{iq\varphi} \left( C_{\omega q}^P e^{-i\delta_{\omega q}} (-2\eta V)^{i\omega/\eta} + C_{\omega q}^{P'} e^{i\delta_{\omega q}} (-2\eta U)^{-i\omega/\eta} \right) \right. \\
&\quad \left. + e^{-iq\varphi} \left( C_{\omega q}^{P*} e^{i\delta_{\omega q}} (-2\eta V)^{-i\omega/\eta} + C_{\omega q}^{P'^*} e^{-i\delta_{\omega q}} (-2\eta U)^{i\omega/\eta} \right) \right] . \tag{E.49}
\end{aligned}$$

At the future horizon  $U = 0$ , (E.49) has to be matched with the expression (E.43) in Region II, whereas at the past horizon  $V = 0$ , it has to be matched with the expression (E.42) in Region I.

We get

$$C_{\omega q}^P = \tilde{a}_{\omega q} , \quad C_{\omega q}^{P'} = a_{\omega q}^\dagger , \tag{E.50}$$

so that the mode expansion in Region P is

$$\phi(t_P, \tilde{r}, \varphi) = \frac{1}{\sqrt{2\pi r_h}} \sum_{q \in \mathbb{Z}} \int_0^\infty \frac{d\omega}{\sqrt{4\pi\omega}} \left( \tilde{a}_{\omega q} G_{\omega q}^{1*} + a_{\omega q}^\dagger G_{\omega q}^{2*} + \text{c.c.} \right) . \tag{E.51}$$

## E.6 Analytic continuation to regions F and P

In the previous subsections, we solved the Klein-Gordon equation separately in each Region and then matched the expressions across the horizons. These mode functions were analytic in the lower-half  $t$  plane (where  $t$  has to be replaced by its counterpart in each Region). One can also consider functions which are analytic in the lower-half  $U$  or  $V$  planes. This consideration is motivated by the simple observation, due to Unruh [69], that translations in the  $V$  coordinate are a symmetry of the metric on the future horizon  $U = 0$  (and similarly, translations in  $U$  on the future horizon  $V = 0$ ). One can then naturally write down mode functions  $e^{-i\omega V}$  which are analytic in the lower-half  $V$  plane. Following Unruh, let us try to obtain appropriate analytic continuations of the mode functions  $F_{\omega q}^i$  such that they are analytic in the lower-half  $U$  and  $V$  planes. For better readability, we reproduce the mode functions  $F_{\omega q}^i$  and  $G_{\omega q}^i$  below:

$$\begin{aligned}
F_{\omega q}^1 &= e^{-i\omega t - iq\varphi} e^{i\delta_{\omega q}} (\rho - 1)^\alpha \rho^\gamma {}_2F_1(a, b; a + b - c + 1; 1 - \rho) , \\
F_{\omega q}^2 &= e^{-i\omega t - iq\varphi} e^{-i\delta_{\omega q}} (\rho - 1)^{-\alpha} \rho^\gamma {}_2F_1(c - a, c - b; c - a - b + 1; 1 - \rho) . \tag{E.52}
\end{aligned}$$

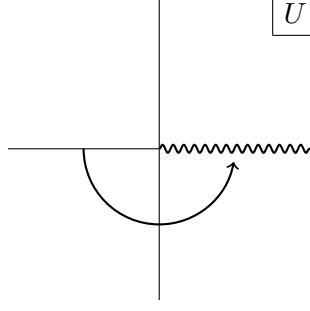


Figure 8: Analytic continuation in the lower-half  $U$ -plane.

$$\begin{aligned} G_{\omega q}^1 &= e^{i\delta\omega q} e^{-i\omega t_F - iq\varphi} (1 - \rho)^\alpha \rho^\gamma {}_2F_1(a, b; a + b - c + 1; 1 - \rho) , \\ G_{\omega q}^2 &= e^{-i\delta\omega q} e^{-i\omega t_F - iq\varphi} (1 - \rho)^{-\alpha} \rho^\gamma {}_2F_1(c - a, c - b; c - a - b + 1; 1 - \rho) . \end{aligned} \quad (\text{E.53})$$

The mode functions  $F_{\omega q}^i$  in Region I are valid for  $U < 0$ ,  $V > 0$ , and are certainly not analytic in the lower-half  $U$  and  $V$  planes. However, one can make them analytic in the lower-half  $U$  plane by appropriately defining their continuation to  $U > 0$ , across the future horizon  $U = 0$  (and similarly, across the past horizon  $V = 0$ ). Recall from (E.26) that  $F_{\omega q}^1 \sim V^{-i\omega/\eta}$ . Hence, this continues uneventfully across  $U = 0$ . The function  $F_{\omega q}^2 \sim U^{i\omega/\eta}$  requires the introduction of a branch cut in the complex  $U$  plane to be well-defined. Let us take the branch cut along the positive  $U$  axis and define

$$\text{For } U > 0, \quad \underbrace{U}_{\text{in F}} = e^{i\pi} \underbrace{(-U)}_{\text{in I}} . \quad (\text{E.54})$$

This corresponds to a rotation by  $\pi$  in the counter-clockwise direction in the lower-half  $U$  plane, see Figure 8. This ensures that  $U^{i\omega/\eta}$  is analytic in the lower-half plane. How do we implement this for the full function  $F_{\omega q}^2$  and not just its near-horizon expression? Recall the definition of the Kruskal  $U$  in Regions I and F:

$$\text{Region I: } U = -\eta^{-1} e^{-\eta(t-r_*)} , \quad \text{Region F: } U = \eta^{-1} e^{-\eta(t_F - r_{*F})} . \quad (\text{E.55})$$

To get formulas in Region F, we replace  $t - r_*$  by  $t - r_* - i\pi/\eta$  in all formulas in Region I. But since the local coordinates in Region F are called  $t_F$  and  $r_F$ , we relabel  $t$  and  $r_*$  as  $t_F$  and  $r_F$  respectively, after the replacement. Effectively, we have

$$t - r_* \rightarrow t_F - r_{*F} - i\pi/\eta , \quad t + r_* \rightarrow t_F + r_{*F} , \quad (\text{E.56})$$

that is,

$$\text{Region I} \rightarrow \text{Region F: } t \rightarrow t_F - i\pi/2\eta , \quad r_* \rightarrow r_{*F} + i\pi/2\eta \quad \Rightarrow \quad \rho - 1 \rightarrow e^{i\pi}(1 - \rho) . \quad (\text{E.57})$$

Next, the continuation across the past horizon  $V = 0$  involves taking  $V$  to  $-V$  through the lower half complex  $V$  plane while keeping  $U$  fixed:

$$\text{For } V < 0, \quad \underbrace{V}_{\text{in P}} = e^{-i\pi} \underbrace{(-V)}_{\text{in I}} = -e^{-i\pi} \eta^{-1} e^{\eta(t+r_*)} , \quad (\text{E.58})$$

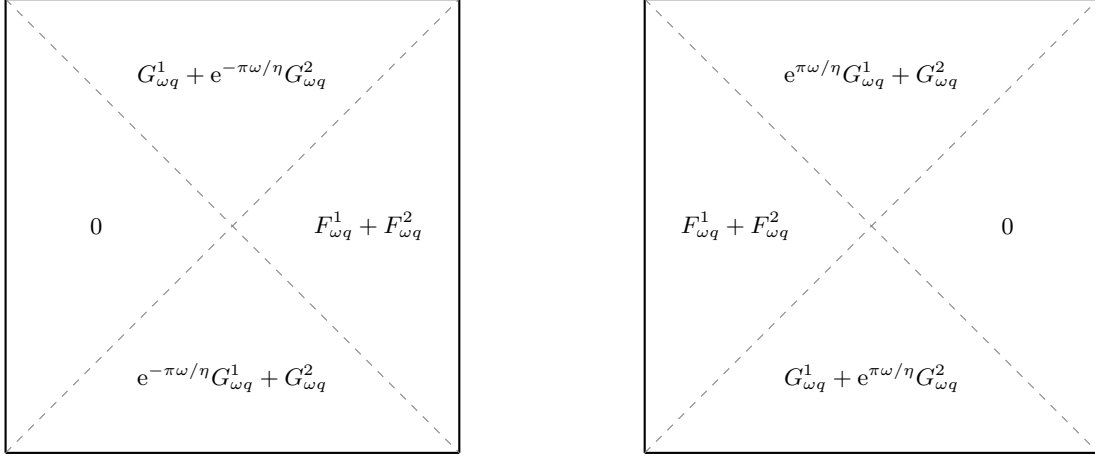


Figure 9: The above are Penrose diagrams for the fully extended BTZ black hole. **Left:** The analytic continuation of Region I mode  $F_{\omega q} = F_{\omega q}^1 + F_{\omega q}^2$  to rest of the fully extended BTZ spacetime. **Right:** The analytic continuation of Region II conjugate modes  $\tilde{F}_{\omega q}^* = F_{\omega q}^1 + F_{\omega q}^2$ .

which corresponds to

$$\text{Region I} \rightarrow \text{Region P: } t \rightarrow t_P - i\pi/2\eta, \quad r_* \rightarrow r_{*P} - i\pi/2\eta \quad \Rightarrow \quad \rho - 1 \rightarrow e^{-i\pi}(1 - \tilde{\rho}). \quad (\text{E.59})$$

Thus, we apply the above rules to  $F_{\omega q}^i$  to obtain the appropriate analytic continuation to Regions F and P. We then get

$$\begin{aligned} \text{Region I to F: } & F_{\omega q}^1(t, r, \varphi) \rightarrow G_{\omega q}^1(t_F, r, \varphi), \quad F_{\omega q}^2(t, r, \varphi) \rightarrow e^{-\pi\omega/\eta} G_{\omega q}^2(t_F, r, \varphi), \\ \text{Region I to P: } & F_{\omega q}^1(t, r, \varphi) \rightarrow e^{-\pi\omega/\eta} G_{\omega q}^1(t_P, \tilde{r}, \varphi), \quad F_{\omega q}^2(t, r, \varphi) \rightarrow G_{\omega q}^2(t_P, \tilde{r}, \varphi). \end{aligned} \quad (\text{E.60})$$

The analytic continuation of the  $F_{\omega q}^i$  are then

$$F_{\omega q}^1 = \begin{cases} F_{\omega q}^1 & \text{Region I} \\ G_{\omega q}^1 & \text{Region F} \\ e^{-\pi\omega/\eta} G_{\omega q}^1 & \text{Region P} \\ 0 & \text{Region II.} \end{cases} \quad F_{\omega q}^2 = \begin{cases} F_{\omega q}^2 & \text{Region I} \\ e^{-\pi\omega/\eta} G_{\omega q}^2 & \text{Region F} \\ G_{\omega q}^2 & \text{Region P} \\ 0 & \text{Region II.} \end{cases} \quad (\text{E.61})$$

This is summarized on the left of Figure 9.

**Note:** Most importantly, the function presented (E.61) is analytic for negative values of  $\omega$  as well, since the procedure above did not involve positivity of  $\omega$ .

Similarly, we can work out the continuation rules for Region II to Regions F and P:

$$\begin{aligned} \text{Region II} \rightarrow \text{Region F: } & \tilde{t} \rightarrow t_F + i\pi/2\eta, \quad \tilde{r}_* \rightarrow r_{*F} + i\pi/2\eta \quad \Rightarrow \quad \tilde{\rho} - 1 \rightarrow e^{i\pi}(1 - \rho), \\ \text{Region II} \rightarrow \text{Region P: } & \tilde{t} \rightarrow t_P + i\pi/2\eta, \quad \tilde{r}_* \rightarrow r_{*P} - i\pi/2\eta \quad \Rightarrow \quad \tilde{\rho} - 1 \rightarrow e^{-i\pi}(1 - \tilde{\rho}). \end{aligned} \quad (\text{E.62})$$

The Region II modes (E.35) involve  $F^{i*}$ . Under the rules (E.62), the analytic continuation to



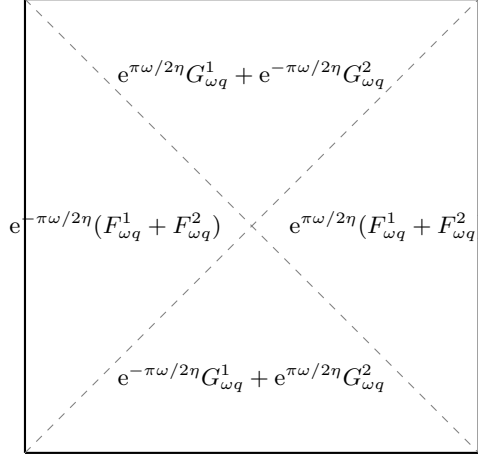


Figure 10: The definition of the Hartle-Hawking modes  $h_{\omega q}$  by the Unruh procedure.

Regions F and P are

$$\begin{aligned}
\text{Region II to F : } & F_{\omega q}^{1*}(\tilde{t}, \tilde{r}, \varphi) \rightarrow e^{-\pi\omega/\eta} G_{\omega q}^{1*}(t_F, r, \varphi) , \quad F_{\omega q}^{2*}(\tilde{t}, \tilde{r}, \varphi) \rightarrow G_{\omega q}^{2*}(t_F, r, \varphi) , \\
\text{Region II to P : } & F_{\omega q}^{1*}(\tilde{t}, \tilde{r}, \varphi) \rightarrow G_{\omega q}^{1*}(t_P, \tilde{r}, \varphi) , \quad F_{\omega q}^{2*}(\tilde{t}, \tilde{r}, \varphi) \rightarrow e^{-\pi\omega/\eta} G_{\omega q}^{2*}(t_P, \tilde{r}, \varphi) . \quad (\text{E.63})
\end{aligned}$$

We also need the analytic continuation of the conjugate mode functions in Region II. These simply involve the  $F_{\omega q}^i$ . Applying the rules (E.62), we get

$$\begin{aligned}
\text{Region II to F : } & F_{\omega q}^1(\tilde{t}, \tilde{r}, \varphi) \rightarrow e^{\pi\omega/\eta} G_{\omega q}^1(t_F, r, \varphi) , \quad F_{\omega q}^2(\tilde{t}, \tilde{r}, \varphi) \rightarrow G_{\omega q}^2(t_F, r, \varphi) , \\
\text{Region II to P : } & F_{\omega q}^1(\tilde{t}, \tilde{r}, \varphi) \rightarrow G_{\omega q}^1(t_P, \tilde{r}, \varphi) , \quad F_{\omega q}^2(\tilde{t}, \tilde{r}, \varphi) \rightarrow e^{\pi\omega/\eta} G_{\omega q}^2(t_P, \tilde{r}, \varphi) . \quad (\text{E.64})
\end{aligned}$$

The analytic continuations of the Region II conjugate modes are summarized on the right in Figure 9. Observe that the analytic continuation of the rescaled Region I mode function  $e^{\pi\omega/2\eta}F_{\omega q} = e^{\pi\omega/2\eta}(F^1 + F^2)$  and the rescaled Region II mode function  $e^{-\pi\omega/2\eta}\tilde{F}_{\omega q}^* = e^{-\pi\omega/2\eta}(F^1 + F^2)$  agree on Region F and Region P. Using these analytic continuations, we can define a function on the fully extended BTZ black hole that is analytic in the lower half  $U, V$  planes as

$$h_{\omega}(U, V, \varphi) = \frac{1}{\sqrt{4\pi\omega}\sqrt{2\sinh(\pi\omega/\eta)}} \begin{cases} e^{\pi\omega/2\eta}(F_{\omega q}^1 + F_{\omega q}^2) & \text{Region I} \\ e^{\pi\omega/2\eta}G_{\omega q}^1 + e^{-\pi\omega/2\eta}G_{\omega q}^2 & \text{Region F} \\ e^{-\pi\omega/2\eta}G_{\omega q}^1 + e^{\pi\omega/2\eta}G_{\omega q}^2 & \text{Region P} \\ e^{-\pi\omega/2\eta}(F_{\omega q}^1 + F_{\omega q}^2) & \text{Region II .} \end{cases} \quad (\text{E.65})$$

Note that these modes are analytic in the lower half  $U$  and  $V$  planes for both positive and negative  $\omega$ . Thus,  $\omega$  is a label running over all real numbers for these modes, and only when we include  $\omega$  of both signs do we get a complete set of modes.

## E.7 The Hartle-Hawking modes and Bogoliubov coefficients

The scalar field can then be expanded in terms of these Hartle-Hawking modes:

$$\phi(U, V, \varphi) = \frac{1}{\sqrt{2\pi r_h}} \sum_{q \in \mathbb{Z}} \int_{-\infty}^{\infty} d\omega c_{\omega q} h_{\omega q} + \text{c.c.} . \quad (\text{E.66})$$

For future use, we define  $\tilde{c}_{\omega q} = c_{-\omega, -q}$  for  $\omega > 0$ . Restricting to Region I, we get

$$\begin{aligned} & \phi(U, V, \varphi)|_{\text{I}} \\ &= \sum_{q \in \mathbb{Z}} \int_{-\infty}^{\infty} \frac{d\omega}{\sqrt{4\pi\omega} \sqrt{2 \sinh \frac{\pi\omega}{\eta}}} (c_{\omega q} e^{\pi\omega/2\eta} F_{\omega q} + c_{\omega q}^\dagger e^{\pi\omega/2\eta} F_{\omega q}^*) , \\ &= \sum_{q \in \mathbb{Z}} \int_0^{\infty} \frac{d\omega}{\sqrt{4\pi\omega} \sqrt{2 \sinh \frac{\pi\omega}{\eta}}} (c_{\omega q} e^{\pi\omega/2\eta} F_{\omega q} + \tilde{c}_{\omega q} e^{-\pi\omega/2\eta} F_{-\omega, -q} \\ & \quad + c_{\omega q}^\dagger e^{\pi\omega/2\eta} F_{\omega q}^* + \tilde{c}_{\omega q}^\dagger e^{-\pi\omega/2\eta} F_{-\omega, -q}^*) , \\ &= \sum_{q \in \mathbb{Z}} \int_0^{\infty} \frac{d\omega}{\sqrt{4\pi\omega} \sqrt{2 \sinh \frac{\pi\omega}{\eta}}} ((c_{\omega q} e^{\pi\omega/2\eta} + \tilde{c}_{\omega q}^\dagger e^{-\pi\omega/2\eta}) F_{\omega q} \\ & \quad + (\tilde{c}_{\omega q} e^{-\pi\omega/2\eta} + c_{\omega q}^\dagger e^{\pi\omega/2\eta}) F_{\omega q}^*) . \end{aligned} \quad (\text{E.67})$$

Comparing with the mode expansion in Region I (E.16), we get the following relations between the operators  $a_{\omega q}$  and  $c_{\omega q}, \tilde{c}_{\omega q}$ :

$$a_{\omega q} = \frac{c_{\omega q} e^{\pi\omega/2\eta} + \tilde{c}_{\omega q}^\dagger e^{-\pi\omega/2\eta}}{\sqrt{2 \sinh(\pi\omega/\eta)}} , \quad a_{\omega q}^\dagger = \frac{c_{\omega q}^\dagger e^{\pi\omega/2\eta} + \tilde{c}_{\omega q} e^{-\pi\omega/2\eta}}{\sqrt{2 \sinh(\pi\omega/\eta)}} . \quad (\text{E.68})$$

Similarly, restricting the global mode expansion (E.66) to Region II, and comparing with the mode expansion in Region II (5.25), we get

$$\tilde{a}_{\omega q} = \frac{\tilde{c}_{\omega q} e^{\pi\omega/2\eta} + c_{\omega q}^\dagger e^{-\pi\omega/2\eta}}{\sqrt{2 \sinh(\pi\omega/\eta)}} , \quad \tilde{a}_{\omega q}^\dagger = \frac{\tilde{c}_{\omega q}^\dagger e^{\pi\omega/2\eta} + c_{\omega q} e^{-\pi\omega/2\eta}}{\sqrt{2 \sinh(\pi\omega/\eta)}} . \quad (\text{E.69})$$

We can invert the relations (E.68) and (E.69) together to get the Bogoliubov transformations

$$c_{\omega q} = \frac{a_{\omega q} e^{\pi\omega/2\eta} - \tilde{a}_{\omega q}^\dagger e^{-\pi\omega/2\eta}}{\sqrt{2 \sinh(\pi\omega/\eta)}} , \quad \tilde{c}_{\omega q} = \frac{\tilde{a}_{\omega q} e^{\pi\omega/2\eta} - a_{\omega q}^\dagger e^{-\pi\omega/2\eta}}{\sqrt{2 \sinh(\pi\omega/\eta)}} , \quad (\text{E.70})$$

and their conjugates. The commutation relations for  $c_{\omega q}, \tilde{c}_{\omega q}$  for  $\omega > 0$  can be obtained from those of the  $a_{\omega q}, \tilde{a}_{\omega q}$ :

$$[c_{\omega q}, c_{\omega' q'}^\dagger] = [\tilde{c}_{\omega q}, \tilde{c}_{\omega' q'}^\dagger] = \delta(\omega - \omega') \delta_{qq'} , \quad [c_{\omega q}, \tilde{c}_{\omega' q'}] = [c_{\omega q}, c_{\omega' q'}] = [\tilde{c}_{\omega q}, \tilde{c}_{\omega' q'}] = 0 . \quad (\text{E.71})$$

## E.8 Normalization of the Klein-Gordon mode functions

The Klein-Gordon inner product between two solutions  $\phi_1$  and  $\phi_2$  of the Klein-Gordon equation is defined by

$$(\phi_1, \phi_2)_{\text{KG}} = i \int_{\Sigma} d^{d-1} x \sqrt{g} \eta^\mu (\phi_1^* D_\mu \phi_2 - D_\mu \phi_1^* \phi_2) , \quad (\text{E.72})$$

where  $\Sigma$  is a constant time slice and  $n^\mu$  is the future directed unit vector normal to it. In a static spacetime with metric

$$-N^2 dt^2 + g_{ij} dx^i dx^j , \quad (\text{E.73})$$

the normal to the constant time  $t$  slice in the coordinate basis  $(\partial/\partial t, \partial/\partial x^i)$  is given by

$$n^\mu \partial_\mu = N^{-1} \partial_t . \quad (\text{E.74})$$

Thus, the Klein-Gordon inner product becomes

$$(\phi_1, \phi_2)_{\text{KG}} = i \int d^{d-1}x \sqrt{g} N^{-1} (\phi_1^* \dot{\phi}_2 - \dot{\phi}_1^* \phi_2) . \quad (\text{E.75})$$

For the BTZ black hole, we have

$$N(r) = f(r)^{1/2} , \quad g_{rr} = f(r)^{-1} , \quad g_{\varphi\varphi} = r^2 , \quad \sqrt{g} = r f(r)^{-1/2} . \quad (\text{E.76})$$

Since  $\partial_t$  and  $\partial_\varphi$  are Killing vectors, we can separate variables and write

$$F_{\omega q}(t, r, \varphi) = \frac{1}{\sqrt{2\pi}} e^{-i\omega t} e^{-iq\varphi} f_{\omega q}(r) . \quad (\text{E.77})$$

In this case, the Klein-Gordon norm between the modes  $F_{\omega q}$  and  $F_{\omega' q'}$  becomes

$$\begin{aligned} (F_{\omega' q'}, F_{\omega q})_{\text{KG}} &= \frac{1}{2\pi} (\omega + \omega') e^{i(\omega' - \omega)t} \int dr d\varphi r f^{-1} f_{\omega' q'}^* f_{\omega q} e^{i(q' - q)\varphi} , \\ &= (\omega + \omega') e^{i(\omega' - \omega)t} \delta_{qq'} \int dr r f^{-1} f_{\omega' q'}^* f_{\omega q} , \\ &= \frac{\ell^2}{2} (\omega + \omega') e^{i(\omega' - \omega)t} \delta_{qq'} \int \frac{d\rho}{\rho - 1} f_{\omega' q'}^* f_{\omega q} , \\ &= -\frac{\ell^2 \eta}{2} (\omega + \omega') e^{i(\omega' - \omega)t} \delta_{qq'} \int dr_* \coth \eta r_* f_{\omega' q'}^* f_{\omega q} . \end{aligned} \quad (\text{E.78})$$

We are interested in the norm in Region I so that the limits of the integral above are

$$r_h < r < \infty , \quad 1 < \rho < \infty , \quad -\infty < r_* < 0 . \quad (\text{E.79})$$

The equation for  $f_{\omega q}(r)$  becomes the following ordinary differential equation in  $r$ :

$$\frac{1}{r} \frac{d}{dr} \left( r f \frac{df_{\omega q}}{dr} \right) = (-f^{-1} \omega^2 + q^2 r^{-2} + m^2) f_{\omega q} , \quad (\text{E.80})$$

which, in terms of  $\rho = r^2/r_h^2$ , becomes

$$\frac{d}{d\rho} \left( \rho(\rho - 1) \frac{df_{\omega q}}{d\rho} \right) = \left( -\frac{1}{4(\rho - 1)} \frac{\omega^2}{\eta^2} + \frac{q^2 \ell^2}{4\rho r_h^2} + \frac{\ell^2 m^2}{4} \right) f_{\omega q} . \quad (\text{E.81})$$

This gives

$$f_{\omega'q}^* \frac{d}{d\rho} \left( \rho(\rho-1) \frac{df_{\omega q}}{d\rho} \right) - f_{\omega q} \frac{d}{d\rho} \left( \rho(\rho-1) \frac{df_{\omega'q}^*}{d\rho} \right) = -\frac{1}{4(\rho-1)} \frac{(\omega^2 - \omega'^2)}{\eta^2} f_{\omega'q}^* f_{\omega q} . \quad (\text{E.82})$$

Integrating both sides over  $\rho$ , we get

$$\int d\rho f_{\omega'q}^* \frac{d}{d\rho} \left( \rho(\rho-1) \frac{df_{\omega q}}{d\rho} \right) - \int d\rho f_{\omega q} \frac{d}{d\rho} \left( \rho(\rho-1) \frac{df_{\omega'q}^*}{d\rho} \right) = -\frac{(\omega^2 - \omega'^2)}{4\eta^2} \int \frac{d\rho}{\rho-1} f_{\omega'q}^* f_{\omega q} . \quad (\text{E.83})$$

Integrating by parts in both terms on the left-hand side, we see that the volume terms cancel each other, and there is only a surface contribution left:

$$\left[ \rho(\rho-1) \left( f_{\omega'q}^* \frac{df_{\omega q}}{d\rho} - f_{\omega q} \frac{df_{\omega'q}^*}{d\rho} \right) \right]_{\rho_0}^{\rho_1} = -\frac{(\omega^2 - \omega'^2)}{4\eta^2} \int_{\rho_0}^{\rho_1} \frac{d\rho}{\rho-1} f_{\omega'q}^* f_{\omega q} . \quad (\text{E.84})$$

The right hand side is proportional to the Klein-Gordon inner product of  $\phi_{\omega'q}$  and  $\phi_{\omega q}$ :

$$\left[ \rho(\rho-1) \left( f_{\omega'q}^* \frac{df_{\omega q}}{d\rho} - f_{\omega q} \frac{df_{\omega'q}^*}{d\rho} \right) \right]_{\rho_0 \rightarrow 1}^{\rho_1 \rightarrow \infty} = \frac{(\omega' - \omega)}{2\eta^2 \ell^2} e^{-i(\omega' - \omega)t} (F_{\omega'q}, F_{\omega q})_{\text{KG}} . \quad (\text{E.85})$$

Let us first study the boundary term at  $\rho = \infty$ . The two solutions of the Klein-Gordon equation can be written in terms of solutions of the hypergeometric equation that are regular at  $\infty$ :

$$f_{\omega q}^{\pm}(\rho) = C_{\omega q}^{\pm} (\rho-1)^{\alpha} \rho^{-\alpha - \frac{1}{2}\Delta_{\pm}} {}_2F_1 \left( \alpha + \gamma + \frac{1}{2}\Delta_{\pm}, \alpha - \gamma + \frac{1}{2}\Delta_{\pm}; \Delta_{\pm}; \frac{1}{\rho} \right) . \quad (\text{E.86})$$

As  $\rho \rightarrow \infty$ , we have

$$f_{\omega q}^{\pm}(\rho) = C_{\omega q}^{\pm} \rho^{-\Delta_{\pm}/2} \left( 1 + \frac{4(\alpha^2 - \gamma^2) + \Delta_{\pm}^2}{4\Delta_{\pm}} \frac{1}{\rho} + \mathcal{O}(\rho^{-2}) \right) , \quad (\text{E.87})$$

$$\frac{df_{\omega q}^{\pm}}{d\rho} = C_{\omega q}^{\pm} \rho^{-\Delta_{\pm}/2-1} \left( -\frac{\Delta_{\pm}}{2} + \frac{(4(\alpha^2 - \gamma^2) + \Delta_{\pm}^2)(2 + \Delta_{\pm})}{8\Delta_{\pm}} \frac{1}{\rho} + \mathcal{O}(\rho^{-2}) \right) . \quad (\text{E.88})$$

Plugging this into the left hand side at  $\rho = \infty$ , the leading contribution cancels, whereas the subleading contribution is

$$\left[ \rho(\rho-1) \left( f_{\omega'q}^{\pm*} \frac{df_{\omega q}^{\pm}}{d\rho} - f_{\omega q}^{\pm} \frac{df_{\omega'q}^{\pm*}}{d\rho} \right) \right]_{\rho \rightarrow \infty} = C_{\omega'q}^{\pm*} C_{\omega q}^{\pm} \frac{(2 + \Delta_{\pm})(\omega^2 - \omega'^2)}{8\Delta_{\pm}\eta^2} \rho^{-\Delta_{\pm}} \Big|_{\rho \rightarrow \infty} . \quad (\text{E.89})$$

Thus, when  $m^2 > 0$ ,  $f_{\omega q}^+$  is normalizable since  $\Delta_+ > 0$  whereas  $f_{\omega q}^-$  is not normalizable since  $\Delta_- < 0$ . We choose to work with the normalizable solution  $f_{\omega q}^+$  and thus the upper limit in (E.85) simply vanishes.

The normalizable solution  $f_{\omega q}^+(\rho)$  can be rewritten in terms of hypergeometric functions which

are regular near  $\rho = 1$ , see (E.23). Near the horizon in region I as  $\rho \rightarrow 1^+$ , we then get

$$\begin{aligned}
f_{\omega q}^+ &= C_{\omega q}^+ N_{\omega q} \left( e^{i\delta_{\omega q}} 2^{-i\omega/\eta} e^{-i\omega r_*} + e^{-i\delta_{\omega q}} 2^{i\omega/\eta} e^{i\omega r_*} \right) + \mathcal{O}(e^{2\eta r_*}) \\
&= 2 C_{\omega q}^+ N_{\omega q} \cos \left( \delta_{\omega q} - \omega r_* - \frac{\omega}{\eta} \log 2 \right) + \mathcal{O}(e^{2\eta r_*}) , \\
\rho(\rho - 1) \frac{df_{\omega q}^+}{d\rho} &= C_{\omega q}^+ N_{\omega q} \alpha \left( e^{i\delta_{\omega q}} (\rho - 1)^\alpha - e^{-i\delta_{\omega q}} (\rho - 1)^{-\alpha} \right) + \mathcal{O}(\rho - 1) \\
&= C_{\omega q}^+ N_{\omega q} \frac{\omega}{\eta} \sin \left( \delta_{\omega q} - \omega r_* - \frac{\omega}{\eta} \log 2 \right) + \mathcal{O}(e^{2\eta r_*}) . \tag{E.90}
\end{aligned}$$

Recall that to calculate the Klein-Gordon inner product, we need to find the LHS of (E.85). The upper limit vanished for the normalizable mode and we only have to calculate the lower limit. From the above equations, we get

$$\begin{aligned}
&f_{\omega' q}^{+*} \rho(\rho - 1) \frac{df_{\omega q}^+}{d\rho} \\
&= C_{\omega' q}^{+*} N_{\omega' q} C_{\omega q}^+ N_{\omega q} \frac{\omega}{\eta} \left[ \sin \left( \delta_{\omega q} + \delta_{\omega' q} - (\omega + \omega') r_* - \frac{\omega + \omega'}{\eta} \log 2 \right) \right. \\
&\quad \left. + \sin \left( \delta_{\omega q} - \delta_{\omega' q} - (\omega - \omega') r_* - \frac{\omega - \omega'}{\eta} \log 2 \right) \right] + \mathcal{O}(e^{2\eta r_*}) . \tag{E.91}
\end{aligned}$$

Using

$$\lim_{r_* \rightarrow -\infty} \frac{\sin(-\omega r_*)}{\omega} = \pi \delta(\omega) , \tag{E.92}$$

we get

$$\frac{1}{(\omega - \omega')} \lim_{r_* \rightarrow -\infty} f_{\omega' q}^{+*} \rho(\rho - 1) \frac{df_{\omega q}^+}{d\rho} = |C_{\omega' q}^+|^2 N_{\omega q}^2 \frac{\pi \omega}{\eta} \delta(\omega - \omega') . \tag{E.93}$$

Since  $\omega, \omega' \geq 0$ , the other delta function never clicks. Therefore we have

$$\frac{1}{(\omega - \omega')} \left[ \rho(\rho - 1) \left( f_{\omega' q}^{+*} \frac{df_{\omega q}^+}{d\rho} - f_{\omega q}^+ \frac{df_{\omega' q}^{+*}}{d\rho} \right) \right]_{\rho \rightarrow 1^+} = |C_{\omega' q}^+|^2 N_{\omega q}^2 \frac{\pi}{\eta} 2\omega \delta(\omega - \omega') , \tag{E.94}$$

from which we find the Klein-Gordon inner product

$$(F_{\omega' q}, F_{\omega q})_{\text{KG}} = |C_{\omega' q}^+|^2 N_{\omega q}^2 2\pi r_h 2\omega \delta(\omega - \omega') . \tag{E.95}$$

Setting

$$C_{\omega q}^+ = \frac{1}{N_{\omega q} \sqrt{2\pi r_h}} , \tag{E.96}$$

we get

$$f_{\omega q}^+(\rho) = \frac{1}{N_{\omega q} \sqrt{2\pi r_h}} (\rho - 1)^\alpha \rho^{-\alpha - \frac{1}{2}\Delta_+} {}_2F_1 \left( \alpha + \gamma + \frac{1}{2}\Delta_+, \alpha - \gamma + \frac{1}{2}\Delta_+; \Delta_+; \frac{1}{\rho} \right) , \tag{E.97}$$

so that the modes  $F_{\omega q} = \frac{1}{\sqrt{2\pi}} e^{-i\omega t} e^{-iq\varphi} f_{\omega q}$  satisfy the canonical Klein-Gordon norm

$$(F_{\omega'q'}, F_{\omega q})_{\text{KG}} = 2\omega\delta(\omega - \omega')\delta_{qq'} . \quad (\text{E.98})$$

## References

- [1] P. A. M. Dirac, “Generalized Hamiltonian dynamics”, in: *Can. J. Math.* 2 (1950), pp. 129–148, DOI: [10.4153/CJM-1950-012-1](https://doi.org/10.4153/CJM-1950-012-1).
- [2] P. Dirac, *Lectures on Quantum Mechanics*, Belfer Graduate School of Science, monograph series, Dover Publications, 2001, URL: <https://books.google.co.in/books?id=GVwzb1rZW9kC>.
- [3] Y. Choquet-Bruhat, J. Isenberg, and D. Pollack, “The Einstein-scalar field constraints on asymptotically Euclidean manifolds”, in: (June 2005), arXiv: [gr-qc/0506101](https://arxiv.org/abs/gr-qc/0506101).
- [4] Y. Choquet-Bruhat, J. Isenberg, and D. Pollack, “The Constraint equations for the Einstein-scalar field system on compact manifolds”, in: *Class. Quant. Grav.* 24 (2007), pp. 809–828, DOI: [10.1088/0264-9381/24/4/004](https://doi.org/10.1088/0264-9381/24/4/004), arXiv: [gr-qc/0610045](https://arxiv.org/abs/gr-qc/0610045).
- [5] E. Hebey, F. Pacard, and D. Pollack, “A Variational analysis of Einstein-scalar field Lichnerowicz equations on compact Riemannian manifolds”, in: *Commun. Math. Phys.* 278 (2008), pp. 117–132, DOI: [10.1007/s00220-007-0377-1](https://doi.org/10.1007/s00220-007-0377-1), arXiv: [gr-qc/0702031](https://arxiv.org/abs/gr-qc/0702031).
- [6] A. Sakovich, “Constant mean curvature solutions of the Einstein-scalar field constraint equations on asymptotically hyperbolic manifolds”, in: *Class. Quant. Grav.* 27 (2010), p. 245019, DOI: [10.1088/0264-9381/27/24/245019](https://doi.org/10.1088/0264-9381/27/24/245019), arXiv: [0910.4178 \[gr-qc\]](https://arxiv.org/abs/0910.4178).
- [7] E. Witten, “A note on the canonical formalism for gravity”, in: *Adv. Theor. Math. Phys.* 27.1 (2023), pp. 311–380, DOI: [10.4310/ATMP.2023.v27.n1.a6](https://doi.org/10.4310/ATMP.2023.v27.n1.a6), arXiv: [2212.08270 \[hep-th\]](https://arxiv.org/abs/2212.08270).
- [8] E. Witten, Canonical Quantization in Anti de Sitter Space, [\[LINK\]](#), Talk at Princeton Center for Theoretical Science, Oct. 2017.
- [9] M. Henneaux and C. Teitelboim, “Asymptotically anti-De Sitter Spaces”, in: *Commun. Math. Phys.* 98 (1985), pp. 391–424, DOI: [10.1007/BF01205790](https://doi.org/10.1007/BF01205790).
- [10] J. D. Brown and M. Henneaux, “Central Charges in the Canonical Realization of Asymptotic Symmetries: An Example from Three-Dimensional Gravity”, in: *Commun. Math. Phys.* 104 (1986), pp. 207–226, DOI: [10.1007/BF01211590](https://doi.org/10.1007/BF01211590).
- [11] V. Moncrief, “Reduction of the Einstein equations in (2+1)-dimensions to a Hamiltonian system over Teichmuller space”, in: *J. Math. Phys.* 30 (1989), pp. 2907–2914, DOI: [10.1063/1.528475](https://doi.org/10.1063/1.528475).
- [12] L. Andersson, V. Moncrief, and A. J. Tromba, “On the global evolution problem in (2+1) gravity”, in: *J. Geom. Phys.* 23 (1997), p. 191, DOI: [10.1016/S0393-0440\(97\)87804-7](https://doi.org/10.1016/S0393-0440(97)87804-7), arXiv: [gr-qc/9610013](https://arxiv.org/abs/gr-qc/9610013).

- [13] P. T. Chruściel, W. Cong, T. Quéau, and R. Wutte, “Cauchy problems for Einstein equations in three-dimensional spacetimes”, in: (Nov. 2024), arXiv: [2411.07423 \[gr-qc\]](https://arxiv.org/abs/2411.07423).
- [14] M. Banados, C. Teitelboim, and J. Zanelli, “The Black hole in three-dimensional space-time”, in: *Phys. Rev. Lett.* 69 (1992), pp. 1849–1851, DOI: [10.1103/PhysRevLett.69.1849](https://doi.org/10.1103/PhysRevLett.69.1849), arXiv: [hep-th/9204099](https://arxiv.org/abs/hep-th/9204099).
- [15] M. Banados, M. Henneaux, C. Teitelboim, and J. Zanelli, “Geometry of the (2+1) black hole”, in: *Phys. Rev. D* 48 (1993), [Erratum: *Phys.Rev.D* 88, 069902 (2013)], pp. 1506–1525, DOI: [10.1103/PhysRevD.48.1506](https://doi.org/10.1103/PhysRevD.48.1506), arXiv: [gr-qc/9302012](https://arxiv.org/abs/gr-qc/9302012).
- [16] J. M. Maldacena, “The Large N limit of superconformal field theories and supergravity”, in: *Adv. Theor. Math. Phys.* 2 (1998), pp. 231–252, DOI: [10.4310/ATMP.1998.v2.n2.a1](https://doi.org/10.4310/ATMP.1998.v2.n2.a1), arXiv: [hep-th/9711200](https://arxiv.org/abs/hep-th/9711200).
- [17] S. S. Gubser, I. R. Klebanov, and A. M. Polyakov, “Gauge theory correlators from noncritical string theory”, in: *Phys. Lett. B* 428 (1998), pp. 105–114, DOI: [10.1016/S0370-2693\(98\)00377-3](https://doi.org/10.1016/S0370-2693(98)00377-3), arXiv: [hep-th/9802109](https://arxiv.org/abs/hep-th/9802109).
- [18] E. Witten, “Anti-de Sitter space and holography”, in: *Adv. Theor. Math. Phys.* 2 (1998), pp. 253–291, DOI: [10.4310/ATMP.1998.v2.n2.a2](https://doi.org/10.4310/ATMP.1998.v2.n2.a2), arXiv: [hep-th/9802150](https://arxiv.org/abs/hep-th/9802150).
- [19] T. Banks, M. R. Douglas, G. T. Horowitz, and E. J. Martinec, “AdS dynamics from conformal field theory”, in: (Aug. 1998), arXiv: [hep-th/9808016](https://arxiv.org/abs/hep-th/9808016).
- [20] V. Balasubramanian, P. Kraus, and A. E. Lawrence, “Bulk versus boundary dynamics in anti-de Sitter space-time”, in: *Phys. Rev. D* 59 (1999), p. 046003, DOI: [10.1103/PhysRevD.59.046003](https://doi.org/10.1103/PhysRevD.59.046003), arXiv: [hep-th/9805171](https://arxiv.org/abs/hep-th/9805171).
- [21] J. R. David, G. Mandal, and S. R. Wadia, “Microscopic formulation of black holes in string theory”, in: *Phys. Rept.* 369 (2002), pp. 549–686, DOI: [10.1016/S0370-1573\(02\)00271-5](https://doi.org/10.1016/S0370-1573(02)00271-5), arXiv: [hep-th/0203048](https://arxiv.org/abs/hep-th/0203048).
- [22] A. Hamilton, D. N. Kabat, G. Lifschytz, and D. A. Lowe, “Local bulk operators in AdS/CFT: A Boundary view of horizons and locality”, in: *Phys. Rev. D* 73 (2006), p. 086003, DOI: [10.1103/PhysRevD.73.086003](https://doi.org/10.1103/PhysRevD.73.086003), arXiv: [hep-th/0506118](https://arxiv.org/abs/hep-th/0506118).
- [23] A. Hamilton, D. N. Kabat, G. Lifschytz, and D. A. Lowe, “Holographic representation of local bulk operators”, in: *Phys. Rev. D* 74 (2006), p. 066009, DOI: [10.1103/PhysRevD.74.066009](https://doi.org/10.1103/PhysRevD.74.066009), arXiv: [hep-th/0606141](https://arxiv.org/abs/hep-th/0606141).
- [24] S. Leutheusser and H. Liu, “Causal connectability between quantum systems and the black hole interior in holographic duality”, in: *Phys. Rev. D* 108.8 (2023), p. 086019, DOI: [10.1103/PhysRevD.108.086019](https://doi.org/10.1103/PhysRevD.108.086019), arXiv: [2110.05497 \[hep-th\]](https://arxiv.org/abs/2110.05497).
- [25] S. A. W. Leutheusser and H. Liu, “Emergent Times in Holographic Duality”, in: *Phys. Rev. D* 108.8 (2023), p. 086020, DOI: [10.1103/PhysRevD.108.086020](https://doi.org/10.1103/PhysRevD.108.086020), arXiv: [2112.12156 \[hep-th\]](https://arxiv.org/abs/2112.12156).

- [26] S. Leutheusser and H. Liu, “Subregion-subalgebra duality: emergence of space and time in holography”, in: (Dec. 2022), arXiv: [2212.13266 \[hep-th\]](#).
- [27] K. Papadodimas and S. Raju, “An Infalling Observer in AdS/CFT”, in: *JHEP* 10 (2013), p. 212, DOI: [10.1007/JHEP10\(2013\)212](#), arXiv: [1211.6767 \[hep-th\]](#).
- [28] K. Papadodimas and S. Raju, “Black Hole Interior in the Holographic Correspondence and the Information Paradox”, in: *Phys. Rev. Lett.* 112.5 (2014), p. 051301, DOI: [10.1103/PhysRevLett.112.051301](#), arXiv: [1310.6334 \[hep-th\]](#).
- [29] K. Papadodimas and S. Raju, “State-Dependent Bulk-Boundary Maps and Black Hole Complementarity”, in: *Phys. Rev. D* 89.8 (2014), p. 086010, DOI: [10.1103/PhysRevD.89.086010](#), arXiv: [1310.6335 \[hep-th\]](#).
- [30] D. Harlow, “Jerusalem Lectures on Black Holes and Quantum Information”, in: *Rev. Mod. Phys.* 88 (2016), p. 015002, DOI: [10.1103/RevModPhys.88.015002](#), arXiv: [1409.1231 \[hep-th\]](#).
- [31] E. Bahiru, A. Belin, K. Papadodimas, G. Sarosi, and N. Vardian, “State-dressed local operators in the AdS/CFT correspondence”, in: *Phys. Rev. D* 108.8 (2023), p. 086035, DOI: [10.1103/PhysRevD.108.086035](#), arXiv: [2209.06845 \[hep-th\]](#).
- [32] S. H. Shenker and D. Stanford, “Black holes and the butterfly effect”, in: *JHEP* 03 (2014), p. 067, DOI: [10.1007/JHEP03\(2014\)067](#), arXiv: [1306.0622 \[hep-th\]](#).
- [33] J. Maldacena, S. H. Shenker, and D. Stanford, “A bound on chaos”, in: *JHEP* 08 (2016), p. 106, DOI: [10.1007/JHEP08\(2016\)106](#), arXiv: [1503.01409 \[hep-th\]](#).
- [34] T. Regge and C. Teitelboim, “Role of Surface Integrals in the Hamiltonian Formulation of General Relativity”, in: *Annals Phys.* 88 (1974), p. 286, DOI: [10.1016/0003-4916\(74\)90404-7](#).
- [35] V. Balasubramanian and P. Kraus, “A Stress tensor for Anti-de Sitter gravity”, in: *Commun. Math. Phys.* 208 (1999), pp. 413–428, DOI: [10.1007/s002200050764](#), arXiv: [hep-th/9902121](#).
- [36] R. Emparan, C. V. Johnson, and R. C. Myers, “Surface terms as counterterms in the AdS / CFT correspondence”, in: *Phys. Rev. D* 60 (1999), p. 104001, DOI: [10.1103/PhysRevD.60.104001](#), arXiv: [hep-th/9903238](#).
- [37] S. R. Lau, “Light cone reference for total gravitational energy”, in: *Phys. Rev. D* 60 (1999), p. 104034, DOI: [10.1103/PhysRevD.60.104034](#), arXiv: [gr-qc/9903038](#).
- [38] R. B. Mann, “Misner string entropy”, in: *Phys. Rev. D* 60 (1999), p. 104047, DOI: [10.1103/PhysRevD.60.104047](#), arXiv: [hep-th/9903229](#).
- [39] P. Kraus, F. Larsen, and R. Siebelink, “The gravitational action in asymptotically AdS and flat space-times”, in: *Nucl. Phys. B* 563 (1999), pp. 259–278, DOI: [10.1016/S0550-3213\(99\)00549-0](#), arXiv: [hep-th/9906127](#).



- [40] P. A. M. Dirac, “The Hamiltonian form of field dynamics”, in: *Can. J. Math.* 3 (1951), pp. 1–23, DOI: [10.4153/CJM-1951-001-2](https://doi.org/10.4153/CJM-1951-001-2).
- [41] C. Teitelboim, “How commutators of constraints reflect the space-time structure”, in: *Annals Phys.* 79 (1973), pp. 542–557, DOI: [10.1016/0003-4916\(73\)90096-1](https://doi.org/10.1016/0003-4916(73)90096-1).
- [42] E.ourgoulhon, “3+1 formalism and bases of numerical relativity”, in: (Mar. 2007), arXiv: [gr-qc/0703035](https://arxiv.org/abs/gr-qc/0703035).
- [43] P. A. M. Dirac, “Fixation of coordinates in the Hamiltonian theory of gravitation”, in: *Phys. Rev.* 114 (1959), ed. by J.-P. Hsu and D. Fine, pp. 924–930, DOI: [10.1103/PhysRev.114.924](https://doi.org/10.1103/PhysRev.114.924).
- [44] L. Andersson, P. Chrusciel, and H. Friedrich, “On the Regularity of solutions to the Yamabe equation and the existence of smooth hyperboloidal initial data for Einsteins field equations”, in: *Commun. Math. Phys.* 149 (1992), pp. 587–612, DOI: [10.1007/BF02096944](https://doi.org/10.1007/BF02096944).
- [45] L Andersson and P. T. Chrusciel, “On asymptotic behaviour of solutions of the constraint equations in general relativity with 'hyperboloidal boundary conditions'”, in: *Diss. Math.* 355 (1996), pp. 1–100.
- [46] P. T. Chruściel and G. J. Galloway, “Maximal hypersurfaces in asymptotically Anti-de Sitter spacetime”, in: (Aug. 2022), arXiv: [2208.09893 \[gr-qc\]](https://arxiv.org/abs/2208.09893).
- [47] P. Senjanovic, “Path Integral Quantization of Field Theories with Second Class Constraints”, in: *Annals Phys.* 100 (1976), [Erratum: *Annals Phys.* 209, 248 (1991)], pp. 227–261, DOI: [10.1016/0003-4916\(76\)90062-2](https://doi.org/10.1016/0003-4916(76)90062-2).
- [48] K. Krasnov and J.-M. Schlenker, “Minimal surfaces and particles in 3-manifolds”, in: *Geom. Dedicata* 126 (2007), pp. 187–254, DOI: [10.1007/s10711-007-9132-1](https://doi.org/10.1007/s10711-007-9132-1), arXiv: [math/0511441](https://arxiv.org/abs/math/0511441).
- [49] F. Bonsante and J.-M. Schlenker, “Maximal surfaces and the universal Teichmüller space”, in: *Inventiones mathematicae* 182.2 (Nov. 2010), pp. 279–333, DOI: [10.1007/s00222-010-0263-x](https://doi.org/10.1007/s00222-010-0263-x), arXiv: [0911.4124](https://arxiv.org/abs/0911.4124), URL: <https://doi.org/10.1007/s00222-010-0263-x>.
- [50] C. Scarinci and K. Krasnov, “The universal phase space of  $AdS_3$  gravity”, in: *Commun. Math. Phys.* 322 (2013), pp. 167–205, DOI: [10.1007/s00220-012-1655-0](https://doi.org/10.1007/s00220-012-1655-0), arXiv: [1111.6507 \[hep-th\]](https://arxiv.org/abs/1111.6507).
- [51] D. Borthwick, *Spectral theory of infinite-area hyperbolic surfaces*, Switzerland: Publ: Birkhäuser, 2016.
- [52] A. R. Steif, “Time symmetric initial data for multibody solutions in three-dimensions”, in: *Phys. Rev. D* 53 (1996), pp. 5527–5532, DOI: [10.1103/PhysRevD.53.5527](https://doi.org/10.1103/PhysRevD.53.5527), arXiv: [gr-qc/9511053](https://arxiv.org/abs/gr-qc/9511053).
- [53] D. R. Brill, “Multi - black hole geometries in (2+1)-dimensional gravity”, in: *Phys. Rev. D* 53 (1996), pp. 4133–4176, DOI: [10.1103/PhysRevD.53.R4133](https://doi.org/10.1103/PhysRevD.53.R4133), arXiv: [gr-qc/9511022](https://arxiv.org/abs/gr-qc/9511022).

- [54] L. Smarr and J. W. York Jr., “Kinematical conditions in the construction of space-time”, in: *Phys. Rev. D* 17 (1978), pp. 2529–2551, DOI: [10.1103/PhysRevD.17.2529](https://doi.org/10.1103/PhysRevD.17.2529).
- [55] F. Estabrook, H. Wahlquist, S. Christensen, B. DeWitt, L. Smarr, and E. Tsiang, “Maximally slicing a black hole”, in: *Phys. Rev. D* 7 (1973), pp. 2814–2817, DOI: [10.1103/PhysRevD.7.2814](https://doi.org/10.1103/PhysRevD.7.2814).
- [56] T. W. Baumgarte and S. L. Shapiro, *Numerical Relativity: Solving Einstein’s Equations on the Computer*, Cambridge University Press, 2010, DOI: [10.1017/CB09781139193344](https://doi.org/10.1017/CB09781139193344).
- [57] A. Kaushal, N. S. Prabhakar, and S. R. Wadia, “Emergent Time in Hamiltonian General Relativity”, in: (May 2024), arXiv: [2405.18486](https://arxiv.org/abs/2405.18486) [[hep-th](https://arxiv.org/abs/2405.18486)].
- [58] S. J. Avis, C. J. Isham, and D. Storey, “Quantum Field Theory in anti-De Sitter Space-Time”, in: *Phys. Rev. D* 18 (1978), p. 3565, DOI: [10.1103/PhysRevD.18.3565](https://doi.org/10.1103/PhysRevD.18.3565).
- [59] P. Breitenlohner and D. Z. Freedman, “Positive Energy in anti-De Sitter Backgrounds and Gauged Extended Supergravity”, in: *Phys. Lett. B* 115 (1982), pp. 197–201, DOI: [10.1016/0370-2693\(82\)90643-8](https://doi.org/10.1016/0370-2693(82)90643-8).
- [60] P. Breitenlohner and D. Z. Freedman, “Stability in Gauged Extended Supergravity”, in: *Annals Phys.* 144 (1982), p. 249, DOI: [10.1016/0003-4916\(82\)90116-6](https://doi.org/10.1016/0003-4916(82)90116-6).
- [61] S. W. Hawking, “The Boundary Conditions for Gauged Supergravity”, in: *Phys. Lett. B* 126 (1983), pp. 175–177, DOI: [10.1016/0370-2693\(83\)90585-3](https://doi.org/10.1016/0370-2693(83)90585-3).
- [62] M. Henneaux and C. Teitelboim, “Hamiltonian Treatment of Asymptotically Anti-de Sitter Spaces”, in: *Phys. Lett. B* 142 (1984), pp. 355–358, DOI: [10.1016/0370-2693\(84\)91339-X](https://doi.org/10.1016/0370-2693(84)91339-X).
- [63] L. Mezincescu and P. K. Townsend, “Stability at a Local Maximum in Higher Dimensional Anti-de Sitter Space and Applications to Supergravity”, in: *Annals Phys.* 160 (1985), p. 406, DOI: [10.1016/0003-4916\(85\)90150-2](https://doi.org/10.1016/0003-4916(85)90150-2).
- [64] G. Lifschytz and M. Ortiz, “Scalar field quantization on the (2+1)-dimensional black hole background”, in: *Phys. Rev. D* 49 (1994), pp. 1929–1943, DOI: [10.1103/PhysRevD.49.1929](https://doi.org/10.1103/PhysRevD.49.1929), arXiv: [gr-qc/9310008](https://arxiv.org/abs/gr-qc/9310008).
- [65] I. Ichinose and Y. Satoh, “Entropies of scalar fields on three-dimensional black holes”, in: *Nucl. Phys. B* 447 (1995), pp. 340–372, DOI: [10.1016/0550-3213\(95\)00197-Z](https://doi.org/10.1016/0550-3213(95)00197-Z), arXiv: [hep-th/9412144](https://arxiv.org/abs/hep-th/9412144).
- [66] E. Keski-Vakkuri, “Bulk and boundary dynamics in BTZ black holes”, in: *Phys. Rev. D* 59 (1999), p. 104001, DOI: [10.1103/PhysRevD.59.104001](https://doi.org/10.1103/PhysRevD.59.104001), arXiv: [hep-th/9808037](https://arxiv.org/abs/hep-th/9808037).
- [67] A. Ishibashi and R. M. Wald, “Dynamics in nonglobally hyperbolic static space-times. 3. Anti-de Sitter space-time”, in: *Class. Quant. Grav.* 21 (2004), pp. 2981–3014, DOI: [10.1088/0264-9381/21/12/012](https://doi.org/10.1088/0264-9381/21/12/012), arXiv: [hep-th/0402184](https://arxiv.org/abs/hep-th/0402184).

- [68] N. D. Birrell and P. C. W. Davies, *Quantum Fields in Curved Space*, Cambridge Monographs on Mathematical Physics, Cambridge, UK: Cambridge University Press, 1982, DOI: [10.1017/CB09780511622632](https://doi.org/10.1017/CB09780511622632).
- [69] W. G. Unruh, “Notes on black hole evaporation”, in: *Phys. Rev. D* 14 (1976), p. 870, DOI: [10.1103/PhysRevD.14.870](https://doi.org/10.1103/PhysRevD.14.870).
- [70] *NIST Digital Library of Mathematical Functions*, <https://dlmf.nist.gov/>, Release 1.2.3 of 2024-12-15, F. W. J. Olver, A. B. Olde Daalhuis, D. W. Lozier, B. I. Schneider, R. F. Boisvert, C. W. Clark, B. R. Miller, B. V. Saunders, H. S. Cohl, and M. A. McClain, eds., URL: <https://dlmf.nist.gov/>.